FISSION PRODUCT IMPACT REDUCTION VIA PROTRACTED IN-CORE RETENTION IN VERY HIGH TEMPERATURE REACTOR (VHTR) TRANSMUTATION SCENARIOS

A Dissertation

by

AYODEJI BABATUNDE ALAJO

Submitted to the Office of Graduate Studies of
Texas A&M University
in partial fulfillment of the requirements for the degree of

DOCTOR OF PHILOSOPHY

May 2010

Major Subject: Nuclear Engineering

FISSION PRODUCT IMPACT REDUCTION VIA PROTRACTED IN-CORE RETENTION IN VERY HIGH TEMPERATURE REACTOR (VHTR) TRANSMUTATION SCENARIOS

A Dissertation

by

AYODEJI BABATUNDE ALAJO

Submitted to the Office of Graduate Studies of
Texas A&M University
in partial fulfillment of the requirements for the degree of

DOCTOR OF PHILOSOPHY

Approved by:

Chair of Committee,	Pavel V. Tsvetkov
Committee Members,	Yassin A. Hassan
	Sean M. McDeavitt
	Joseph E. Pasciak
Head of Department,	Raymond J. Juzaitis

May 2010

Major Subject: Nuclear Engineering

ABSTRACT

Fission Product Impact Reduction via Protracted In-core Retention in Very High Temperature Reactor (VHTR) Transmutation Scenarios. (May 2010)

Ayodeji Babatunde Alajo, B.Sc., University of Ibadan; M.S., Texas A&M University

Chair of Advisory Committee: Dr. Pavel V. Tsvetkov

The closure of the nuclear fuel cycle is a topic of interest in the sustainability context of nuclear energy. The implication of such closure includes considerations of nuclear waste management. This originates from the fact that a closed fuel cycle requires recycling of useful materials from spent nuclear fuel and discarding of non-usable streams of the spent fuel, which are predominantly the fission products. The fission products represent the near-term concerns associated with final geological repositories for the waste stream. Long-lived fission products also contribute to the long-term concerns associated with such repository. In addition, an ultimately closed nuclear fuel cycle in which all actinides from spent nuclear fuels are incinerated will result in fission products being the only source of radiotoxicity. Hence, it is desired to develop a transmutation strategy that will achieve reduction in the inventory and radiological parameters of significant fission products within a reasonably short time.

In this dissertation, a transmutation strategy involving the use of the VHTR is developed. A set of specialized metrics is developed and applied to evaluate performance characteristics. The transmutation strategy considers six major fission products: ^{90}Sr, ^{93}Zr, ^{99}Tc, ^{129}I, ^{135}Cs and ^{137}Cs. In this approach, the unique core features of VHTRs operating in equilibrium fuel cycle mode of 405 effective full power days are used for

transmutation of the selected fission products. A 30 year irradiation period with 10 post-irradiation cooling is assumed. The strategy assumes no separation of each nuclide from its corresponding material stream in the VHTR fuel cycle. The optimum locations in the VHTR core cavity leading to maximized transmutation of each selected nuclides are determined.

The fission product transmutation scenarios are simulated with MCNP and ORIGEN-S. The results indicate that the developed fission product transmutation strategy offers an excellent potential approach for the reduction of inventories and radiological parameters, particularly for long-lived fission products (^{93}Zr, ^{99}Tc, ^{129}I and ^{135}Cs). It has been determined that the in-core transmutation of relatively short-lived fission products (^{90}Sr and ^{137}Cs) has minimal advantage over a decay-only scenario for these nuclides. It is concluded that the developed strategy is a viable option for the reduction of radiotoxicity contributions of the selected fission products prior to their final disposal in a geological repository. Even in the cases where the transmutation advantage is minimal, it is deemed that the improvement gained, coupled with the virtual storage provided for the fission products during the irradiation period, makes the developed fission product transmutation strategy advantageous in the spent fuel management scenarios. Combined with the in-core incineration options for TRU, the developed transmutation strategy leads to potential achievability of engineering time scales in the comprehensive nuclear waste management.

To God and for Ibukun Mi Owon

ACKNOWLEDGEMENTS

My gratitude goes to my adviser, Dr. Pavel Tsvetkov, for his support during the course of this dissertation. I appreciate his dedication to the subject of the research and his guidance throughout my academic pursuit at Texas A&M University. I also thank Drs. Yassin Hassan, Sean McDeavitt and Joe Pasciak for serving on my graduate committee. They were invaluable resources when I needed expert judgment during the research effort.

I would like to acknowledge the financial support of my research by the US Department of Energy as part of the Nuclear Energy Research Initiative (NERI) project Award Number DE-FC07-05ID14655 (05-094).

I also acknowledge the support of friends and family. I appreciate the prayers and goodwill from my parents, brothers, in-laws, the Abikoyes, the Ruwases, the Ames, the Salamis, the Ewumis and the Akinwales. The encouragement you all gave to me is priceless. Thanks for being a part of my success.

To all of my GCI, UI and UCH crews, friends from Andersen, KPMG, Chicago, Dallas, Austin, College Station and Houston, CFC, BGSA and ASA friends, my buddies in the Nuke department, I thank you all for being good friends.

Also to my wife, Ibukunoluwa, thanks for being the pillar of support that you are. I appreciate everything you have sacrificed to make this journey a success. Above all, I thank God, who is the Wise and Holy One for seeing me through this endeavor. He has been true to His words.

NOMENCLATURE

ADS	Accelerator Driven System
ANL	Argonne National Laboratory
AVR	Arbeitsgemeinschaft Versuchs Reaktor
BNL	Brookhaven National Laboratory
BOC	Beginning of Cycle
BOEC	Beginning of Equilibrium Cycle
DOE	U.S. Department of Energy
EFC	Equilibrium Fuel Cycle
ENDF/B	Evaluated Nuclear Data Files – Basic
EOC	End of Cycle
EOEC	End of Equilibrium Cycle
EPA	Environmental Protection Agency
FP	Fission Products
GTCC	Greater Than Class-C
HLW	High Level Waste
HTGR	High Temperature Gas Reactor
HTR	High Temperature Reactor
HTTR	High Temperature Test Reactor
ICRP	International Commission on Radiological Protection
JENDL	Japanese Evaluated Nuclear Data Library
JNDC	Japanese Nuclear Data Committee
KAERI	Korea Atomic Energy Research Institute

LANL	Los Alamos National Laboratory
LLFP	Long Lived Fission Product
LLW	Low Level Waste
LWR	Light Water Reactor
MCNP	Monte Carlo N – Particle
MCNPX	Monte Carlo N – Particle Extended
MT	Metric Tons
MTHM	Metric Tons of Heavy Metal
MTIHM	Metric Tons of Initial Heavy Metal
MTU	Metric Tons of Uranium
NRC	Nuclear Regulatory Commission
ORNL	Oak Ridge National Laboratory
OTOC	Once-Through-and-Out Cycle
P&T	Partitioning and Transmutation
PWR	Pressurized Water Reactor
SNF	Spent Nuclear Fuel
THTR	Thorium High Temperature Reactor
TRISO	Tri-structural Isotropic
TRU	Transuranium Nuclide
VHTR	Very High Temperature Reactor

TABLE OF CONTENTS

CHAPTER Page

CHAPTER Page

LIST OF FIGURES

FIGURE Page

LIST OF TABLES

TABLE Page

CHAPTER I

INTRODUCTION

Nuclear energy has a potential to offer a sustainable reliable source of energy. This potential can only be realized if the major issues associated with nuclear energy are resolved. Today those issues are because of the need to handle nuclear waste and proliferation concerns. This dissertation addresses nuclear waste management challenges by offering an inventory minimization approach to the near-term component of the nuclear waste – fission products (FP). The flow of the body of work presented in this dissertation is provided in Figure 1. The flowchart identifies the focus of each chapter and provides a complete view of the work done.

I.A RADIOTOXICITY: TRANSURANIUM NUCLIDES AND FISSION PRODUCTS

The active part of a fresh nuclear fuel consists of uranium isotopes. At this stage, the radiotoxicity of the fuel is relatively low. Once the fuel is deployed in a reactor, the irradiation leads to incineration and/or transmutation of uranium isotopes. A uranium atom may absorb a neutron in the reactor and then fission resulting in the creation of fission products. A uranium atom that is not fissioned after neutron absorption will be transmuted to another isotope. The new isotope may experience series of decays and neutron absorptions, thereby progressively changing into TRU. The increasing presence of FP and TRU in the nuclear fuel increases the radiotoxicity of spent fuels.

This dissertation follows the style of *Nuclear Science and Engineering*.

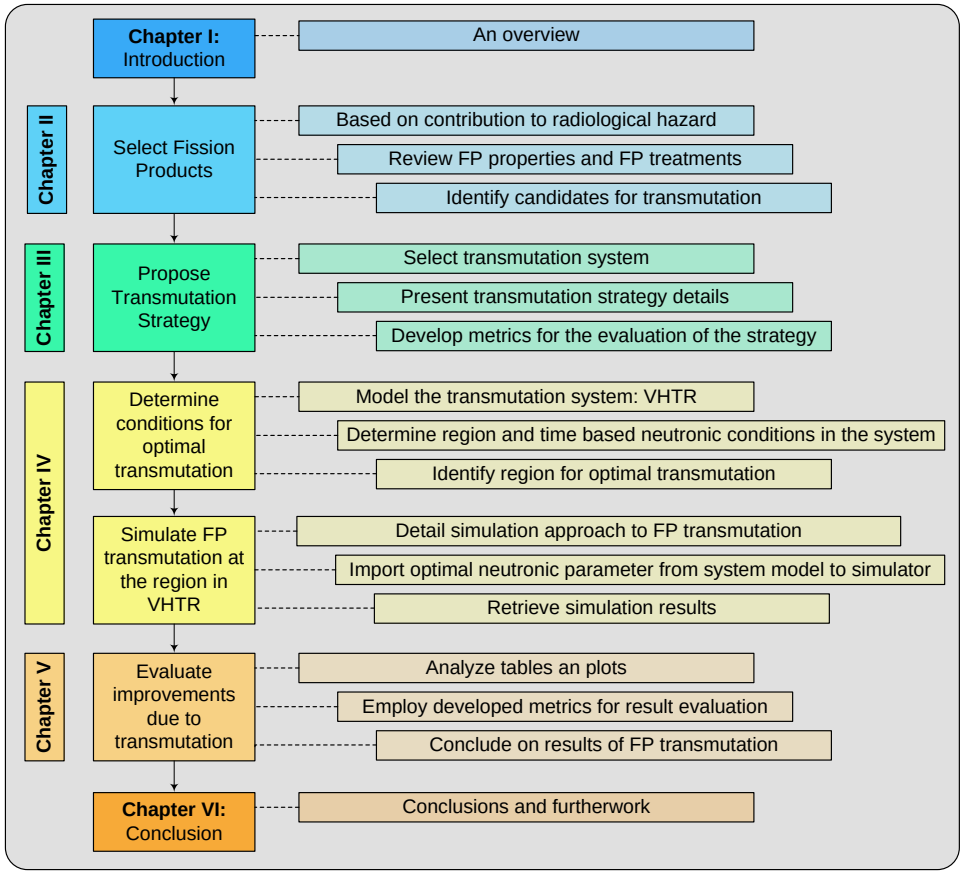

Fig. 1. Flowchart representation of the dissertation.

Radiotoxicity refers to the hazardous effects of radioactive materials on living organisms. Radiotoxicity is an attribute of spent nuclear fuel stemming from the FP and TRU content of the fuel. In discharged spent nuclear fuels (SNF), the reduction of radiotoxicity is mainly driven by the decay of the radionuclides. The time required to attain a tolerable level of toxicity is governed by the half lives of the radioactive nuclides. The transmutation path of the radionuclides may not be accelerated once the fuel is discharged from the reactor. TRU generally have longer half-lives than the FP nuclides. Fission products are the main contributors to the spent fuel hazard during the first 300 to 500 years after irradiation. Beyond this timeframe, the total radiotoxicity is mainly from the TRU.

Transuranics account for most of the long-term radiotoxicity of spent fuel due to the radioactive decay of most of FP nuclides. TRU have half-lives in the order of thousands to millions of years. A trivial answer to the question 'how can radiotoxicity of spent nuclear fuel be reduced?' is the elimination of FP and TRU.

I.B SPENT NUCLEAR FUEL MANAGEMENT

Spent fuel management options include geological disposal scenarios and nuclear fuel recycling technologies. The U.S. department of Energy (DOE) estimated that 57,700 metric tons of spent fuels were stored at nuclear power plants and other facilities at the end of 2007 [1,2]. In a geological disposal scenario, all U.S. commercial spent fuel would be permanently moved to a repository – a disposal site designated to accommodate spent fuel inventory. The spent fuel estimate is 82% of the 70,000 metric tons capacity of the proposed Yucca Mountain repository. As a result of the increasing spent fuel inventory to be stored, the disposal option has some concerns associated with it. These concerns cover aspects such as health concerns of local communities, environmental impact, safety issues, and proliferation risks. The DOE estimated the worst case of exposure to an individual over a period of 70 years at 7.6 mrem annually [3]. In addition, researchers would have to demonstrate that standards such as the Environmental Protection Agency (EPA) individual radiation exposure limit of 15 mrem over the first 10,000 years of disposal [4] are achievable. These doses are below the EPA annual limit of 25 mrem [5], demonstrating that geological disposal scenarios can be safely implemented.

The recycling option is a technological approach designed to address the concerns associated with the direct geological disposal option. Recycling scenarios involve the recovery and reuse of potential fuel materials in spent fuel to reduce the amount of wastes requiring permanent geological disposal. The reduced waste inventory will further lower the current estimates for individual doses. Assuming that spent nuclear fuel reprocessing is performed, the spent fuel can be partitioned and separated into 3 streams: depleted uranium (to be recycled with plutonium in reactors), TRU and FP. The TRU content of spent fuel is potentially a useable material. TRU can be recycled in advanced reactors as nuclear fuel. Unlike the other 2 streams, the FP stream does not have any recycling potential. Thus FP is the true waste in nuclear fuel. Moreover, the FP stream represents a near-term radiotoxicity concern due to its high radioactivity coupled with relatively short half-lives of the constituents of the FP stream. In addition the long-lived fission products contribute to the long term radiotoxicity concerns. Hence it is desirable to seek ways through which the radiotoxicity of the FP stream can be reduced in order to reduce its impact on the environment.

I.C FISSION PRODUCTS MANAGEMENT OPTIONS

The current management of FP inventory is focused on disposal in geological repositories. For example, a research effort by the Japan Atomic Energy Agency is focused on the isolation of FP through various Partitioning and Transmutation (P&T) schemes. In this effort, the FP are partitioned and made into forms suitable for geological disposal. The FP waste forms are designed to mitigate difficulties caused by long-term nature of radioactivity and extend the capacity of a repository [6]. Similarly, the

European Commission research efforts focused on this option through its RED IMPACT program [7]. The program was established to assess the impact of P&T on geological disposal and waste management. In addition, the program would assess economic, environmental and societal costs/benefits of spent fuel P&T [8].

Geological disposal will require the FP nuclides to be isolated from the environment for as long as 500 years before attaining a negligible radioactivity level. The repository needs to maintain its integrity over this period. This may not be very long time, but there are not many examples of man-made facilities with their integrities kept intact for hundreds of years. In addition, uncertainties in the design and construction of facilities required for the disposal may be too large to quantify over such long time frame. This will place low confidence on the integrity of the disposal facility over time. Suppose there is a strategy that will achieve reduction in the radiotoxicity of FP, then spent nuclear fuel will ultimately become environmentally benign within a short time frame. In addition, higher confidence can be placed on disposal facilities since much shorter time is required for the isolation of the final waste-form.

One way through which the radiotoxicity of FP can be reduced is via transmutation of the FP nuclides into stable nuclides or nuclides with shorter half-lives than the initial FP nuclides. FPs placed in the core of a reactor absorb neutrons in capture reactions. Unlike uranium isotopes, FP nuclides are not capable of fission. They can only be progressively transmuted to other nuclides through a series of radioactive decays and neutron absorption reactions. The transmutation chain is expected to lead to various combinations of stable nuclides and very short-lived nuclides. This is the premise upon which this research effort is situated.

The studies and experiments on the transmutation of FPs have been reported in several articles [9 – 14]. These studies focus on transmutation in fast reactors, fusion system and accelerator driven systems. All these efforts are aimed at using various nuclear energy systems to reduce FP inventories. The FP incineration strategy for each nuclear system takes advantage of the system's energy spectrum, flux levels, reactor operation cycle and any combination thereof. Moreover, the transmutation studies are focused on a particular fission product in a selected reactor system; for example, technetium transmutation in JOYO fast reactor [13]. Another literature on the utilization of gas-cooled reactor technologies for transmutation of nuclear waste suggested Technetium and Iodine transmutation in systems driven by advanced fuels containing plutonium and minor actinides [15]. These various approaches to FP management will be discussed further in section II.C of Chapter II.

The transmutation strategy being proposed though this research effort will address the incineration of all significant FP from current LWR spent fuel in a selected system. The ultimate FP incinerator would optimally combine flux levels, energy spectrum and core lifetime to achieve the highest conversion of radioactive FP to stable nuclides in the shortest time possible. Such ultimate incineration may be derived through the use of advanced nuclear systems.

I.D ADVANCED REACTOR SYSTEMS: VHTR

The DOE leads an international collaborative effort to develop advanced nuclear energy systems known as the Gen-IV systems. The systems are expected to broaden the opportunities for implementing nuclear energy globally. In addition, the systems promise

to be economically viable, environmentally benign, and ultimately minimize nuclear waste. One of the six systems identified for this purpose is the Very High Temperature Reactor (VHTR) [16].

The VHTR is the most near-term of the Gen-IV reactor systems. It is based on a well proven technology that has been implemented in High Temperature Gas Reactors (HTGRs) such as the German AVR and THTR prototypes, and the United States' Fort Saint Vrain and Peach Bottom prototypes. The VHTR builds on the capabilities of HTGR by improvements in thermal efficiency and deployment for high-temperature applications such as hydrogen production, sea-water desalination and industrial process heat supply [17]. The VHTR is a graphite-moderated helium-cooled reactor that supplies heat at core outlet temperatures above 750^0C. It can be in prismatic block configuration like the HTTR operating in Japan, or a pebble bed core such as the Chinese High Temperature Test Module (HTR-10) [18, 19].

The VHTR is one of the reactors being conceptually designed for thermal neutron transmutation of nuclear wastes. Much of the research efforts by General Atomics and Argonne National Laboratory in this area have been focused on TRU transmutation in VHTR. The VHTR-based transmutation concept takes advantage of the higher number of steps it takes for a neutron to slow-down to thermal energies in graphite than the steps required in conventional LWR. The reduced slowing-down rate in graphite media favors the attainment of the right spectra for transmutation of different nuclides [20]. This spectral effect of graphite on neutron moderation will be taken advantage of for FP transmutation in VHTR.

I.E DISSERTATION OBJECTIVES

The present doctoral research effort is focused on the reduction of the impact of fission product radiotoxicity via protracted retention in the core of a VHTR system in thermal and epithermal neutron spectrum transmutation scenarios. This objective leads to a set of quantifiable sub-objectives:

1. Development of the irradiation strategies and evaluation methodology and quantification of reduction factors for LLFP inventories during the in-core retention period of the FP targets.
2. Development of the evaluation methodology and quantification of radiation reduction factors at the geological disposal stage.
3. Development of the evaluation methodology and minimization of time required for final waste radiotoxicity to attain tolerable levels.
4. Development of the evaluation methodology and minimization of time required for FP decay heat to reach acceptable levels at the geological disposal stage.

The expected advantage of the in-core retention of FPs in the VHTR-based fuel cycle scenarios is the opportunity to attain engineering time scales in the nuclear waste management scenarios. The overall constraint for introducing specialized irradiation targets containing FPs is to avoid significant flux fluctuations in the VHTR while retaining FPs in the reactor system.

I.F OUTLINE AND STRATEGY

An approach is proposed herein to reduce the radiotoxicity of the SNF. It takes advantage of transmutation of FPs via protracted in-core retention in VHTRs. In the present effort, Because of spectral options in VHTRs and 3D irradiation location flexibilities, the VHTR cores offer a potential to attain conditions for efficient transmutation of FPs. The adequacy of the applied VHTR models has been confirmed in a series of experiment-to-code benchmark evaluations [21, 22].

The proposed approach involves strategic placement of irradiation targets with FPs in favorable in-core locations so that the FP are transmuted to stable or shorter lived radionuclides more efficiently allowing for a potential of engineering time scales in nuclear waste management. The strategy focuses on FPs with half lives greater than 25 years. A 25 year half-life cut-off is set to include ^{90}Sr and ^{137}Cs in the group of FPs for transmutation consideration. The phases of the proposed analysis are described as follow:

1. Determine the spectrum conditions under which selected LLFPs can be effectively transmuted. The review of each LLFP's neutronic properties is discussed in Chapter II. Calculated spectral conditions for the transmutation are presented in section IV.C.1.
2. Determine the locations in the VHTR core that will achieve maximum transmutation of FP with little or no distortion in the power profile of the reactor in its original configuration. This is done by deriving the core power map in a 3-D full core MCNP/MCNPX model of the VHTR with spatial flux tallies and energy binning (See section IV.C.2). Since the VHTR as proposed

under Gen-VI program has not been built, a representative 600MWt VHTR power core is modeled. The representative VHTR core follows the prescription of G. Aliberti et al. [23]. The prismatic blocks of the VHTR are based Japan's HTTR. The fuel kernel is uranium oxide as fabricated for the HTTR.

3. Optimize the placement of FP target at locations that will result in the fastest and/or highest transmutation-induced reduction in radioactive FP inventory. The anticipated result of this approach is the quick reduction of FP radiotoxicity contribution. The reduced toxicity will insure less storage time to the attainment of a tolerable level of toxicity. The full core model required for this phase involves the use of MCNP/MCNPX and ORIGEN-S code systems. This is presented in section IV.D.
4. Develop a methodology for the systemic characterization of the FP nuclides before and after transmutation. The method will be based on the fact that the radiotoxicity of a nuclide may be reduced via reduction in the magnitude of contributing parameters or shortening of the duration of the nuclides' existence. The contributing parameters include quantities of materials, radioactivity levels, decay heat data, gamma-ray emission rates, dose equivalents, and residence times in reactor core. The methodology utilizes several metrics and their combinations thereof to determine the optimal transmutation scenario.

This research approach will take advantage of neutrons outside the active core of reactor systems for transmutation. The active core region will be avoided so that flux

profile in the core is preserved. The FP target placement locations will be optimized for the outer radial and center reflectors of the VHTR.

There is a number of advantages in the method being suggested in the presented dissertation. First, the protracted in-core residence serves as a virtual storage facility for the FP inventories over the transmutation period. In addition, reduction in the radiotoxicity term is achieved through the possible reductions in quantities of radioactive materials and transmutation of FPs to shorter-lived nuclides. This will lead to reduction in magnitude of waste quantities as well as size of facilities required for waste disposal. It will also result in the reduction of nuclear fuel cycle's ecological footprint, thereby improving nuclear energy's environmental friendliness. Other aspects of the nuclear fuel cycle that will be positively impacted by the successful implementation of the transmutation-induced reduction in radioactive FP inventory are HLW disposal, LLW management and SNF repository utilization.

CHAPTER II

FISSION PRODUCT VECTOR, SOURCE AND TREATMENT

There have been discussions and efforts to provide a permanent geological repository for the existing spent fuel inventory in the United States of America. The location of such facility, quantities of radioactive wastes to be accommodated and the potential impact of concentrating HLW in one location are the main questions to be addressed to assure viability of such a disposal facility. While the selection of a site is outside the scope of this research, the waste quantity and its impact to the site are cardinal to this effort.

The site selection process identified Yucca Mountain as the location for the disposal facility. The proposed facility was specified to hold a maximum of 70,000 MT of high level wastes. Analyses were performed to determine the impact of the current spent fuel inventory on the selected site [24]. While the analyses have shown that waste inventories can be safely disposed at the proposed site, it would be better if the waste quantities and their environmental impact can be reduced. To determine a strategy that would lead to the desired reduction, it is important to understand the properties of the principal radionuclides in the waste stream.

The present research effort focuses on the fission product streams in the high level nuclear waste. It is understood that the main players in long term radiotoxicity of the spent nuclear fuel are the higher actinides; however, this would not be such a problem if and when actinide recycling is adopted. It can be argued that once a complete and ultimate incineration of transuranium nuclides is established, all that will be left are fission products. Thus the ultimate contributor to the radiotoxicity of spent nuclear fuel

will be the fission products. Thus, there is a need to explore fission product vectors, source terms and develop potential treatment options.

This chapter discusses the fission product content in the current spent fuel inventory. It starts with the review of the fission product vector in the spent fuel inventory at the end of 2007. Based on the inventory and activities of the constituent radionuclides, a few fission products are selected for further consideration. The analysis accounts for neutronics properties, physical properties and chemical forms for the selected fission products. A later section of this chapter is dedicated to the analysis of the current treatment approaches of fission product inventories as well as some proposed outlook across the globe.

II.A LWR FISSION PRODUCT INVENTORIES

The United States of America has about 57,700 MT of spent nuclear fuel from commercial reactors stored at nuclear power plants across the country. The spent fuel consists of actinides and fission products. The exact fission product quantification (by mass) would require extensive assay of the spent nuclear fuels. However, a fairly adequate estimate can be determined.

Previous work, which led to this research indicated that a UO_2 fueled LWR operating at 85% load factor up to 45GWd/MTU burnup contains approximately 4.6 weight percent of fission products, 94.3 weight percent depleted uranium and 1.1 percent higher actinides [25]. Based on the 4.6w/o fission product content, it can be estimated that 10GWd/MTU burnup corresponds to about 1.0w/o of fission products in the spent fuel. Given the burnup of U.S. legacy spent fuel, a conservative assumption of

40 GWd/MTU burnup is made for the current spent fuel inventory; thereby assuming a 4.0w/o fission product content in the 57,700 MT spent fuel inventory. Hence the fission product inventory is estimated as 2,308 MT. The mass quantification varies with burnup and age of the spent nuclear fuels. The burnup of spent nuclear fuels affects the initial quantities heat load and radiotoxicity of FPs, while the age affects the stream of nuclides contributing to the FP's continuing heat generation and radiotoxicity hazards.

Quantitative analysis of known fission product inventories provides basis for identifying constituents of the FP inventories with significant contributions to the overall hazards. The 2002 Yucca Mountain Report [24] establishes a quantitative basis for characterizing fission product inventories in spent nuclear fuel compositions. Emphasis is placed on the fission product vector from legacy PWR spent fuel – a 23 year old spent fuel at 41.2 GWd/MTU burnup. The vector forms the basis of selection of significant FP nuclides in section II.B.

II.B SIGNIFICANT FISSION PRODUCTS

Table I shows the individual fission products in the legacy spent fuel as well as their contributions to the quantity and radioactivity of the fission products in PWR spent fuel. The selenium, strontium, zirconium, niobium-94, technetium, palladium, tin, iodine, cesium (except ^{134}Cs) and Samarium radionuclides have half-lives greater than 25 years. These nuclides are probable candidates for transmutation in order to reduce their inventory within a relatively short time frame. The primary candidates from this group are nuclides with significant contribution to the radioactivity of FP vector. These are ^{90}Sr and ^{137}Cs, which represent 95.55% of the FP vector's radioactivity (see Table I). Both

nuclides also have the highest heat load impact from the group of FP nuclides. The rest of the nuclides in this group are significantly less radioactive. Radiotoxicity hazard qualifies ^{129}I and ^{99}Tc as candidates for transmutation. Environmental concerns are associated with both nuclides. ^{129}I is a highly mobile nuclide. Iodine is known to sublime at low temperature and highly soluble in water when in salt form. ^{99}Tc is also mobile in geological environment. Both nuclides have significant quantities in the FP vector. Addition candidates for transmutation are identified in this group by their contribution to the inventory size. ^{93}Zr and ^{135}Cs are selected. It should be noted that while ^{107}Pd represents 6.33% of the FP radionuclide inventory, its radioactivity contribution is merely 0.0001% of the total for all FP radionuclides and its specific heat generation is least of all the FP nuclides (see Table I). Its contribution to the overall radiotoxicity of the FP vector is negligible.

The radionuclides with half-lives between 5 and 25 years fall in a class where other considerations such as their inventory and radioactivity contributions are important in the determination of the most appropriate treatment. Nuclides in this category include ^{93m}Nb, ^{113m}Cd and ^{154}Eu. The ^{154}Eu represents 1.59% of the total radioactivity of the FP vector. It also generates 2.43 W/g of decay heat (see Table I). However, it has little quantity in the FP vector. With its half-life less than 10 years, this radionuclide will completely decay in a short time. The nuclides ^{93m}Nb and ^{113m}Cd have small contributions to the radioactivity and inventory of the FP vector. They can be stored or disposed at a repository without significant radiotoxicity hazard.

A number of radionuclides (see Table I) have half-lives less than 5 years. This group generally has the highest decay heat contribution to the FP vector. Particularly,

^{125}Sb and ^{134}Cs have specific decay heat of 3.3 W/g and 13.2 W/g respectively. This group of radionuclides is a candidate for decay-only treatment since almost all of each nuclide's radioactivity will be gone in 6 half-lives.

Table I. Fission products in legacy PWR spent fuels.[1]

Nuclide	ID	Half-life (yr)	Decay heat[2] (W/g)	Atom % in Total FP inventory	Radioactivity Contribution (%)
Selenium-79	^{79}Se	290000.	1.36E-6	1.0290	0.0004
Krypton-85	^{85}Kr	10.76	5.34E-1	0.1872	1.8959
Strontium-90	^{90}Sr	28.78	1.42E-1	10.2124	38.6774
Zirconium-93	^{93}Zr	1500000.	2.86E-7	27.1351	0.0020
Niobium-93m	^{93m}Nb	16.10	4.37E-2	0.0002	0.0014
Niobium-94	^{94}Nb	20000.	1.96E-3	0.1809	0.0010
Technetium-99	^{99}Tc	213000.	8.54E-6	23.7119	0.0121
Ruthenium-106	^{106}Ru	1.02	1.98E-1	0.0000	0.0001
Palladium-107	^{107}Pd	6500000.	2.83E-8	6.3315	0.0001
Cadmium-113m	^{113m}Cd	14.10	2.47E-1	0.0025	0.0190
Antimony-125	^{125}Sb	2.76	3.30E+0	0.0011	0.0425
Tin-126	^{126}Sn	230000.	1.31E-5	1.5683	0.0007
Iodine-129	^{129}I	15700000.	8.86E-8	4.2602	0.0000
Cesium-134	^{134}Cs	2.07	1.32E+1	0.0014	0.0720
Cesium-135	^{135}Cs	2300000.	6.10E-7	9.2816	0.0004
Cesium-137	^{137}Cs	30.07	9.67E-2	15.6914	56.8785
Promethium-147	^{147}Pm	2.62	3.40E-1	0.0051	0.2123
Samarium-151	^{151}Sm	90.	3.10E-3	0.2630	0.3185
Europium-154	^{154}Eu	8.59	2.43E+0	0.1256	1.5926
Europium-155	^{155}Eu	4.75	3.57E-1	0.0119	0.2730
Total				**100.0000**	**100.0000**

After assessing all the FP radionuclides in the light of the aforementioned considerations (i.e. half-life, inventory and radioactivity/radiotoxicity), the following nuclides are considered as significant fission product, which would be better eliminated via transmutation: ^{90}Sr, ^{93}Zr, ^{99}Tc, ^{129}I, ^{135}Cs and ^{137}Cs. The properties of these radionuclides will be discussed in following sub-sections.

[1] Data based on spent fuel vectors in Table A-11 of reference no. 24.
[2] Data from www.nucleonica.net

II.B.1 Strontium – 90

Strontium is a naturally occurring alkaline earth metal, which exists in solid phase at standard temperature and pressure. The strontium metal has a density of 2.64g/cc at room temperature with a melting point of 1050 K. The boiling point is at 1655 K. Strontium has a normal oxidation state of +2. Being a metal, it has good thermal conductivity. It is softer than calcium and decomposes water more vigorously. It is a lustrous metal, which tarnishes on exposure to air and can spontaneously combust in air if finely divided into bits. Three allotropes of strontium exist, with transition points at 508 K and 813 K. There 4 naturally occurring isotopes of strontium, which are stable. The existence of 32 other unstable isotopes and isomers is known, the most important of which is ^{90}Sr [26 – 31].

The naturally occurring isotopes are ^{84}Sr, ^{86}Sr, ^{87}Sr and ^{88}Sr. Strontium-90 on the other hand, is radioactive and it is a byproduct of fission reaction in actinides. The fission yield of each isotope varies depending on the splitting actinide, however, in the thermal fission of ^{235}U and ^{239}Pu, ^{90}Sr is about 48% of the total strontium yield. The balance is comprised of varying distributions of ^{86}Sr, ^{87}Sr and ^{88}Sr [32, 33].

In the incineration of strontium isotopes, it is imperative to understand if there would be significant production of ^{90}Sr from lighter isotopes. Table II provides the capture cross sections for some strontium isotopes. The ^{87}Sr thermal neutron and resonance integral capture cross sections are higher than those of the others. This indicates a preferential transformation of ^{87}Sr transmutation target to ^{88}Sr. However, the capture cross sections ^{88}Sr are the smallest of the strontium isotopes. This indicates a limited transformation of ^{88}Sr to ^{89}Sr, which is the neutron link to ^{90}Sr. Moreover,

subsequent transformation of produced ^{89}Sr to ^{90}Sr would not be prominent since ^{89}Sr has small cross sections (see Table II). This indicates that ^{90}Sr buildup from lighter strontium isotopes is unlikely.

Table II. Radiative capture cross section of principal zirconium isotopes.

Nuclide	Thermal neutron capture cross section (b)	Resonance integral capture cross section (b)
^{87}Sr	14.3400	118.5000
^{88}Sr	0.0058	0.0058
^{89}Sr	0.3740	0.4919
^{90}Sr	0.8008	0.4812

The ^{90}Sr isotope is a fairly long-lived high-energy beta emitter with 28.8 year half-life. The energy of the beta emitted is 546 keV. The resultant nuclide is still unstable. The isotope transitions to a stable nuclide after 2 beta decays. The first beta decay creates an Yttrium isotope, ^{90}Y. The ^{90}Y decays to stable ^{90}Zr via the emission of 2.281 MeV beta and associated gamma with energy 2.186 MeV. The half-life of the ^{90}Y is 2.67 days [34].

For transmutation ^{90}Sr, the most important neutron interaction data is the capture cross section of the nuclide. Figure 2 shows the energy dependent capture cross section of ^{90}Sr from both ENDF/B-VI.8 and ENDF/B-VII.0 nuclear data libraries. At energies beyond 10 keV, there is no significant difference between the data from both libraries. However, below 10 keV, there is a difference of about 2 orders on magnitude between the cross sections provided in both libraries. Specifically, the data values from the ENDF/B-VII.0 are lower than those of the earlier evaluations (i.e. ENDF/B-VI.8). The ^{90}Sr ENDF/B-VII.0 data are adapted from Japanese Nuclear Data Committee (JNDC) evaluation of March 1990 [32]. The ENDF/B-VI.8 data were based on Schenter and

Schmittroth's evaluation of April 1974 [33]. Thus it appears that the ENDF/B-VII.0 data for ^{90}Sr is better since it is the more recent evaluation. Moreover, if a conservative result is desired in the transmutation analysis of ^{90}Sr, the evaluation with lower cross section value would be better.

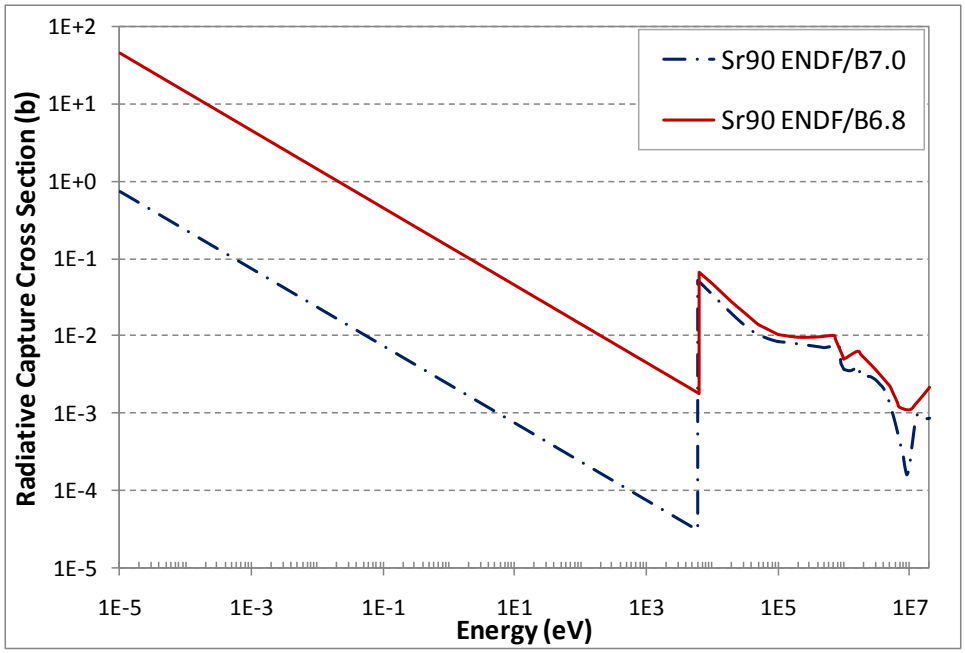

Fig. 2. Energy dependent radiative capture cross sections of ^{90}Sr.

In the consideration of ^{90}Sr transmutation, a practical and reasonable approach will involve the transmutation of the strontium element as a whole. The fission of actinides creates various isotopes of strontium, most of which have half-lives less than 1 day. The isotopes ^{82}Sr, ^{85}Sr and ^{89}Sr have half-lives between 25 and 65 days, which means in about 1 year of decay, these 3 isotopes would no longer be of significance in the fission yield of strontium isotopes. Thus the resultant strontium vector consists of the 4 stable isotopes and ^{90}Sr. Since isotopic separation may neither be economically viable

nor practical for light elements, it is deemed appropriate that transmutation approach should be intended for a strontium target, which consists of the 5 significant isotopes.

Fig. 3 shows the transmutation path of the strontium isotopes. The several combinations of radioactive decay and neutron absorption lead to production of stable nuclides as well as radioactive nuclides. However, most of the radionuclides produced have short half-lives. Thus post irradiation decay of the discharged strontium target would ensure almost complete elimination of the new radionuclides. It should be noted that long lived radionuclides such as ^{93}Zr and ^{99}Tc are 5 proton numbers from strontium isotopes. Hence a protracted irradiation of strontium may very well lead to creation of these long lived nuclides. Since the main goal of the transmutation strategy is the reduction of long lived radionuclides, the creation of ^{93}Zr and ^{99}Tc becomes counterproductive to the objective of the strategy. Based on this hypothesis, the creation of ^{93}Zr and ^{99}Tc becomes a limiting condition for the length of irradiation time of the strontium target.

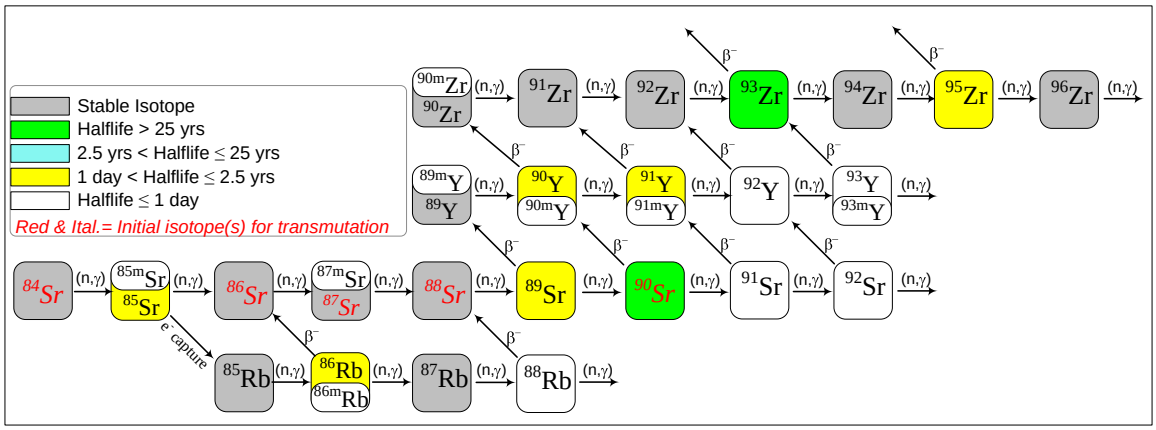

Fig. 3. Transformation path for strontium isotopes in transmutation scenario.

The physical form of the strontium targets is another important consideration. The projected operating temperature in a VHTR system is about 763K at the cold leg and up to 1273K at the hot leg. Strontium metal has a melting point lower than the hot leg temperature. This make strontium metal target impractical. Moreover, strontium reacts with carbon to produce the carbide SrC_2. The chemical interaction can degrade the graphite material in the VHTR core. Pure metals have also been known to undergo physical degradation in a neutron flux environment. Effects such as swelling and creep are the common degradations. Rapid progression of these effects may limit the irradiation time in transmutation scenarios. Thus the preferred target form should be chemically stable and resistant to degradation.

Chemically stable targets include strontium compounds such as the oxide and carbide. Studies on oxide and carbide fuel forms have shown that theses oxides and carbides are more resistant to radiation induced degradations than metals. This may also hold true for targets in form of these compounds. However, it is important to consider the changes in the stoichiometric balance of the resultant compounds as transmutation of the target progresses. Table III shows the elements that are progressively formed from the transmutation of strontium. For each element, the composition stoichiometry of the oxide and carbide are provided. It should be noted that there is progressive increase in the valence of the metals. The effect of this valence change in the oxide form is the requirement of excess oxygen atom as strontium is being transformed to higher Z metals. For example, the ratio of strontium to oxygen in strontium oxide is 1-to-1. Once the strontium is transformed to yttrium or zirconium, the metal-oxygen ratio required for the new oxides becomes 1-to-1.5 or 1-to-2 respectively.

Table III. Compounds of strontium and its derivative elements.

Element (Z)	Valences	Oxides (Melting Point, K)	Carbides (Melting Point, K)
Strontium (38)	2	SrO (2804)	SrC_2 (1973)
Yttrium (39)	3	Y_2O_3 (2712)	YC_2 (2673)
Zirconium (40)	2, 3, 4	ZrO_2 (2983)	ZrC (3805)
Niobium (41)	2, 3, 4, 5	NbO (2210), NbO_2 (2174)	NbC (3881), Nb_2C (3353)
Molybdenum (42)	2, 3, 4, 5, 6	Mo_2O_3, MoO_2 (2073[1])	MoC (2850), Mo_2C (2960)

Note: [1] is the decomposition temperature of the compound.

In order to keep a balanced stoichiometry in the oxide transformation, the representation below becomes plausible:

$$6SrO \xrightarrow{transmutation} 2Y_2O_3 + 2Y_{metal} \xrightarrow{transmutation} 3ZrO_2 + 3Zr_{metal}$$

This transformation chain suggests that the transmutation of strontium oxide target will lead to a combination of oxides and metals in the target as transmutation progresses. If it is undesirable to create metals, then the use of oxide as a target form becomes a limitation. Precipitation of metals as transmutation progresses may be eliminated if a carbide target is considered. This is shown in the transformation below:

$$SrC_2 \xrightarrow{transmutation} YC_2 \xrightarrow{transmutation} ZrC + C_{residue}$$

II.B.2 Zirconium – 93

Zirconium is a naturally occurring element found across the globe. Its principal ore is zirconium silicate – a white powdery mineral. Elemental zirconium is a grayish-white lustrous metal, which has a density of 6.52g/cc at 293 K. Its melting point and boiling point are 2128 K and 4682 K respectively. The element has valences of +2, +3 and +4. It ignites spontaneously in air when finely divided, especially at high temperatures. However, the solid metal does not readily ignite. Zirconium is very

resistant to corrosion by most acids and alkalis, and other corrosive agents. However, it is soluble in hot concentrated acid. Zirconium based materials are particularly bio-friendly since its compounds exhibit low inherent chemical toxicity. Zirconium also has very low neutron absorption cross section, which makes it useful for in-core materials such as cladding and metal fuel alloying in nuclear reactors [26 – 31].

Natural zirconium has 5 isotopes: ^{90}Zr, ^{91}Zr, ^{92}Zr, ^{94}Zr and ^{96}Zr – all of which are stable. There are 31 other isotopes known to exist – all of which are radioactive. The radioactive isotopes are produce from nuclear reactions. The principal isotopes of the radioactive set are ^{93}Zr and ^{95}Zr. In the thermal fission of ^{235}U, these 2 radionuclides represent about 30% of total zirconium yield. This fraction increases to 34% in the thermal fission of ^{239}Pu. The balances of these fractions mainly consist of the stable zirconium isotopes [32, 33].

The ^{95}Zr is somewhat short-lived with half-life of 64 days to produce ^{95}Nb or ^{95m}Nb. It decays with emission of both beta particle and gamma ray with prominent energies of 368 keV and 756.7 keV respectively. Less prominent energies associated with the decay are 400 keV betas and 724.2 keV gammas. The daughter nuclides have shorter half-life than ^{95}Zr. The ^{95m}Nb has a 3.61 day half-live for isomeric transition to ground state. The ground state ^{95}Nb has a beta decay half-life of 35 days. The associated total decay energy is 925.6 keV to produce ^{95}Mo – a stable nuclide. Thus it takes about a net half-life of 100 day for ^{95}Zr to decay to ^{95}Mo. Given that in 6 half-lives, all initial radioactive isotope would have been transformed, this translates to about 2 years for all initial ^{95}Zr to become stable ^{95}Mo [34].

Unlike ^{95}Zr, the ^{93}Zr isotope is very long lived with a half-life of 1.5 million years to produce ^{93m}Nb. The ^{93}Zr emits low beta energy of 60 keV and delayed gamma with energy of 30.8 keV. The delay gamma is emitted in the isomeric transition of ^{93m}Nb to ground state (stable) ^{93}Nb. The isomeric transition has a half-life of 16.1 years [34].

Considering the high yield of ^{93}Zr and its very long half-life, transmutation is the viable way to reduce its inventory. Due to the impracticability of isotopic separation for light elements, the transmutation scheme would have to incorporate the incineration of all zirconium isotopes from fission product stream. Thus it is imperative to understand if there would be significant production of ^{93}Zr from isotopes with lower atomic massed. Table IV provides the capture cross sections for ^{93}Zr and the 5 stable isotopes. The ^{93}Zr thermal neutron capture cross section is higher than those of the other isotopes except ^{91}Zr. In addition, the resonance integral capture cross section for ^{93}Zr is much higher than all other isotopes combined. This suggests a preferential transformation of ^{93}Zr in the zirconium transmutation target. Moreover, the capture cross sections of the isotopes immediately before and immediately after ^{93}Zr are very small in comparison to the ^{93}Zr cross section. This indicates a limited transformation of ^{92}Zr to ^{93}Zr. It also suggests that upon the transformation of the ^{93}Zr isotope to ^{94}Zr, subsequent transformation to isotopes with higher atomic masses would not be as prominent.

Table IV. Radiative capture cross section of principal zirconium isotopes.

Nuclide	Thermal neutron capture cross section (b)	Resonance integral capture cross section (b)
Zr90	0.010	0.20
Zr91	1.200	5.40
Zr92	0.200	0.60
Zr93	1.000	15.00
Zr94	0.050	0.28
Zr96	0.022	5.10

Figure 4 shows the energy-dependent capture cross section of ^{93}Zr from both ENDF/B-VI.8 and ENDF/B-VII.0 nuclear data libraries. At energies beyond 10 keV, there is no significant difference between the data from both libraries. However, between 0.1 keV and 10 keV, ENDF/B-VII.0 data shows a defined resonance absorption region. The capture cross section from ENDF/B-VI.8 within this energy band appears to be a piecewise 1/V profile. Both data libraries have 1/V capture cross sections below 0.1 keV but ENDF/B-VII.0 values are lower than those of ENDF/B-VI.8. The ^{93}Zr ENDF/B-VII.0 data are based on S. Mughabghab's evaluation of March 2005 (for energies less than 6.8 keV) as well as adaptation of Japanese Nuclear Data Committee's JENDL-3.3 evaluation of March 1990 (for energies of 6.8 keV and above) [32]. The ENDF/B-VI.8 data were based on Schenter and Schmittroth's evaluation of April 1974 [33]. The more recent nature of the ENDF/B-VII.0 evaluation for ^{93}Zr indicates a better and more reliable cross section data. More so, if a conservative result is desired in the transmutation analysis of ^{93}Zr, the evaluation with lower cross section value would be better.

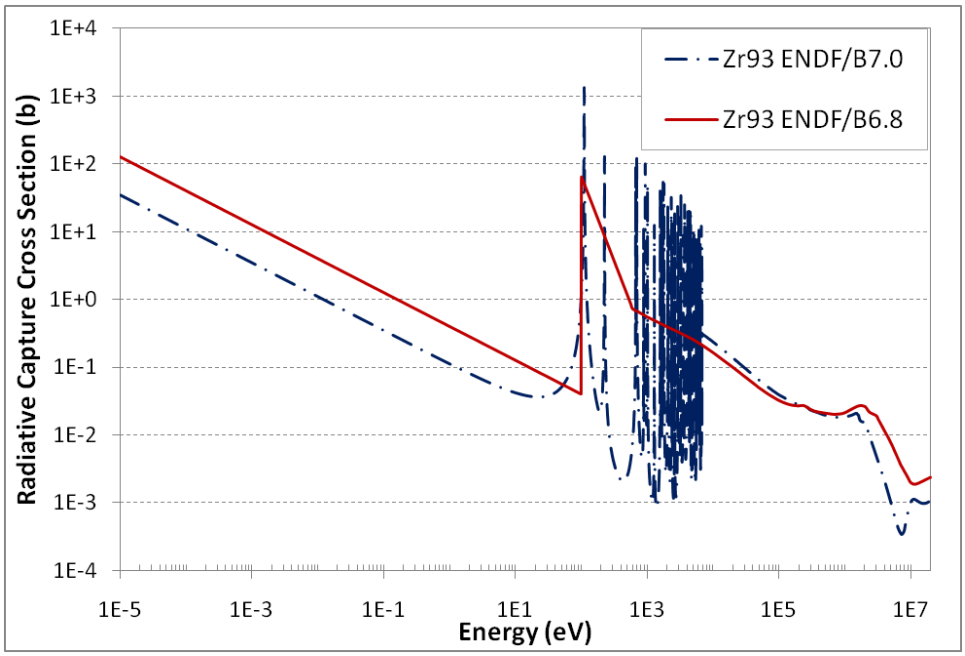

Fig. 4. Energy dependent radiative capture cross sections of ^{93}Zr

In a strategy that involves the transmutation of elemental zirconium, the isotopes to be considered are those with significant yield in the fission product stream. These are the 5 stable isotopes, ^{93}Zr and ^{95}Zr. Since ^{95}Zr is relatively short lived, the other 6 isotopes become the principal nuclides of interest in the transmutation of zirconium. Fig. 5 illustrates the transformation path of the selected zirconium isotopes. Note that only ^{93m}Nb ($T_{1/2}$ = 16.1 yrs), ^{94}Nb ($T_{1/2}$ = 20,000 yrs) and ^{99}Tc ($T_{1/2}$ = 213,000 yrs) have medium to long half-lives. The nuclide ^{93m}Nb has a thermal neutron capture cross section of 0.9 barns [34], which is comparable to that of ^{93}Zr (see Table IV). However, the resonance integral capture cross section of ^{93m}Nb is 6.2 barns [34], which is lower than the same cross section for ^{93}Zr by a factor of approximately 2.5. Thus given the same neutronic conditions, the transmutation of ^{93m}Nb will be slower than that of ^{93}Zr. However, since ^{93m}Nb is only created in the transmutation of zirconium via the beta decay of ^{93}Zr, the accumulation of ^{93m}Nb is unlikely due to the slow decay of ^{93}Zr.

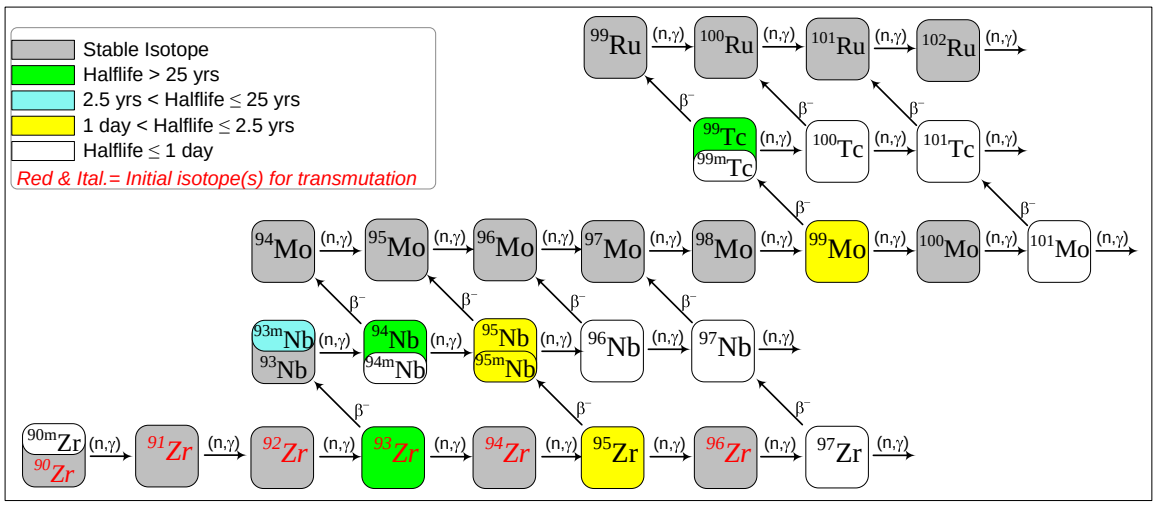

Fig. 5. Transformation path for zirconium isotopes in transmutation scenario.

The transmutation of ^{93m}Nb/^{93}Nb via neutron capture creates ^{94}Nb, which is long lived. The nuclide ^{94}Nb has a thermal neutron capture cross section of 15.4 barns and the resonance integral capture cross section of ^{93m}Nb is 130 barns. These values are significantly greater than those of zirconium isotopes. Thus in the unlikely event of a significant production of this nuclide, it's further transmutation to a short-lived ^{95}Nb is highly probable due to the relatively high capture cross section of ^{94}Nb. This in effect, mitigates the accumulation of ^{94}Nb.

The last of the likely long-lived nuclide that may be generated from the transmutation of zirconium isotopes is ^{99}Tc. There are 2 other elements that could be created before the production of ^{99}Tc. Niobium is the first of these elements, with 2 of its isotopes – ^{93m}Nb and ^{94}Nb – being long-lived. Other isotopes of niobium are rather short-lived and thus would be lost in a few years of post irradiation decay of the zirconium target. The 2nd element is molybdenum. Most of its isotopes that could be created from transmutation of zirconium are stable (see Fig. 5). The radioactive molybdenum isotopes are very short-lived. The nuclide ^{99}Mo – one of the short-lived isotopes – is the possible

parent of ^{99}Tc. It is possible for the ^{99}Tc to be further transmuted (this will be discussed in the next section). However, if a significant quantity of ^{99}Tc is produced, then the possible accumulation of ^{99}Tc over time becomes a limiting factor in the transmutation of ^{93}Zr.

Table V. Compounds of zirconium and its derivative elements.

Element	MP (K)	Valences	Oxides (Melting Pt., K)	Carbides (Melting Pt., K)
Zirconium (40)	2128	2, 3, 4	ZrO_2 (2983)	ZrC (3805)
Niobium (41)	2750	2, 3, 4, 5	NbO (2210), NbO_2 (2174)	NbC (3881), Nb_2C (3353)
Molybdenum (42)	2896	2, 3, 4, 5, 6	Mo_2O_3, MoO_2 (2073[1])	MoC (2850), Mo_2C (2960)
Technetium (43)	2430			
Ruthenium (44)	2606	3, 4, 6, 8	RuO_2 (1573[3]), RuO_4 (298)	RuC

Note: [1] is the decomposition temperature of the compound.

In the transmutation of zirconium, the physical form of the target is an important factor. The target has to withstand the operating temperature and other conditions in the reactor for the transmutation strategy to be practicable. The target may be zirconium metal/alloys or compounds of zirconium that are heat resistant and chemically stable. The melting points of zirconium metal, oxide and carbide are given in Table V. These temperatures are higher than the peak temperature in a VHTR system. Thus, there is the possibility of the target being in any of the 3 forms. The Table also provides the elements that are progressively generated from the transmutation of zirconium. For each element, the composition stoichiometries of the oxide and carbide – as well as the melting point of each compound – are provided. As described in the section dealing with strontium, stoichiometric compositions may play significant role in the choice of target forms. The possible stoichiometric changes in the early transformation of zirconium oxide are given below:

$$4ZrO_2 \xrightarrow{transmutation} \begin{bmatrix} & 4NbO_2 \\ & \\ 2O_2 + 4NbO & \end{bmatrix} \xrightarrow{transmutation} \begin{bmatrix} 4MoO_2 & \\ & \\ 2Mo_2O_3 + O_2 & \end{bmatrix}$$

The production of niobium in the target may lead to release of oxygen molecule if niobium (II) oxide is preferentially created. On the other hand, there is no oxygen release in the creation of niobium (IV) oxide. Further transformation of both niobium oxides may create molybdenum (III) oxide, which also comes with liberation of excess oxygen. However, the creation of molybdenum (IV) oxide completely mitigates the generation of oxygen.

The determination of the preferred stoichiometric path in the transmutation process is a difficult proposition – a topic of special interest and research on its own. Nonetheless, the liberation of oxygen in a VHTR core is a safety concern since spontaneous combustion of the graphite material can ensue. Thus, it suffices to conclude that whatever stoichiometric path is dominant will affect the safety feature that would be necessary in the implementation of the transmutation strategy involving zirconium oxide target.

Also, given the high temperatures attainable in the VHTR, a zirconium oxide target may lead to the creation of zirconium carbide. Zirconium carbide can be produced through carbothermal reduction of zirconium (IV) oxide in the presence of graphite dust/powder [35, 36]. Carbon dioxide – which results from the combustion of oxygen from the zirconium oxide with the graphite – is a byproduct of this reaction. The main concern with possibility of this reaction is the degradation of the structural graphite in the reactor core. Thus is also a safety concern that should be investigated in the implementation of in-core transmutation of the zirconium stream of the fission products.

The possible stoichiometric changes in the early transformation of zirconium carbide are given below:

$$2ZrC \xrightarrow{transmutation} \begin{bmatrix} 2NbC \\ \\ C_{residue} + Nb_2C \end{bmatrix} \xrightarrow{transmutation} \begin{bmatrix} 2MoC \\ \\ Mo_2C + C_{residue} \end{bmatrix}$$

The production of carbon residue from a carbide target is not a significant issue in the transmutation scheme. However, the transport of the residue within the reactor core may result in other system issues. For example, residues that may be transported through the coolant may cause damage to heat exchangers and/or energy conversion components of the reactor system. Thus, such residue may have to be contained within the location of the target.

A good containment of residues can be achieved by encapsulating the zirconium target. Encapsulation would also work well in the case of metal/alloy target. Zirconium metal (particularly when finely divided) at elevated temperatures ignites in the presences of graphite dust to form zirconium carbide [35]. In a severe case, run-away ignition of zirconium target in graphite may result. This is a potential mechanism for the degradation of structural graphite over time. In order to prevent this reaction, a capsule preventing direct contact between the metal and graphite is required. Such capsule may be made from refractory materials such as zirconium carbide.

II.B.3 Technetium – 99

The element technetium is not known to occur naturally on earth. It is artificially produced in reactors as part of the fission product streams. Elemental technetium is a silvery-gray metal, which has a density of 11.5g/cc at 293 K. Its melting point and

boiling point are 2430 K and 4538 K respectively. The chemistry of technetium is similar to that of rhenium. Which has multiple valences from -1 to +7 [37]. It tarnishes slowly in moist air. It dissolves in nitric acid, aqua regia and concentrated sulfuric acid, but it is insoluble in hydrochloric acid.

There are 43 isotopes and isomers known to exist. The atomic masses range from 86 to 114. All of the isotopes and isomers are radioactive. The principal isotopes are shown in Table VI with their respective half-lives and decay/radiation modes. All other isotopes and isomers have half-lives less than 1 day. Three of these isotopes – ^{97}Tc, ^{98}Tc and ^{99}Tc – are very long lived. However, in the fission of uranium and transuranics, the production of ^{99}Tc is almost 100% yield of the technetium stream in fission products. The production of ^{97}Tc, ^{98}Tc and other isotopes of technetium is very small to the extent that they are nonexistent in fission product vector [32, 33].

Table VI. Principal isotopes of technetium and their decay modes.

Nuclide	Half-life	Decay type/ Radiation
Tc95m	61 days	electron capture, γ, isomeric transition, β^+
Tc96	4.3 days	electron capture, γ
Tc97m	91 days	isomeric transition, conversion electron, electron capture
Tc97	2,600,000 years	electron capture
Tc98	4,200,000 years	β^+, γ,
Tc99[1]	213,000 years	β^-

Note: [1] has gamma ray signature of 89.7 keV, however, it has an abundance of less than 0.001%.

The ^{99}Tc has a half-life of 213 thousand years. It decays with emission of beta particle of energy 294 keV. The daughter nuclide is ^{99}Ru, which is a stable nuclide [34]. The long half-life of ^{99}Tc implies that it will take a few million years before all initial inventories will transform to a stable nuclide. The isotope has a specific activity of

6.25×10^6 Bq/g. With the annual limit of intake for inhalation being 1.54×10^6 Bq [38], 1 gram of ^{99}Tc will pose a radiotoxicity hazard over a period of 4 times its half-live. Hence this activity level should be contained in other to prevent contamination hazard.

The isotope ^{99}Tc has a high yield in the fission product vector from LWR (see Table I). Thus it is a very suitable candidate for a transmutation scheme that will reduce its inventory. The capture cross section of the isotope from both ENDF/B-VI.8 and ENDF/B-VII.0 nuclear data libraries is plotted in Figure 6. The data from ENDF/B-VI.8 are based on the August 1999 evaluation by J. Chang (KAERI), S. Mughabghab (BNL) and R. Schenter (BNL) [33]. The ENDF/B-VII.0 data are based on the May 2006 evaluations by BNL's D. Rochman, M. W. Herman, P. Oblozinsky, S. Mughabghab and T. Kawano (LANL) [32]. The data from both libraries are virtually the same except in the resonance region. The ENDF/B-VI.8 have unresolved resonances at energies greater than 1 keV. In the ENDF/B-VII.0 data, all resonances below 6.37 keV are resolved. The unresolved resonances are from 6.37 keV to 141 keV. Both data libraries should give similar result especially if the resonance integral valuation between 6.37 keV and 141 keV are similar for both libraries.

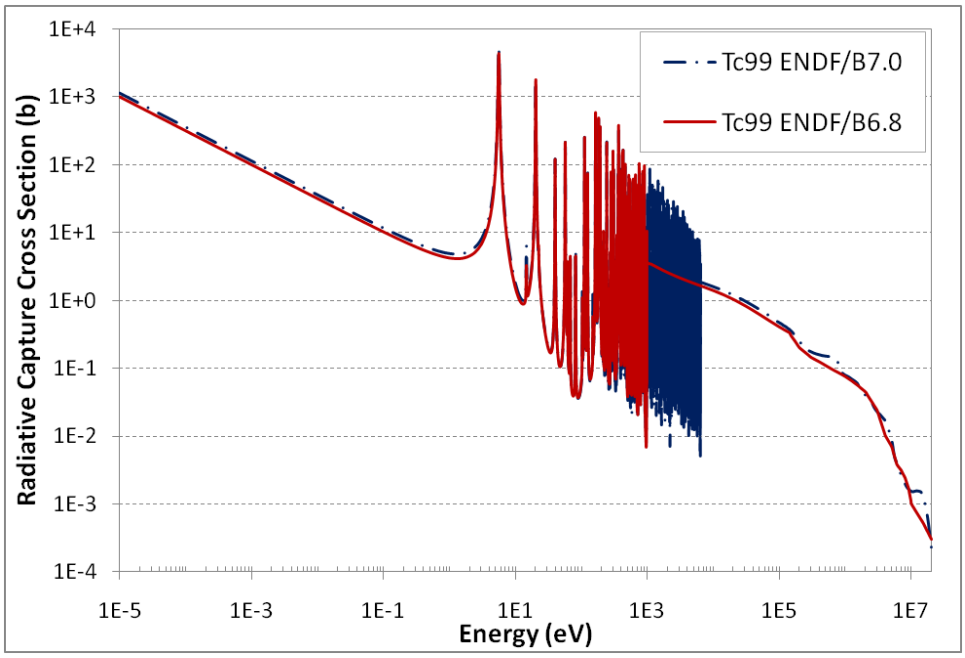

Fig. 6. Energy dependent radiative capture cross sections of ^{99}Tc

Figure 7 shows the transmutation path of ^{99}Tc. A neutron capture in the isotope results in the creation of ^{100}Tc, which has a half-life of 15.8 seconds and decays to ^{100}Ru – a stable isotope of ruthenium. Subsequent transmutation of ^{100}Ru produces another stable nuclide. The progressive transmutation of nuclides being created generally leads to either a stable nuclide or very short-lived radio nuclide, with the exception of ^{107}Pd and ^{108m}Ag. The palladium isotope ^{107}Pd has a half-life of 6.5 million years. It has a specific activity of 1.9×10^{7} Bq/g, which is greater than that of ^{99}Tc, and an annual limit of intake for inhalation of 3.4×10^{7} Bq [38]. This suggests that ^{107}Pd poses higher radiotoxicity hazard than similar quantity of ^{99}Tc. The high radiotoxicity value for ^{107}Pd coupled with its long half-life makes its production a limiting factor in the transmutation of ^{99}Tc. Likewise, the production of ^{108m}Ag becomes a limitation since the nuclide has a half life of 418 years and specific activity of 2.93×10^{11} Bq/g.

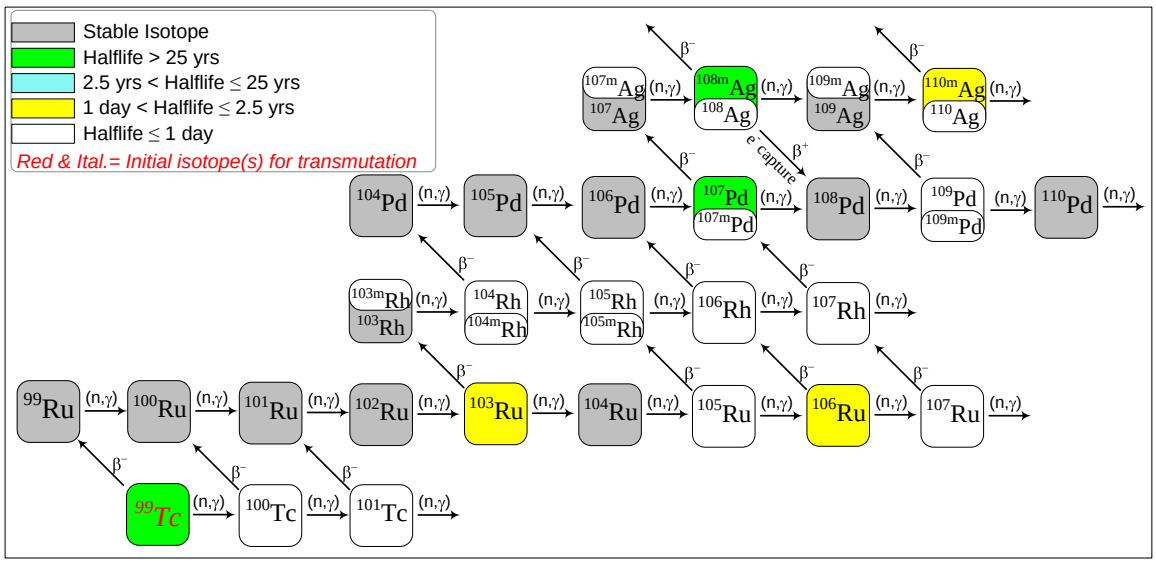

Fig. 7. Transformation path for technetium-99 in transmutation scenario.

The physical form of a technetium target is expected to withstand the conditions within a transmutation reactor. Not many compounds of technetium are known since it does not exist naturally. Moreover, the several oxidation states of technetium may make the stoichiometry of its compounds fluctuate under transmutation scenario. Thus it may be more practical to have a technetium metal or alloy target. Table VII provides the possible derivative elements of technetium in transmutation scenario. The melting point of each metal is higher than the operating temperature of the VHTR with the exception of silver. Since the production of silver may occur in the protracted irradiation of technetium target, it would be important to prevent the circulation of molten metal in the reactor core. An encapsulated target would provide containment for the target and mitigate possible transport of molten metal.

Table VII. Technetium and its derivative elements.

Element	Valences	Melting point (K)
Technetium (43)	-1 to 7	2430
Ruthenium (44)	3, 4, 6, 8	2606
Rhodium (45)	3, 4, 6	2237
Palladium (46)	2	1828
Silver (47)	1, 2	1235

II.B.4 Iodine – 129

Iodine is a halogen which occurs sparingly in nature. Its natural forms are iodides from sea water, saltpeter and brines. Iodine is less reactive than other halogen. Hence it is easily displaced from its compound by the other halogens. Pure iodine is a bluish-black lustrous solid with a melting point of 387 K. Although iodine is known to sublime at its melting point, under the right conditions, liquid iodine can be formed. The liquid iodine has a boiling point of 457 K. Iodine has a density of 4.93g/cc in solid phase at 293 K, while the density of iodine gas is 1.127×10^{-2}g/cc. It has oxidation states of +1, +3, +5 and +7. Many of its compounds have low melting point and/or decomposition temperature. There are 42 known isotopes and isomers. However, only 1 stable isotope exists. The radioactive isotopes ^{125}I and ^{129}I are the most significant of the other known isotopes [26 – 31].

Table VIII provides the principal isotopes of iodine. Aside from the 5 isotopes on the Table, every other isotope has half-life less than 1 day. The isotope ^{127}I is the stable, naturally occurring isotope. Other isotopes are byproducts from fission reaction of actinides. The yield of each iodine isotopes varies with the actinide fissioned. However, ^{127}I and ^{129}I are the remaining isotopes of iodine present in the fission product stream. This is due to the stability and ultra-long half-life of the isotopes respectively. Other

principal isotopes are essentially lost within a short period through radioactive decay. The longest lived of these other isotopes is ^{125}I, which has a half-life of 59.4 days. The ^{125}I decays through electron capture to produce ^{125}Te – a stable nuclide. This decay of ^{125}I is accompanied by gamma of energy 35.5 keV. The combination of its short half-life and low energy gamma makes it useful in bioassays and radiation therapy. The isotope has very negligible yield from direct fission of actinides. The combination of its low yield from fission and short half life makes it almost nonexistent in the iodine stream of fission products.

Table VIII. Principal isotopes of iodine and their decay modes.

Nuclide	Half-life	Decay type/ Radiation
I124	4.18 days	electron capture, β^+, γ
I125	59.40 days	electron capture, γ, conversion electron
I126	13.00 days	electron capture, β^-, γ, β^+
I127	Stable	none
I129	15,700,000 years	β^-, γ
I131	8.02 days	β^-, γ

Given that the iodine stream of fission products effectively consists of one radioactive isotope, ^{129}I; which happens to be very long-lived, a transmutation of the isotope becomes strategic in the reduction of its inventory. The ^{129}I decays with a 150 keV beta and associated low energy gamma of 39.6 keV. The daughter nuclide is ^{129}Xe, which is a stable nuclide. It is also possible for ^{129}I decay to result in the creation of ^{129m}Xe. The ^{129m}Xe with 8.9 day half-life undergoes isomeric transition to ground state ^{129}Xe with decay energy of 236 keV [34]. The long half-life of ^{129}I makes the transformation via decay a less desirable means to achieve stability of the nuclide. Thus a transformation induced by neutron capture promises a faster means to achieve stability.

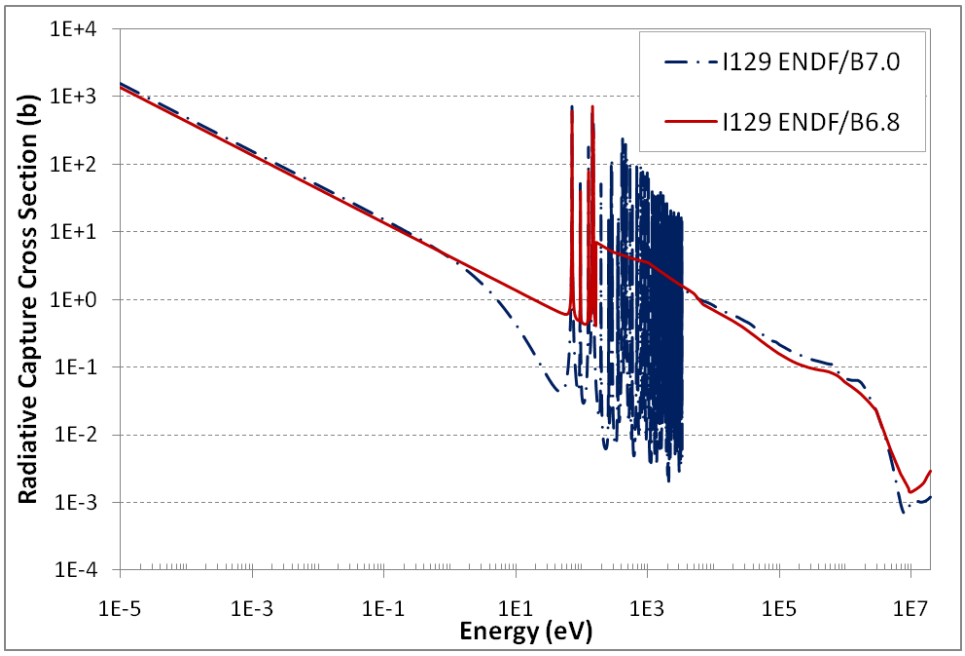

Fig. 8. Energy dependent radiative capture cross sections of ^{129}I

Figure 8 shows the energy dependent capture cross section of ^{129}I from ENDF/B-VI.8 and ENDF/B-VII.0 nuclear data libraries. The ENDF/B-VII.0 data are adapted from the January 2005 evaluations by BNL's S. Mughabghab and JNDC. The cross sections for energies below 3.4 keV are obtained from BNL's evaluation. The cross sections for other energies were adopted for JNDC's JENDL-3.3 data files [32]. The ENDF/B-VI.8 data were based on Schenter and Schmittroth's evaluation of February 1980 [33]. It should be noted that the capture cross sections from both ENDF data libraries are similar except within the energy band of 10 eV to 3.4 keV – a resonance region. The ENDF/B-VII.0 library has resolved resonance data within this range, unlike the ENDF/B-VI.8 library, which has its unresolved resonance data starting at 170 eV. In addition, the evaluation of the resolved resonance in ENDF/B-VI.8 library is quite different from the evaluations in ENDF/B-VII.0 for the same energy range. This is apparently due to the

more recent evaluations in ENDF/B-VII.0 library. It should also be noted that both data libraries have unresolved resonance data between 3.4 keV and 100 keV. However, the evaluated data for this energy band are similar for both libraries. Hence if either library is used in the analysis of ^{129}I transmutation, the difference in results would be attributable to the valuation differences within the 10 eV to 3.4 keV energy band. In addition, the results from an analysis involving the use of ENDF/B-VII.0 data would be more accurate since it would be based on a more recent evaluated nuclear data.

Figure 9 shows the transformation path for iodine isotopes. In the transmutation of ^{129}I, a neutron capture in the isotope creates ^{130}I, which has a half-life of 12.4 hours. The daughter nuclide undergoes beta decay to produce ^{130}Xe – a stable nuclide. Since a practical transmutation scheme would involve the transformation of the other iodine isotope in fission product vector, the transmutation path of ^{127}I is equally important. A neutron capture in ^{127}I would produce ^{128}I, which has a half-life of 25 minutes. The ^{128}I isotope could either undergo beta decay to produce stable nuclide ^{128}Xe or a positron decay, which creates another stable nuclide ^{128}Te. The production of ^{129}I from neutron capture in ^{128}I is possible. However, the buildup of ^{129}I from this reaction is unlikely due to the very short half-life of ^{128}I. Further irradiation of the iodine isotopes will result in the production of a combination of several stable, short-lived and a couple of long-lived nuclides (see Fig. 9). The short-lived nuclides are easily lost by radioactive decay over a short time. However, the long-lived nuclides – possibly ^{135}Cs and ^{137}Cs – could become limiting factors in the transmutation scheme.

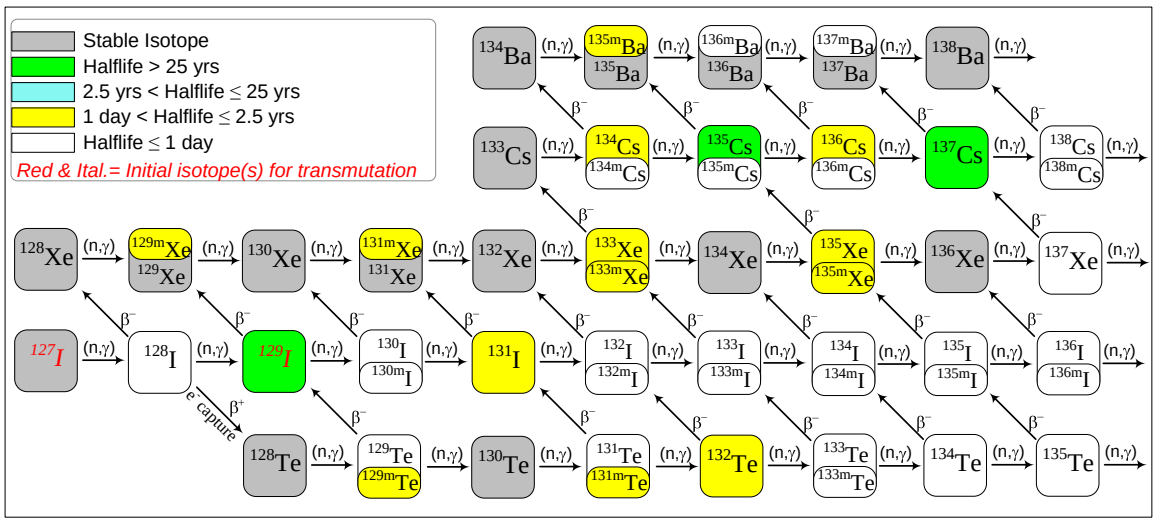

Fig. 9. Transformation path for iodine isotopes in transmutation scenario.

The transmutation of iodine poses a difficult challenge from the view point of its target form as well as the possible changes in the physical form of the target during irradiation. Iodine in its elemental form is unlikely to be a suitable target form due to its low melting point. Elemental (free) iodine is volatile enough to become airborne. Also, the mobility of iodine is enhanced if the free element makes contact with moisture since iodine is slightly soluble in water. Thus the transmutation of iodine in its elemental form is impractical. The only other form iodine target can take would be in a stable compound form.

The compounds of iodine exist in the following forms: iodine oxides, iodine halides, iodates and iodides. All known oxides and halides of iodide have melting points below 450 K or decompose at temperatures below 600 K. These temperatures are very much below the operating temperatures expected in a VHTR system. This makes the oxides and halides unsuitable target forms in the transmutation of iodine. Also, the iodates are unsuitable target forms for similar reasons as the oxides and halides. All know iodates either melt or decompose at temperatures below 860 K. Moreover, iodates

are oxygen-rich [30]. The decomposition of iodates could result in the liberation of oxygen from the target, creating an opportunity for graphite combustion in the VHTR core – a safety concern. Iodides on the other hand have melting points and decomposition temperatures that vary over a wide temperature range. For example: hydrogen iodide becomes gas at 237 K, gold (III) iodide decomposes at 293 K, boron tri-iodide melts at 323 K, and thulium (III) iodide melts at 1294 K. Thus, iodine transmutation targets should be an iodide.

A number of iodides with melting points greater than 950 K are known. Table IX provides a list of some iodides with melting points sufficiently high to be considered as target forms in a VHTR based transmutation scheme. The iodides of americium, plutonium and uranium have melting points above 1000 K. The elements required for the formation of these iodides are available in the spent fuel vector. Thus the availability of materials for the fabrication of such target makes the actinide based iodide a practical option. However, the main drawback for the actinide based iodides is the creation of higher actinides as transmutation progresses. Higher actinides are generally long-lived and are more radiotoxic than the fission products intended for transmutation. Thus the use of actinide based iodide in the transmutation of ^{129}I could worsen the radiotoxicity of the initial transmutation target. In addition, fission of actinides in the target could create undesirable localized perturbation in the reactor core. This could distort power profiles and create safety issues as transmutation progress.

Table IX. Selected iodides and their properties.

Iodide, Formula	MP (K)	Density (g/cc)	Remark
Americium (III) iodide, AmI_3	1223	6.9	Actinide based
Barium iodide, BaI_2	984	5.15	Alkali earth metal based
Calcium iodide, CaI_2	1056	3.96	Alkali earth metal based
Cerium (II) iodide, CeI_2	1081		Lanthanide based
Chromium (II) iodide, CrI_2	1140	5.1	Light element based; Soluble in H_2O
Dysprosium (III) iodide, DyI_3	1251		Lanthanide based
Erbium (III) iodide, ErI_3	1287	5.5	Lanthanide based; Soluble in H_2O
Gadolinium (II) iodide, GdI_2	1104		Lanthanide based
Gadolinium (III) iodide, GdI_3	1203		Lanthanide based
Holmium (III) iodide, HoI_3	1267	5.4	Lanthanide based
Lutetium (III) iodide, LuI_3	1323	5.6	Lanthanide based; Very soluble in H_2O
Molybdenum (III) iodide, MoI_3	1200		Light element based; Insoluble in H_2O
Neodymium (III) iodide, NdI_3	1060	5.85	Lanthanide based; Soluble in H_2O
Nickel (II) iodide, NiI_2	1073	5.22	Light element based; Sublimes at MP
Plutonium (III) iodide, PuI_3	1050	6.92	Actinide based; Soluble in H_2O
Praseodymium (III) iodide, PrI_3	1011	5.8	Lanthanide based; Soluble in H_2O
Praseodymium (II) iodide, PrI_2	1031		Lanthanide based
Samarium (III) iodide, SmI_3	1123		Lanthanide based; Reacts with H_2O
Terbium (III) iodide, TbI_3	1228	5.2	Lanthanide based; Soluble in H_2O
Thulium (III) iodide, TmI_3	1294		Lanthanide based
Thulium (II) iodide, TMI_2	1029		Lanthanide based; Reacts with H_2O
Tungsten (II) iodide, WI_2	1073	6.79	Insoluble in H_2O; Decomposes at MP
Uranium (III) iodide, UI_3	1039		Actinide based; Soluble in H_2O
Ytterbium (II) iodide, YbI_2	1045		Lanthanide based; Reacts with H_2O
Ytterbium (III) iodide, YbI_3	973		Soluble in H_2O; Decomposes at MP
Yttrium iodide, YI_3	1270		Soluble in H_2O
Zirconium (II) iodide, ZrI_2	1100		Light element based
Zirconium (III) iodide, ZrI_3	1000		Light element based

Most of the other iodides with sufficiently high melting point are lanthanide based (see Table IX). The iodides of dysprosium, erbium, gadolinium, holmium, lutetium, terbium and thulium have melting points higher than 1200 K. This makes the lanthanide iodides attractive as target form for iodine transmutation. However, the key drawback for the use of these lanthanides in the target form is their inherent high thermal neutron capture cross section. There could be preferential absorption in the lanthanide atoms since they generally have higher neutron capture cross section than the iodine atoms. In

addition, the neutron capture induced transformation of a lanthanide nuclide usually results in the creation of another lanthanide, which has different neutron absorption cross section. The continual transformation of one lanthanide to another could lead to fluctuating power profile in the core. Moreover, the presence of the lanthanides in iodine target could lead to excessive localized neutron absorption, which would have an adverse effect on the neutron economy in the reactor core.

The rest of the iodides listed on Table IX are alkali earth metal and light element based. These are the iodides of barium, calcium, chromium, nickel, molybdenum and zirconium. All of these iodides have melting points above 1000 K except barium iodide. The light element based iodides, which include chromium, nickel, molybdenum and zirconium iodides are promising target forms. Zirconium and molybdenum have very small thermal neutron capture cross section, which is a desirable property for the reduction of parasitic absorption in targets. However, there is the likelihood of the production of ^{93}Zr and ^{99}Tc in the protracted irradiation of zirconium and molybdenum.

Chromium and nickel equally have small thermal neutron capture compared to iodine. There is a possibility of creating long lived radionuclides from the transmutation of these metals. Chromium could lead to the creation of ^{53}Mn from the possible transformation path below:

$$^{50}Cr \xrightarrow{n,\gamma} {}^{51}Cr \xrightarrow{\beta\ decay} {}^{51}Mn \xrightarrow{n,\gamma} {}^{52}Mn \xrightarrow{n,\gamma} {}^{53}Mn$$

The nuclide ^{53}Mn has a half-life of 3.7 million years. It should be noted that ^{50}Cr is 4.35 atom% of the naturally existing chromium isotopes. Thus the quantity of the nuclides preceding ^{53}Mn would be less abundant. In addition, ^{51}Mn and ^{52}Mn are radionuclides with half-lives 46.2 minutes and 5.6 days respectively. Hence it unlikely that ^{53}Mn

would be created in significant quantity since the transformation of ^{51}Mn and ^{52}Mn would be dominated by radioactive decay.

Similarly, a transformation of nickel could produce ^{59}Ni and ^{63}Ni, with half-life 76 thousand years and 101 years respectively. The transformation paths are shown below:

$$^{58}Ni \xrightarrow{n,\gamma} {}^{59}Ni \ and; \ {}^{62}Ni \xrightarrow{n,\gamma} {}^{63}Ni$$

The nuclides ^{58}Ni and ^{62}Ni have abundances of 68.08 atom% and 3.63 atom% respectively. Thus, given the predominant abundance of ^{58}Ni, the production of ^{59}Ni would be the main concern in a transmutation scheme involving the use of nickel iodide as ^{129}I target.

Calcium iodide is also a possible target form for the transmutation of ^{129}I. Calcium has a small thermal neutron capture cross section. The calcium iodide is particularly suitable as target due to the stability of several calcium isotopes. Naturally occurring calcium has 6 stable isotopes. At 96.9 atom%, ^{40}Ca is the most abundant of the stable isotopes. It also has the lowest atomic mass of the stable isotopes. Hence, progressive transformation of ^{40}Ca to other isotopes of calcium will result in few radioactive calcium isotopes. In addition, other elements that may be produced in short time period from the irradiation of calcium do not have very long lived isotopes. The closest possible long-lived nuclide that may result from the transformation path of calcium isotopes is ^{53}Mn – a nuclide which is 5 proton numbers away from calcium. Given the short life of the precursors to ^{53}Mn, it is unlikely that any significant quantities of the radionuclide will be produced.

All the possible iodide targets discussed have to be considered under another constraint: the nature of the target after the transmutation of iodine. The transformation of iodine isotopes results in the creation of xenon, which is an inert gas. Thus, the other element of the iodide would revert to its elemental state. Hence, it is important that whatever residual element exists in the target should withstand the conditions in the transmutation reactor core. In addition, the derived elements from the transmutation of the target's residual element should also be able to withstand the reactor operating conditions. For example, calcium is the residual element in the transformation of iodine in calcium iodide. Calcium in itself has a melting point and boiling point of 1115 K and 1757 K respectively. The residual calcium may be transmuted in ascending order of proton number to scandium, titanium, vanadium, chromium, manganese, iron and so on. Each of these elements has melting point greater than 1500 K. Thus they should be able to keep a solid form under normal operating condition in a VHTR.

II.B.5 Cesium – 135 and 137

Cesium is a naturally occurring silvery-white metal. One of its main sources is pollucite – a hydrated silicate of aluminum, cesium and sodium. Cesium metal is soft, ductile and has a density of 1.873g/cc at 293 K. Its melting point and boiling point are 302 K and 944 K respectively. It has a normal oxidation state of +1. Cesium is very electropositive and has a great affinity for oxygen. It reacts explosively with water. It also reacts with ice at temperatures above 157 K. There are 52 known isotopes and isomers of cesium, with atomic masses ranging from 112 to 148 [26–31].

The only naturally occurring isotope is ^{133}Cs, which is stable. Other isotopes and isomers are byproducts of fission reactions of actinides. The principal isotopes from fission are ^{131}Cs, ^{132}Cs, ^{133}Cs, ^{134}Cs, ^{135}Cs and ^{137}Cs. Table X provides decay information for the principal isotopes. In addition to the stable isotope, 3 isotopes have decay half-lives of a few days and 3 other isotopes have half-lives greater than 2 years. The isotopes with half-lives in the order of few days would not pose a long term radiotoxicity threat. Of the other 3 radioactive isotopes, ^{134}Cs has a half-life of 2.065 years. It decays to stable ^{134}Ba via beta and gamma radiations of energies 658 keV and 1.401 MeV respectively. It could also transform to stable ^{134}Xe via electron capture with associated energy of 1.229 MeV. Thus while ^{134}Cs does not pose a long term radiotoxicity threat, its high decay energies indicate near term radioactivity concern. The remaining 2 isotopes are ^{135}Cs and ^{137}Cs, which have half-lives of 2.3 million years and 30.07 years respectively. These isotopes are the main long term radiotoxicity concern from the cesium radionuclides.

Table X. Principal isotopes of cesium and their decay modes.

Nuclide	**Half-life**	**Decay type/ Radiation**
Cs131	9.69 days	Electron capture
Cs132	6.48 days	Electron capture, β^+, γ, β^-
Cs133	stable	None
Cs134	2.065 years	β^-, γ, electron capture
Cs135	2,300,000 years	β^-
Cs136	13.16 days	β^-, γ
Cs137	30.07 years	β^-, γ

The isotope ^{135}Cs is a very long lived beta-only emitter. It constitutes 9.28 atom% of the legacy spent fuel fission product content (see Table I). It decays with beta energy of 210 keV to stable nuclide ^{135}Ba. It is not a significant source of decay heat due to its

low specific heat of 6.1×10^{-7} W/g. In addition, its annual limit of intake for inhalation and ingestion are 2.33×10^{6} Bq and 1.00×10^{7} Bq respectively [38]. With its specific activity at 4.26×10^{7} Bq/g, it takes more than a few grams to exceed the annual limits of intake. Thus while ^{135}Cs is not as radiotoxic as other significant nuclides of the fission product vector, its long half-life and significant yield make its transformation via decay a less desirable means to achieve a stable nuclide.

On the other hand, ^{137}Cs has a medium-term half-life. It decays to stable ^{137}Ba through the emission of 514 keV betas and 662 keV gammas. It has a specific activity of 3.22×10^{12} Bq/g. It takes a few micrograms of ^{137}Cs to exceed its annual limit of intake for inhalation and ingestion, which are 5.13×10^{5} Bq and 1.54×10^{6} Bq respectively [38]. Its high intensity is evident in legacy spent fuel where it accounts for 56.9% of the radioactivity of the fission product vector (see Table I). The high radioactivity impact of this nuclide makes it a prime candidate for transmutation.

Figure 10 shows the radiative capture cross section profile for ^{135}Cs and ^{137}Cs from both ENDF/B-VI.8 and ENDF/B-VII.0 libraries. For ^{135}Cs, the ENDF/B-VII.0 data are based on the January 2005 evaluations by BNL and JNDC. The cross sections for energies below 220 eV are obtained from BNL's evaluation. The cross sections for other energies were adopted for JNDC's JENDL-3.3 data files [32]. The ENDF/B-VI.8 data were based on Wright and Schenter's evaluation of August 1998 [33]. The ^{135}Cs radiative capture cross sections from both ENDF data libraries are similar except within the resonance energy region of 0.2 eV to 100 keV. The ENDF/B-VII.0 library has unresolved resonance data between 220 eV and 100 keV. This is similar to the ENDF/B-VI.8 unresolved resonance, which starts at 210 eV. The resolved resonance data as well

as the capture cross section in thermal and fast energies are almost identical in both ENDF/B-VI.8 and ENDF/B-VII.0 libraries. Thus similar results are expected from the use of both libraries in the analysis of ^{135}Cs transmutation.

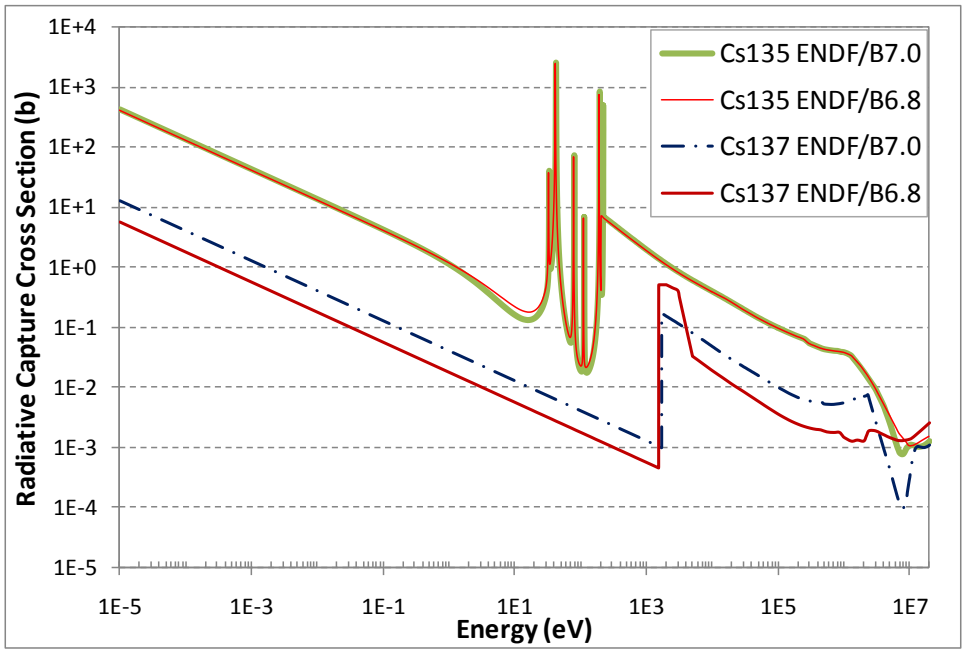

Fig. 10. Energy dependent radiative capture cross sections of ^{135}Cs & ^{137}Cs

The ENDF/B-VII.0 data for ^{137}Cs are based on the March 1990 evaluations by JNDC, while the ENDF/B-VI.8 data are based on Schenter and Schmittroth's evaluation of April 1974. At energies below 1.7 keV, both data libraries have the ^{137}Cs cross sections in the form if 1/V. Beyond 1.7 keV, the libraries have cross sections derived from different modeling methods. Overall, the evaluations in each library are different from the other. The ^{137}Cs cross sections in ENDF/B-VII.0 are greater than the ENDF/B-VI.8 cross sections. While the ENDF/B-VII.0 evaluations are more recent, the ENDF/B-VI.8 evaluations would be more conservative in the transmutation analysis of ^{137}Cs.

Considering the notion that isotopic separation of fission product nuclides is impractical, it is important to evaluate the possibility of transforming ^{135}Cs to ^{137}Cs in a scheme involving the transmutation of cesium element. Table XI provides the capture cross sections for the principal isotopes of cesium. The combined thermal and resonance capture of neutrons in stable ^{133}Cs could create radioactive ^{134}Cs, which has a relatively high thermal capture cross section compared with other isotopes of cesium. Thus it is possible to produce additional ^{135}Cs from the stable isotope. Furthermore, ^{135}Cs can be transformed to ^{136}Cs, which has a half-life of about 13 days and significantly smaller capture cross section than ^{135}Cs. Hence it is expected that the further transmutation of ^{136}Cs would be dominated by beta decay to stable ^{136}Ba. This indicates that subsequent transformation of ^{136}Cs to ^{137}Cs would not be as prominent. The significance of this chain of reactions will be evaluated as part of the cesium transmutation analysis in later chapter.

Table XI. Radiative capture cross sections of principal cesium isotopes.

Nuclide	Thermal neutron capture cross section (b)	Resonance integral capture cross section (b)
Cs133	29.60	421.0
Cs134	140.00	60.0
Cs135	8.70	90.0
Cs136	1.31	39.8
Cs137	0.25	0.4

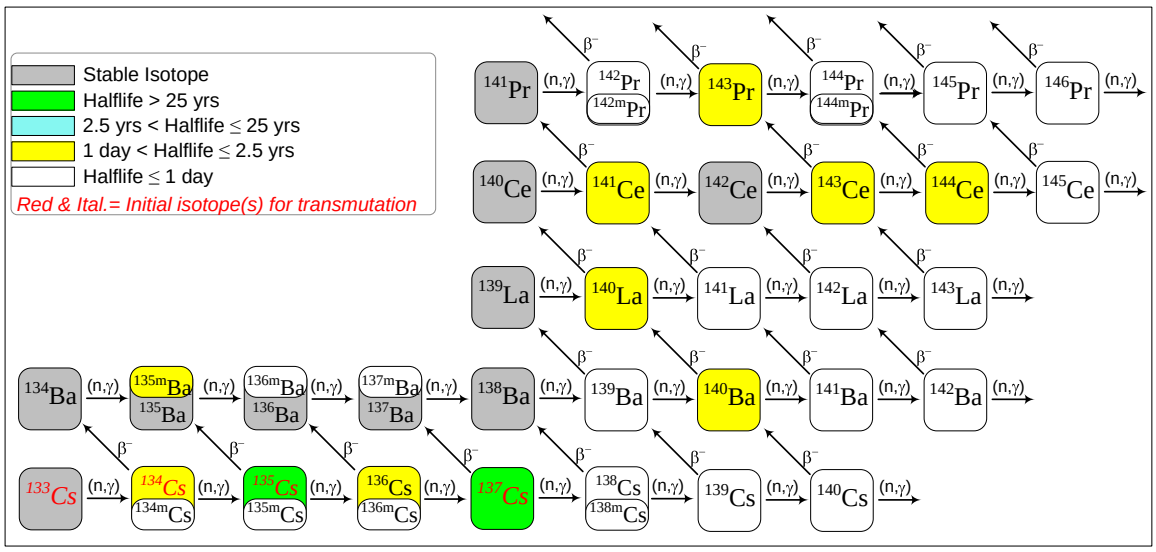

Fig. 11. Transformation path for cesium isotopes in transmutation scenario.

Figure 11 shows the transformation path of the cesium isotopes. The illustration indicates the possibility of transmuting cesium isotope to stable isotopes of barium. The transmutation is plausible given the relatively high capture cross sections of the cesium isotopes with the exception of ^{137}Cs. The transformation chain should accelerate loss of long-lived ^{135}Cs through the creation and decay of ^{136}Cs. However, this does not look as promising for the transmutation of ^{137}Cs, which has a very small capture cross section (see Table XI). The proposed transmutation scheme would need to consider the dominant ^{137}Cs transformation mechanism between radioactive decay to stable ^{137}Ba and transmutation leading to stable ^{138}Ba. If the dominant transformation mechanism is the radioactive decay, then the transmutation scheme is not effective for ^{137}Cs.

In the transmutation of cesium, the elements that could possibly be created (see Fig. 11) either have stable isotopes or short-lived radionuclides. Thus, a transmutation scheme that would transform all cesium isotopes to less radioactive nuclides will significantly reduce the contribution of cesium to the radiotoxicity of fission products.

However, given the small capture cross section of ^{137}Cs and the higher capture cross sections of ^{133}Cs, ^{134}Cs and ^{135}Cs, there is the possibility of ^{137}Cs buildup. This would be a limitation in the transmutation of cesium.

The target form is also a significant consideration in the transmutation of cesium. Cesium in itself has a very low melting point, which makes the metal an unsuitable target form. There are few compounds of cesium with melting points high enough to be a target in high temperature reactors. Table XII provides some of such compounds with their properties. The cesium compounds with melting point above 1000 K are oxygen bearing. Under the operating conditions in a transmutation reactor, there could be liberation of oxygen due to progressive stoichiometric changes in the target. In addition, these compounds consist of additional element aside from cesium and oxygen. Each element may be transmuted, which changes the composition of target made from the compound. This makes the transmutation-induced stoichiometric changes of the compound rather complex.

The simpler compounds are cesium salts with melting points above 900 K. One of these salts is cesium chloride (CsCl), which melts at about 919 K. One of the challenges in the transmutation of CsCl is the stoichiometric changes after transformation of cesium to barium. This is shown in the transformation chain below, which assumes no transmutation of chlorine:

$$6CsCl \xrightarrow{transmutation} 3BaCl_2 + 3Ba_{metal} \xrightarrow{transmutation} 2LaCl_3 + 4La_{metal}$$

Metal are progressively precipitated in the transmutation of CsCl. However, these metals have melting points higher than 1000 K. The stoichiometric balances shown above are simplified by the assumption of untransformed chlorine. Practicality requires that this

assumption be removed, which will make the stoichiometric balance more complex. For example, the neutron capture in chlorine will lead to creation of radionuclides ^{36}Cl and ^{38}Cl. These nuclides beta decay to produce stable argon isotopes. Argon is an inert gas, thus the initial CsCl target would be reduced to Cs metal.

Furthermore, ^{35}Cl is about 76% of naturally existing chlorine and its thermal capture cross section is higher than those of ^{135}Cs and ^{137}Cs. The ^{36}Cl produced from the irradiation of ^{35}Cl is very long-lived with a half-life of 301,000 years and emits 709 keV betas. The small cross section of ^{36}Cl makes its transformation by radiative capture less effective. Hence the production of ^{36}Cl is undesirable.

The complexity arising from the transmutation of CsCl may be reduced by making the target from cesium fluoride (CsF). Fluorine exists as 100% ^{19}F, which has a very small capture cross section. This suggests that a CsF target would readily experience cesium transformation with minimal transmutation of the fluorine in the target.

There are other aspects of cesium targets that need characterization. For example, materials subjected to neutron flux are required to be limited to about 200 dpa from radiation damage. The behavior of targets made from these compounds under protracted neutron flux needs to be understood. In addition, characteristics such as phase changes at elevated temperatures, interaction with surrounding media, and structural changes at grain level need to be understood. Only then will it be possible to completely establish criteria necessary for the safe use of these targets. The studies required to attain this understanding is beyond the scope of this work.

Table XII. Selected cesium compounds and their properties.

Compound, Formula	MP (K)	Density (g/cc)	Remark
Cesium carbonate, Cs_2CO_3	1066	4.24	Crystalline (monoclinic), Hygroscopic
Cesium chloride, CsCl	919	3.99	Crystalline (cubic), Hygroscopic
Cesium chromate (IV), Cs_4CrO_4	1255	4.24	Crystalline
Cesium fluoride, CsF	976	4.64	Crystalline (cubic), Hygroscopic
Cesium molybdenate, Cs_2MoO_4	1229		Crystalline
Cesium sulfate, Cs_2SO_4	1278	4.24	Crystalline, Hygroscopic

II.C GLOBAL OUTLOOK ON FISSION PRODUCT MANAGEMENT

The need to close nuclear fuel cycle has led several countries with nuclear power capability to seek ways to recycle spent fuel, recover usable materials and minimize radioactive waste inventory [39, 40]. This section investigates examples of what some of these countries have done and particularly the outlook on fission product management. The past and current efforts of the European Union, South Korea, Japan and United States of America are presented.

II.C.1 European Union

The approach to fission product management varies across Europe. Countries like Sweden and Finland favored direct disposal of spent nuclear fuel. For instance in 2001, the Finnish government approved a proposed spent fuel storage site at Olkiluoto subsequent to the political and local acceptance of the project. A submission of construction license application is expected no later than 2012. Operating license processing is scheduled around 2020 subject to the completion of the first compartments and encapsulation facility of the repository [41]. In this approach, no special treatment or processing is given to fission products since they are contained in spent fuel assemblies, which would be package for final burial in geologic repository.

On the other hand, countries like France and Russia reprocess most of their spent fuel. The focus of the reprocessing is the recovery of usable materials (generally uranium and plutonium). The waste stream from reprocessing – which includes fission products – is conditioned and stored onsite, awaiting final disposal. Most of the European countries are yet to decide on which approach to adopt. The practice in these countries is the

storage of spent fuel pending the time a decision is made on which alternative to adopt [42, 43]. Such decisions are hinged on the technological developments associated with the options.

In 2004, the European Union established a program called RED-IMPACT, which addresses the disposal of high level wastes. The RED-IMPACT program was aimed at waste reduction, recycling of usable materials and, waste treatment and conditioning of non-reusable materials [44, 45]. The studies under RED-IMPACT primarily assessed transmutation of actinides. However, the transmutation of long-lived fission products such as ^{129}I and ^{99}Tc was implicitly included with actinide transmutation. The program addressed waste management over 3 time frames: short-term options with current reactor fleets, medium-term options with Gen III+ reactors and advanced fuel cycles, and long-term options with Gen IV reactors, ADS with advanced fuels and techniques. Findings from the program suggested that heavy water reactors may be effective in the burning of long-lived fission products due to the reactors' excellent neutron economy. An advanced technique involving LASER transmutation of ^{129}I was identified. The transmutation scheme produces ^{128}I through a (γ,n) reaction in ^{129}I. The short-lived ^{128}I then beta decays to stable ^{128}Xe [45]. Overall, the program did not consider specific transmutation strategy for fission products. The program suggested intermediate storage of other waste stream in vitrified form before final disposal. A variant approach of partitioning cesium and strontium from the waste stream before vitrification was considered. It was however noted that the cesium/strontium stream would require a repository due to the presence of long-lived ^{135}Cs in the stream. The RED-IMPACT program ended in September 2007. The findings from the program are incorporated into the European Atomic Energy

Community's (EURATOM) Framework Programs for the implementation of new nuclear energy strategies.

II.C.2 South Korea

In South Korea, the historical policy to spent fuel management is direct disposal. However, issues such as energy security, waste volume reduction and optimization of repository capacity have led the country to alternative management option involving spent fuel recycling. The favored reprocessing method is pyroprocess. The methodology involves partitioning of fission products from spent fuel vectors. An engineering scale pyroprocess demonstration facility is expected to open by 2011 [46]. In this approach, spent fuel is partitioned into 4 main streams: uranium, TRU, fission products and hull (clad and other structural materials). The uranium stream is store for reuse, while the TRU is recovered for advanced fuel/ transmutation targets. The hull may be considered as low level or high level waste depending on the level of actinide contaminants included in the stream. South Korea plans to remove residual actinides from the hull prior to geologic disposal [47].

Fission product management strategies are being developed by the Korean Atomic Energy Research Institute (KAERI). The fission products are recovered in 3 sub-streams. Iodine and technetium sub-stream recovered to be transmuted along with the TRU. South Korea has adopted the sodium-cooled fast reactor (SFR) as the advanced system for the transmutation of the TRU, iodine and technetium stream. South Korea's prime objective is the reduction and/or elimination of this waste streams, hence the SFR

would be designed to operate as a burner. The reactor is also expected to use recycled fuel materials recovered through the pyroprocess [46, 47].

A second sub-stream of cesium and strontium is recovered for storage and final geologic disposal. This stream poses the main concern in the strategy. Geologic disposal is regulated based on the classification of the waste to be disposed. Wastes are classified based on the activity levels and half-lives of the nuclides in the waste stream. Low level waste (LLW) class is readily permitted by regulation for disposal unlike high level wastes (HLW). Cesium and strontium are very radioactive components of fission products. The inventory size of this sub-stream may determine its classification as either HLW or LLW. This would also affect the time require for its storage before final disposal.

The last fission product sub-stream mostly consists of rare earth (lanthanides) and noble metals. The noble metals may be recovered separately because of their economic value. South Korea plans to recover the rare earth for disposal. The sub-streams for disposal are planned to be made into waste forms that are resistant to leaching, decomposition and dissolution in a geologic repository. The candidate fission products for this waste form are cesium, strontium and rare earth. The fission products would be immobilized in a silicon-aluminum-phosphorus (SAP) matrix. The final form is attained after the addition of other immobilization agents and heat treatment [47].

II.C.3 Japan

The National Policy for Radioactive Waste Management in Japan stipulates amongst other things that steps should be taken to reduce wastes generated. Furthermore, research and development to this end should be actively pursued. Thus, Japan is one of

the countries that have chosen to reprocess its spent fuels. Much like, France, the fission product stream of the wastes is conditioned and stored onsite at the reprocessing facility. This approach is backed by the policy that residual high-level waste after the recovery of useful materials from spent fuel should be solidified in a stable from and stored for up to 50 years, while awaiting final burial in geological repository [48]. The storage time provides a period over which alternative approach to the disposal of the solidified waste is developed.

For the purpose of alternative treatment of the fission products, the stream is classified into 4 categories: usable/economically profitable elements (Ag, Ru, Pd and other platinum group metals), stable waste elements (e.g. Mo), heat generating elements requiring storage for cooling (Cs and Sr), and transmutable elements (Tc and I). The development goals for fission product management includes the reduction of it radiotoxicity contribution [14]. A number of strategies have been explored in the transmutation of specific fission product elements. A transmutation scheme for elemental cesium through the use of fusion neutron source was proposed by Tokyo Institutes of Technology [9]. This is one of the conceptual approaches for specific fission product transmutation. Another of such approaches is the transmutation of technetium and iodine in JOYO experimental fast reactor. The 3D diffusion code CITATION was used in conjunction with depletion code ORIGEN2 to model the transmutation of ^{99}Tc and ^{129}I. Optimal transmutation rates were obtained in cases where local neutron moderation was provided in the vicinity of the fission product targets [13]. Practical research efforts explored the fabrication of suitable LLFP target in fast reactor sub-assemblies. An example of such research was presented in the transmutation of ^{129}I using metal iodide

targets. The candidate targets included MgI_2, CaI_2, CuI and NaI. The research revealed that CaI_2 is a good target material in the absence of air, while CuI performs well in air but reacts with stainless steel. In addition, it was concluded that the slow transmutation rate of ^{129}I makes recycling of the target inevitable [11]. Findings from these experiments and other related studies are expected to be incorporated in future strategies for fission product management in Japan.

II.C.4 United States of America

The United States of America (USA) openly commits to geologic disposal of spent nuclear fuels, which is based on the Nuclear Waste Policy Act of 1982. However, there is ongoing consideration of commercial spent fuel recycling, leading to advanced management strategies for fission products. If there is a change in the policy on commercial spent fuel management that will allow reprocessing, the current spent fuel inventory could be recycled. This future prospect is provided for by requiring the current geologic repository designed to allow retrieval of disposed fuel at a later time when necessary.

As part of the ongoing researches into spent fuel recycling, researchers have considered transmutation of long-lived fission products under different reactor systems. For instance, the United States Department of Energy investigated ^{99}Tc and ^{129}I transmutation using ADS under the Advanced Accelerator Applications program in early 2000 [10]. All other research efforts are similar to those identified in other countries. The focus is on TRU transmutation with long-lived fission product transmutation

incorporated in the strategies. These approaches are aimed at the reduction of HLW and optimization of nuclear resources.

The United States Nuclear Regulatory Commission (NRC) defined HLW to include spent nuclear fuel, liquid wastes resulting from the reprocessing of spent fuel and solids into which the wastes are converted [49]. There are clear regulations spelt out in Part 60 of Title 10 of the Code of Federal Regulations, which govern the disposal of HLW in the USA. Yucca Mountain repository is the sole candidate identified for the disposal HLW from commercial nuclear operations in the USA. However, the disposal facility is yet to be operational. In the event spent fuel reprocessing is pursued in the USA, the identified repository may be used in the disposal of the residual waste steam after stabilization and conditioning. It should be noted that unlike other countries, NRC's definition of HLW is based on the source of the waste and not the characteristics of the waste constituents. Thus it is unlikely that the final waste-form from any advanced fission product management strategy will attain a LLW classification. If the NRC redefines HLW based on the characteristics of the waste, it is possible to reduce fission products to forms considered as LLW. However, it is very likely that the waste will fall into the Greater-Than-Class-C (GTCC) LLW category. By definition, it takes any one of 0.08nCi/g of ^{129}I, 3nCi/g of ^{99}Tc, 4600Ci/m^3 of ^{137}Cs or 7000Ci/m^3 of ^{90}Sr to make a fission product stream GTCC inventory [50]. Much like HLW, there is currently no facility licensed by NRC for the disposal of GTCC LLW. Hence the alternative will be temporary storage of the waste-form.

II.D CONCLUSION

Fission products are not as radiotoxic as TRU nuclides; however, they have significant contribution to the hazards associated with radioactive wastes from the nuclear fuel cycle. Moreover, if the TRU recycling is implemented, the ultimate incineration of actinides will yield more fission product, which becomes the principal source of radiotoxicity. In light of this, the properties of significant fission products have been reviewed. The likely behavior of these fission products under transmutation scenario was also investigated. The inferences from this investigation will serve as the basis of a transmutation strategy, which will be proposed through this dissertation.

In addition, the past approaches and current outlook into fission product management have been studied. Some nations are exploring transmutation strategies for as a fission product management approach. It should be noted that all of the schemes reviewed herein are based on selective treatment of the FP. These schemes utilize transmutation systems such as fast reactors, ADS, and fusion systems. All options agree on the need for a repository for the final waste-form after the fission product transmutation scheme.

In the maintenance of a repository, pre-closure and post-closure concerns are important considerations for the type of waste being disposed. The ^{137}Cs inventory is an important consideration in the pre-closure concerns due to its high activity and potential dose to worker at the facility. On the other hand, ^{99}Tc and ^{129}I inventories are important in the post-closure considerations due to their long-life and mobility in geological environment. Hence a fission product transmutation scheme that can significantly reduce this nuclide will be excellent for waste reduction measure. In addition, if the

transmutation reactor can inherently serve as an in-core storage facility for the fission products over a long time, this will provide addition storage for the cooling of the highly radioactive nuclides such as ^{137}Cs and ^{90}Sr prior to disposal. A VHTR system could serve this purpose. Reflector regions in the VHTR could double as both target locations for the transmutation scheme and also serve as a storage location in the reactor without a significant effect on the power profile in the active core.

CHAPTER III

FISSION PRODUCT TRANSMUTATION STRATEGY AND ANALYSIS METRICS

This chapter discusses the proposed fission product transmutation strategy. Section III.A covers the details and theories behind the strategy. The methodology to demonstrate the transmutation strategy is introduced. The metrics for the analysis of the results of the strategy are also presented in section III.B. Figure 12 shows the summary of this chapter.

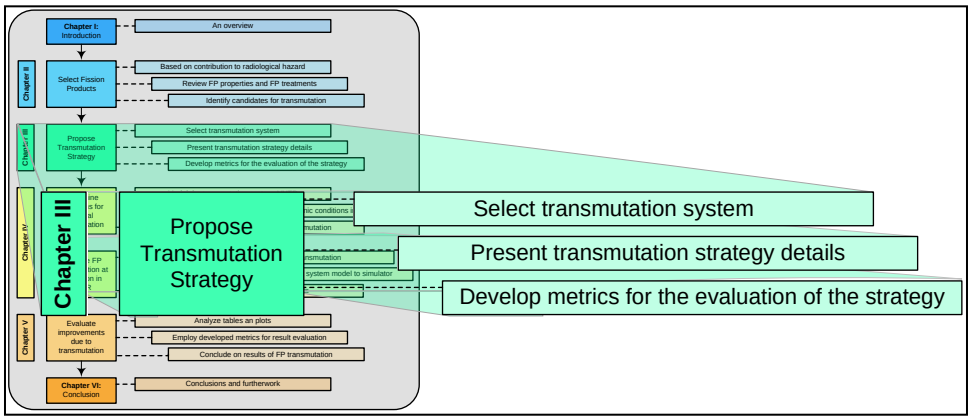

Fig. 12. Key focus of Chapter III.

III.A FISSION PRODUCT TRANSMUTATION STRATEGY

In order to achieve the desired transmutation efficiency of fission products in the VHTR, the necessary conditions must be determined. First let's consider the path of a radioactive fission product without transmutation in a reactor. The reduction in the fission product inventory is driven by decay constant λ. Thus for radionuclides with very small λ, it takes several thousands to millions of years before the radioactivity is reduced to acceptable levels. The decay constant is dependent on the radionuclide itself. Hence

for a particular nuclide that is left to decay, the time required to attain a desired level of activity can neither be accelerated nor slowed-down. If the prospect of transmutation in a reactor system is considered, an addition driver is then involved in the reduction of fission product inventory. This driver is the capture reaction rate per particle $\sigma_c\phi$, which will also be referred to as the transmutation constant.

III.A.1 Decay Constant vs. Transmutation Constant

Unlike the decay constant, which is an intrinsic property of a radionuclide, the transmutation constant is a function of both radionuclide properties and the neutronics condition in the transmutation system. The ability to influence the choice of neutronics condition makes the transmutation constant a prime parameter for the reduction of fission product inventory.

Under a reactor based transmutation scenario, the reduction via decay is still present in addition to the transmutation reaction. Thus the reduction in fission product inventory is governed by an effective transmutation constant $\mathcal{L}_T$, which is defined as:

$$\mathcal{L}_T = (\lambda + \sigma_c\phi) \tag{1}$$

The mean lifetime of a radionuclide under transmutation scenario and radioactive decay mode can be defined as $1/\mathcal{L}_T$ and $1/\lambda$ respectively. It is then obvious that a radionuclide under effective transmutation scenarios will be effectively shorter lived than in decay-only mode since:

$$\frac{1}{\mathcal{L}_T} = \frac{1}{\lambda + \sigma_c\phi} < \frac{1}{\lambda} \tag{2}$$

If a radionuclide with initial concentration N_0 is allowed to decay only, the residual inventory $N_{residual}^{decay}$ of the nuclide after time t is:

$$N_{residual}^{decay} = N_0 e^{-\lambda t} \tag{3}$$

Similarly, the residual inventory under transmutation scenario, $N_{residual}^{xmute}$, over the same time period t is:

$$N_{residual}^{xmute} = N_0 e^{-(\lambda+\sigma_c\phi)t} \tag{4}$$

Now, an improvement factor f_I for radionuclide reduction can be defined as:

$$f_I = \frac{N_{residual}^{decay} - N_{residual}^{xmute}}{N_{residual}^{decay}} \tag{5}$$

The improvement factor is a characterization of the additional reduction of radionuclide inventory when transmutation option is employed. After simplification, the equation (5) reduces to:

$$f_I = 1 - e^{-\sigma_c\phi t} \tag{6}$$

Equation (6) shows that when transmutation constant $\sigma_c\phi$ is zero, improvement factor f_I also becomes zero. This case corresponds to decay-only mode. However, a non-zero $\sigma_c\phi$ will result in a positive improvement factor with time. An optimal improvement factor f_I can be achieved under effective transmutation scenarios through any of the following approaches:

1. Keep a radionuclide in the transmutation system under a given $\sigma_c\phi$ for a very long time; that is, let the transmutation period t to be as long as possible.
2. Increase $\sigma_c\phi$ to the maximum level possible for a given period of time by maximizing flux level and optimizing operation reaction energy range.

3. Effective combination of the approaches above.

If the first approach is considered, the optimal improvement factor will be achieved as time $t \to \infty$. The long time associated with this approach is not particularly desirable. A necessary performance indicator in a transmutation scenario is the reduction in time required to achieve acceptable activity levels compared to decay-only mode. Thus, an infinitely long time period does not provide the justification for transmutation since normal decay over infinitely long time frame will result in significant reduction of the radionuclide.

In the second approach, it is assumed that acceptable level of activity from a particular radionuclide is set to be attained within a stipulated time frame. Thus the optimal improvement factor will be achieved at the highest possible $\sigma_c\phi$ from the transmutation system. Fig. 13 shows the evolution of the improvement factor with transmutation constant $\sigma_c\phi$. The asymptotic behavior of the improvement factor suggests that there is a point at which an increase in $\sigma_c\phi$ provides insignificant increase in the improvement factor. If this point is identified, a clever combination of the $\sigma_c\phi$ and protracted retention of the radionuclide in the transmutation system may offer the optimal fission product inventory reduction desired. This is essentially the third approach stated above.

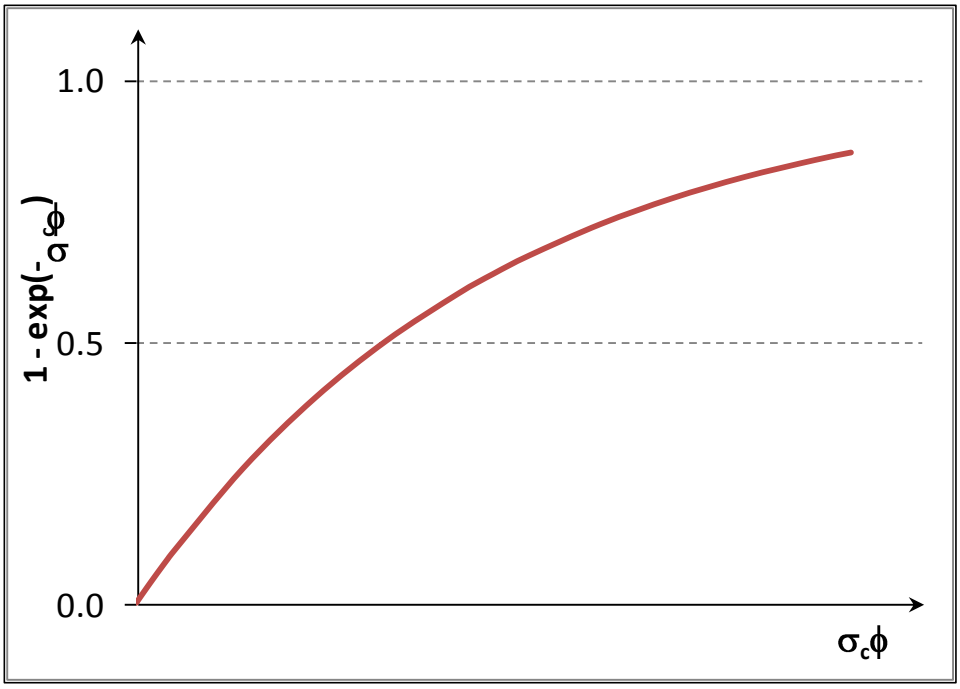

Fig. 13. Improvement factor vs. transmutation constant.

The second and third approaches depend on the optimization strategy of the transmutation constant. The transmutation constant $\sigma_c\phi$ consists of two distinct parameters. One is the radiative capture cross section σ_c, which is an intrinsic property of the radionuclide that cannot be externally influenced. The other is neutron flux ϕ: a system-dependent parameter, which can be optimized to achieve a desired purpose. Both parameters have energy dependence. In addition, neutron flux has spatial dependence. A detailed look at the two parameters would offer insight into the conditions necessary for the transmutation in a reactor system.

III.A.2 Energy-Dependent Transmutation Constant

In any neutron field, the interaction between a neutron and the nucleus of an atom is greatly influenced by the energy E of the incident neutron. Since the neutrons in the

field have various energies, the flux can be represented as $\phi(E)$. Also, the probability that a certain type of interaction will occur in the neutron field is energy dependent. Then the radiative capture cross section of a nuclide in the field can be expressed as $\sigma_c(E)$. Thus, the energy dependent transmutation constant at a particular energy of incident neutron is $\sigma_c(E)\phi(E)$. The behavior of the energy dependent transmutation constant over the energy range must be determined in order to establish the conditions for improved transmutation. To evaluate the behavior of $\sigma_c(E)\phi(E)$, let's consider a family of functions $\{f_i\}$ on a real domain. Suppose for all $i = 1,2,\dots,n$ and within the interval $[a,b]$, the equation

$$F_i = \int_a^b f_i(x)dx = C \tag{7}$$

is satisfied; where C is a constant.

Let's select another function $g(x)$, on a real domain such that two points p and q can be defined on the interval (a,b), such that they satisfy the condition $g(p) \neq g(q)$. Let's define another family of functions $\{h_i\}$ such that:

$$h_i(x) = g(x)f_i(x) \tag{8}$$

Then, the area under the curve of $h_i(x)$ within the interval $[a,b]$ is given by:

$$H_i = \int_a^b h_i(x)dx = \int_a^b g(x)f_i(x)dx \tag{9}$$

Unlike F_i, the value of H_i will depend on i, since $g(x)$ is not constant over the interval $[a,b]$. Thus, H_i is not necessarily a constant for all indices i. A control example is given below, where f_1, f_2 and f_3 are defined as:

$$\begin{aligned} f_1(x) &= x \\ f_2(x) &= 1 - x \\ f_3(x) &= 3x(1-x) \end{aligned} \tag{10}$$

The evaluation of F_i with the family of functions given by (10) over the interval $[0,1]$ gives:

$$F_1 = F_2 = F_3 = 0.5 \tag{11}$$

However, if a function g defined as

$$g(x) = \frac{1}{x} \tag{12}$$

is applied to equation (9), the result is:

$$\begin{aligned} H_1 &= \int_0^1 \frac{1}{x}.xdx && = 1 \\ H_2 &= \int_0^1 \frac{1}{x}.(1-x)dx && = -(1+\ln|0|) \Rightarrow \infty \\ H_3 &= \int_0^1 \frac{1}{x}.3x(1-x)dx && = 1.5 \end{aligned} \tag{13}$$

Thus far, a relationship between $\{f_i\}$ and $\{h_i\}$ has been established. The behavior of both families of functions under a specified set of conditions has been determined. An analogy between the $\{f_i\}/\{h_i\}$ behavioral relationship and the energy dependent transmutation constant can be set forth. The family of functions $\{f_i\}$ can be likened to the set of all possible flux spectra in a transmutation system. This leads to an expression similar to equation (7) for the scalar flux based on the i^{th} spectrum:

$$\phi_i = \int_{E_{min}}^{E_{max}} \phi_i(E)dE \tag{14}$$

The function $g(x)$ is equivalent to the energy dependent capture cross section of a nuclide. The family of functions $\{h_i\}$ is analogous to the set of transmutation constants, which are based on the flux spectra possible in the transmutation system. Thus, an expression similar to equation (9) can be written for the net transmutation constant T_i over the neutron energy range E_{min} to E_{max}:

$$T_i = \int_{E_{min}}^{E_{max}} \sigma_c(E)\phi_i(E)dE \tag{15}$$

Equation (15) can be expanded as:

$$T_i = \left[\sigma_c(E)\int \phi_i(E)dE\right]\Big|_{E_{min}}^{E_{max}} - \int_{E_{min}}^{E_{max}} \left[\int \phi_i(E)dE\right]\frac{d\sigma_c(E)}{dE}dE \tag{16}$$

Equation (16) shows the non-linear coupling of energy dependent cross section and flux spectrum in the determination of the net transmutation constant. As long as $\sigma_c(E)$ is not constant between E_{min} and E_{max}, the net transmutation constant will be dependent on the flux spectrum in the system, not necessarily on the magnitude of the associated scalar flux.

III.A.3 Reaction Rates in Transmutation Scenarios

Figure 14 provides typical examples of flux spectra and energy dependent capture cross section. For a particular nuclide in transmutation under a flux spectrum $\phi_i(E)$, the radiative capture reaction rate $\mathcal{R}_i$ is given by:

$$\mathcal{R}_i = \int_{E_{min}}^{E_{max}} N\sigma_c(E)\phi_i(E)dE = T_i N \tag{17}$$

where N is the number density of the nuclide being transmuted. Suppose the scalar flux derived from each of the 3 flux spectra in Fig. 14(b) are equal to one another, then the nuclide being transmuted is exposed to the same neutron population regardless of the spectrum selected. However, the capture reaction rate is sensitive to the prevailing flux spectrum (see Fig. 14(c)). Thus the optimal transmutation will occur under the spectrum with the highest capture reaction rate.

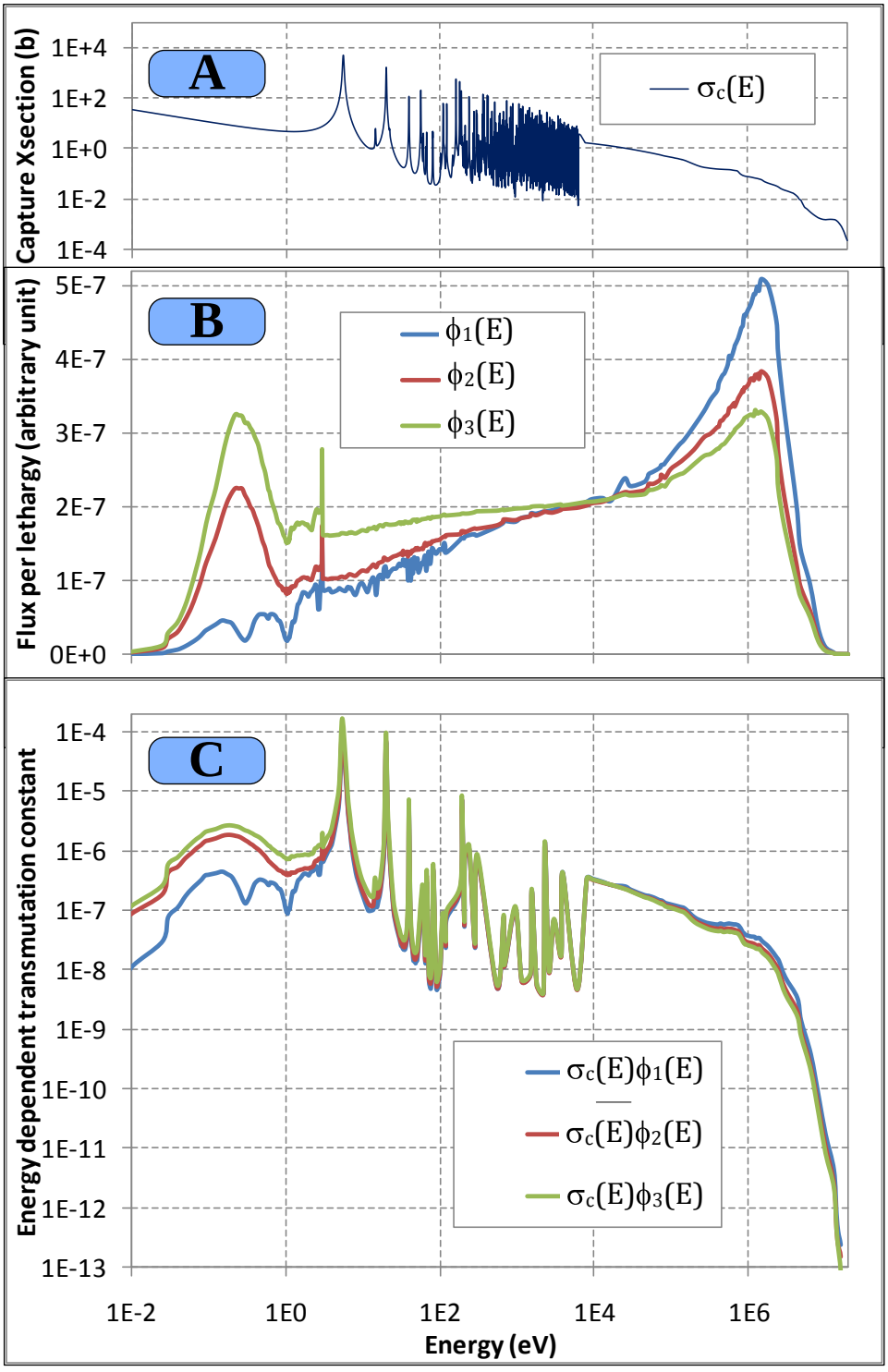

Fig. 14. Typical flux spectra and radiative capture cross section.

In a transmutation system, the various flux spectra may be attainable depending on regions within the system. For example, the spectra $\phi_1(E)$, $\phi_2(E)$ and $\phi_3(E)$ (see Fig. 14(b)) may be described as $\phi(\vec{r}_1, E)$, $\phi(\vec{r}_2, E)$ and $\phi(\vec{r}_3, E)$ respectively, where $\vec{r}_i$ defines the coordinates of region i in the transmutation system. Then regions of the system will influence the capture reaction rate of any nuclide. This is the effect of space induced variation in flux spectra.

There could also be a time induced change in spectrum. This could be a result of changes in the material composition within the transmutation system. Regardless of the cause of the time dependent evolution in flux spectrum, the reaction rate also changes with time. Hence, a location with the optimal reaction rate at a particular point in time may no longer be the optimal region for transmutation after some time.

Spectral change could also be induced by the temperature profile in the transmutation reactor system. Cross sections of materials in and around the core are altered as local temperatures change in different regions of the reactor system. In particular, the alteration of scattering cross-sections in a region of the core will cause changes in the slowing down mechanism of neutrons crossing that region. This in effect leads to a change in the flux spectrum at the region. Thus a region with optimal transmutation reaction rate may no longer be the optimal region once the temperature of that region changes.

There are various parameters that may be perturbed in the reactor system to give a spectral change. For example, any perturbation in the control rod composition or control rod location will have an effect on the flux spectra in the vicinity of the control rods. Exploring all the various perturbations that would lead to spectral shifts in a reactor

system will be a tedious exercise. Moreover, the purpose of this dissertation is to propose strategies for the optimization of fission product reduction through the use of an advanced reactor system. Thus, it will suffice to demonstrate the strategy by considering the perturbation of a few key parameters to induce the spectral changes required in the assessment of the optimal reaction rates for fission product transmutation. For the purpose of this dissertation, space and time induced spectral changes will be used to demonstrate the fission product transmutation strategy proposed herein.

III.A.4 Fission Product Transmutation

For a simplified demonstration of space and time effects on the transmutation strategy being explored, the effect of radioactive decay in the fission products will be neglected. A conservative illustration is made by neglecting contribution of radioactive decay to the loss of the fission product. This has the effect of understating the effective transmutation achievable. Moreover, this neglect is necessary in order to emphasize the effect of time and space changes on transmutation effectiveness in any reactor system.

Suppose there are n local regions in a transmutation system, which are labeled $r_1, r_2, \dots, r_n$. For each region in the given system, it is desirable to determine the neutronic parameters at specific times $t_0, t_1, \dots, t_m$. Figure 15 shows a schematic diagram of spatial and temporal representation for reaction rates R_{ij} for any nuclide in such transmutation system. The reaction rate R_{ij} in this case is defined as

$$R_{i,j} = \int_{E_{min}}^{E_{max}} N\sigma_c(E)\phi(r_i, E, t_j)dE \equiv N\sigma_c\phi(r_i, t_j) \tag{18}$$

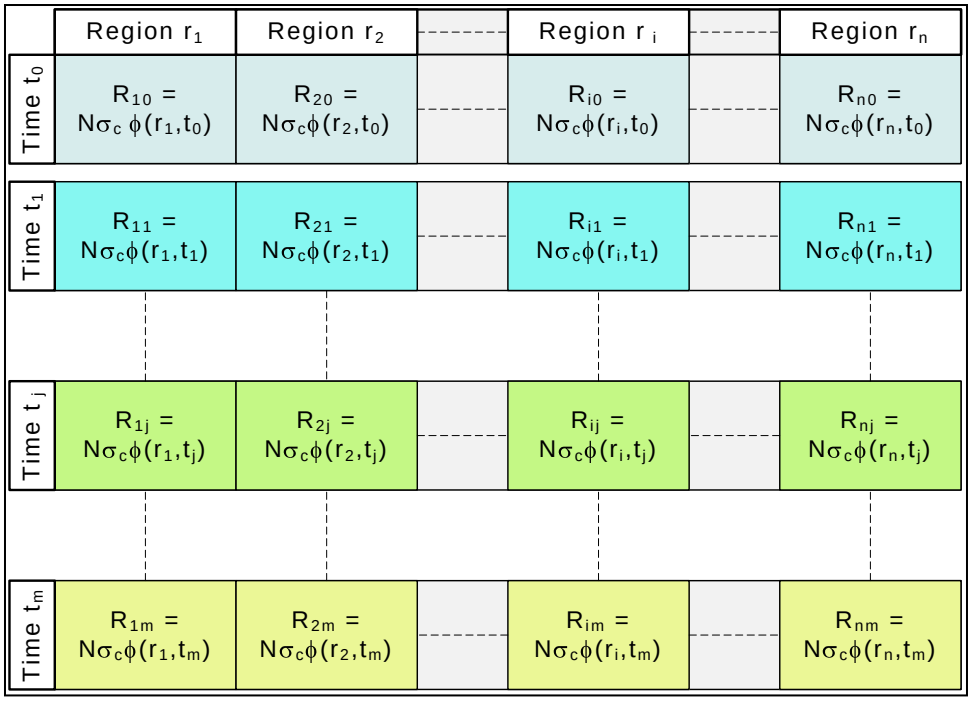

Fig. 15. Time and space dependent reaction rates in any given system.

Consider a situation in which a nuclide of interest with initial concentration N_0 is located in a region r_i. Then, the residual concentration at region r_i after transmutation during time interval t_{j-1} to t_j can be derived as:

$$N_{i,j} = N_0 e^{\frac{-1}{N_0}\int_{t_{j-1}}^{t_j} R_{i,j}dt} \tag{19}$$

At time t_j, there exists a region r_i such that the reaction rate $R_{i,j}$ is optimal for any nuclide that requires transmutation. The optimal reaction rate will be denoted as $R_{max,j}$; where

$$R_{max,j} = \max_{1\le i\le n} R_{i,j} \in \{R_{i,j}: i = 1, 2, \dots, n\} \tag{20}$$

Then the maximum loss possible within time segment t_{j-1} to t_j will result in the minimum residual concentration given by:

$$N_{min,j} = N_0 e^{\frac{-1}{N_0}\int_{t_{j-1}}^{t_j} R_{max,j}dt} \tag{21}$$

Equation (21) essentially provides that for any given time interval t_{j-1} to t_j, there exists a region r_i where transmutation is optimal. Thus, the region at which a nuclide's loss due to transmutation is maximized between times t_{j-1} and t_j becomes the optimal location for the transmutation of the particular nuclide within the specified time interval. Given different time intervals, the region of maximum transmutation could be different. For instance, if the region r_i provides maximum transmutation between times t_{j-1} and t_j, the region may no longer be the optimal location between times t_j and t_{j+1}.

The preceding discussion illustrates the effect of time shifts on the optimization of transmutation. The effect of location changes on the transmutation can be illustrated in a similar way. A change in the spatial region of a target in a transmutation system would affect the outcome of the transmutation scheme. In this case, consider region r_i with nuclide lost by transmutation given by equation (19). The maximum transmutation loss would result a minimum residual concentration given by:

$$N_{i,min} = N_0 e^{\max\limits_{1\le j\le m}\left[\frac{1}{N_0}\int_{t_{j-1}}^{t_j} R_{i,j}dt\right]} \tag{22}$$

This maximum transmutation loss in the region is achieved within a particular time interval t_{j-1} to t_j. Given different region in the transmutation system, the time interval with maximum transmutation could be different. For example, suppose the maximum transmutation in region r_i is observed in the time interval t_{j-1} to t_j. Relocating the target nuclide to another region r_k may change the time interval at which the maximum transmutation is achieved.

The combination of the effects of space and time on transmutation can be effectively used to maximize fission product inventory reduction. Consider again, the

schematic representation of reaction rates in Figure 15. Suppose a fission product target with initial concentration N_0 is placed in region r_i and left at this region to be irradiated over the total period of transmutation, time t_0 to t_m. The residual inventory $N_{i,1}$ after the first time interval t_0 to t_1 is given by:

$$N_{i,1} = N_0 e^{\frac{-1}{N_0}\int_{t_0}^{t_1} R_{i,0}dt} \tag{23}$$

The residual concentration at the end of the first time interval becomes the initial concentration for the next time interval. Hence the residual inventory at the end of the second irradiation interval becomes:

$$N_{i,2} = N_{i,1} e^{\frac{-1}{N_0}\int_{t_1}^{t_2} R_{i,1}dt} = N_0 e^{\frac{-1}{N_0}\int_{t_0}^{t_1} R_{i,0}dt} e^{\frac{-1}{N_0}\int_{t_1}^{t_2} R_{i,1}dt} \tag{24}$$

Thus, at the end of the irradiation period, the residual concentration of the target nuclide in the region is:

$$N_{i,m} = N_0 \exp\left(\frac{-1}{N_0}\sum_{j=1}^{m}\int_{t_{j-1}}^{t_j} R_{i,j}dt\right) \tag{25}$$

Suppose it is impractical to change the location of the target within the system at specific time interval, then the maximum transmutation would be achievable through the placement the target at the location leading to the least residual inventory. The minimum residual $N_{R,m}^{min}$ achievable is then given by:

$$N_{R,m}^{min} = N_0 \exp\left[\frac{-1}{N_0}\left(\max_{1 \le i \le n}\sum_{j=1}^{m}\int_{t_{j-1}}^{t_j} R_{i,j}dt\right)\right] \tag{26}$$

The region which satisfies the minimum residual from equation (26) becomes the location for optimal transmutation. The transmutation achieved through this method provides maximum transmutation possible via the utilization of only one location

throughout the lifetime of the target in the system. This approach is limited by not taking advantage of other locations that would yield more effective transmutation at various time intervals during the irradiation period. Suppose it is possible to shuffle the target's location at specific times during the irradiation period, then a more effective transmutation could be achieved. The minimum residual $N_{Rmax,m}^{min}$ achievable through this additional flexibility would be given by:

$$N_{Rmax,m}^{min} = N_0 \exp\left[\frac{-1}{N_0}\sum_{j=1}^{m}\int_{t_{j-1}}^{t_j} R_{max,j}\,dt\right] \quad ; \tag{27}$$

where $R_{max,j}$ is as defined in equation (20). From equations (26) and (27), it is evident that $N_{Rmax,m}^{min}$ cannot be greater than $N_{R,m}^{min}$ since $R_{i,j} \leq R_{max,j}$. Thus the best transmutation result is achievable when the system allows the flexibility of location changes within itself at various time intervals. This is the ultimate approach to take advantage of time and space effects in a transmutation system.

III.A.5 Demonstration of the Fission Product Transmutation Strategy

Let's demonstrate the transmutation strategy as it has been described in the preceding section. The first aspect is identification of the transmutation system. Based on preliminary reviews, a thermal system would provide better transmutation for the selected fission products. Figure 16 shows the ratio of decay rate (λ) to capture reaction rate $(\sigma_c\phi)$for the selected nuclides. The ratio $\lambda/\sigma_c\phi$ is less than one for ^{93}Zr, ^{99}Tc, ^{129}I and ^{135}Cs, which indicates that transformation by neutron capture dominates the transmutation of these nuclides. In addition for each of the nuclides, the ratio is smaller in thermal spectrum than in fast spectrum. This indicates better results in transmutation

through thermal systems. The $\lambda/\sigma_c\phi$ is greater than one for ^{90}Sr and ^{137}Cs, which indicates that radioactive decay dominates the transmutation for both nuclides. However, the ratios are closer to one in thermal spectrum than in fast spectrum (see Fig. 16). The $\lambda/\sigma_c\phi$ ratio herein are speculative. These values may be improved once actual calculation is done. The higher flux values in the actual transmutation system could contribute to the improvement. In addition, improvement should also result from the contribution of neutrons other than fast and thermal energy neutrons, which were neglected in this preliminary analysis.

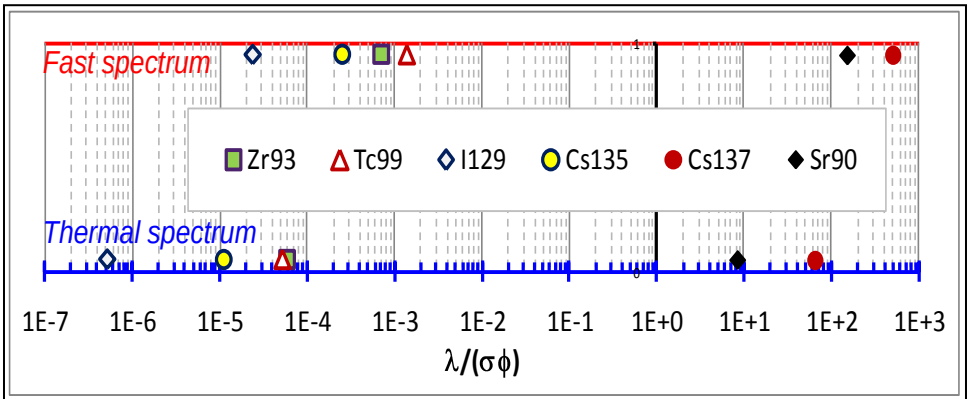

Fig. 16. Transmutation potential for radionuclides in fast and thermal spectrum.

For the purpose of this dissertation, the thermal system of choice is the VHTR. The VHTR intrinsically provides various energy spectra and flux levels depending on location within the reactor. This influences the reaction rates attainable at different location in the reactor system. In addition, changes in flux and energy spectra due to changes in reactor core materials with time influence the reaction rates as time

progresses. Thus the VHTR is an ideal system for the space and time effects on transmutation. The VHTR will be discussed further in Chapter IV.

The next step in this demonstration is the validation of the strategy. This is done in two phases. The first phase addresses the evaluation of transmutation potential in the VHTR. This is done by modeling the VHTR and calculating transmutation parameters at various locations in the system and at different times during the operation of the reactor. The modeling and calculations are accomplished using MCNP5 release 1.51 and MCNPX version 2.6.0 codes developed and maintained by Los Alamos National Laboratory [51 – 53]. These codes were used to calculate neutronic parameters such as energy spectra, neutron fluxes, neutron intensity, k-effective and reaction rates at zero power. The MCNPX was used to simulate the operation of the VHTR at full power over a specific period. In additional to the neutronic parameters, depleted fuel composition and burnup at specific times and locations during full power were also calculate. The reaction rates are the most significant to the evaluation of the transmutation potential. The resulting reaction rates are indicators of locations and time segments combination leading to optimal transmutation for each of the fission product nuclide being considered. The results of this phase are discussed in details in Chapter IV.

The second phase of the validation is the evaluation of transmutation effectiveness in the VHTR. This is done by simulating the transmutation of selected fission products at the identified locations. The other neutronic parameters calculated in the first phase play important roles in the simulation. In the phase, the ORIGEN-S code developed and maintained by Oak Ridge National Laboratory was employed [54]. The code was used for the simulation of fission products transmutation over a period of time.

The neutronics parameters required to simulate transmutation in VHTR were provided to ORIGEN-S from the results of MCNP5/MCNPX codes calculations. The parameters required by ORIGEN-S included neutron fluxes, time intervals, and energy spectra. The results obtained from ORIGEN-S for the transmutation calculations included fission product inventories, heat load, radioactivity and radiotoxicity hazards. The evaluations from this phase are the main subject of Chapter V.

III.B EVALUATION METRICS IN THE TRANSMUTATION STRATEGY

In order to successfully validate the proposed transmutation strategy, methods for the characterization of the FP nuclides before and after transmutation were developed. Some analyses were performed in the course of the demonstration of the transmutation strategy. The characterization was accomplished through a few metrics developed and employed in the analyses. These metrics were in two categories:

- Basic characteristics of radionuclides.
- Transmutation effectiveness characterization.

III.B.1 Basic Characteristics of Radionuclides

This category of metrics is based on the rudimentary characteristics of radionuclides. These characteristics include mass inventory, radioactivity, decay heat and intake doses. They are particularly important in the evaluation of improvements in final repository capacity, pre-closure issues and post-closure issues with selected fission products. Four metrics were derived from these characteristics:

1. Fraction of nuclide i transmuted, f_i: This is based on residual concentrations of each significant fission product nuclide after transmutation. It is a primary measure of the reduction in fission product inventory. This metric is given by equation (28):

$$f_i = \frac{N_{i,in} - N_{i,out}}{N_{i,in}} \tag{28}$$

where $N_{i,in}$ is the initial mass inventory of nuclide i before irradiation and $N_{i,out}$ is the residual inventory of nuclide i after transmutation. The metric is important for the improvement of repository capacity and utilization. The higher the fraction f_i, the better the transmutation achieved and by extension, less inventory would require disposal after discharge.

2. Radioactivity contribution of nuclide i to the discharged fission product target, $f_{A,i\ out}$: This is a fraction of the total radioactivity of discharged fission product target contributed by nuclide i. The metric is a measure of the radiotoxicity of the fission product and is given by equation (29).

$$f_{A,i\ out} = \frac{A_{i,out}}{A_{out}} \tag{29}$$

The parameter $A_{i,out}$ is defined as the activity of nuclide i at discharge, while A_{out} is the total activity of the discharged target. This metric is important since a low fraction indicates that the bulk of the discharged target's radioactivity is from other radionuclides of less significance when compared to the fission product of interest. There is the certainty that the

complimentary radioactivity fraction, $1 - f_{A,i\ out}$ will be lost after a few years of decay.

3. Decay heat contribution of nuclide i to the discharged fission product target, $f_{Q,i\ out}$: This is a fraction of the total decay heat of discharged fission product target contributed by nuclide i. The metric is a measure of potential heat load at storage site or eventual disposal facility. This is calculated for each significant nuclide and is given by equation (30).

$$f_{Q,i\ out} = \frac{Q_{i,out}}{Q_{out}} \tag{30}$$

The parameter $Q_{i,out}$ is defined as the decay heat contributed from nuclide i at discharge, while Q_{out} is the total decay heat from the discharged target. This metric is important since it reflects on the pre-closure issues such as thermal heat generation from the target. Similar to the radioactivity metric above, a low $f_{Q,i\ out}$ indicates that the decay heat from target is mainly driven by secondary radionuclides produced during irradiation. These secondary contributors should completely decay off after a few years of cooling.

4. Fraction of effective dose equivalent contributed by nuclide i at discharge, $f_{D,i\ out}$: This metric is a measure of effective radiotoxicity from the fission product nuclide of interest. This is calculated by using equation (31)

$$f_{D,i\ out} = \frac{D_{i,out}}{D_{out}} \tag{31}$$

The parameter $D_{i,out}$ is defined as the effective dose equivalent contributed from nuclide i at discharge, while D_{out} is the total effective

dose equivalent from the discharged target. This metric is important since it's an indication of the potential reduction in radiotoxicity of the nuclide of interest. A low fraction suggests that total dose equivalent is dominated by secondary radionuclides produced during irradiation. Once the secondary nuclides decay completely, a there would be a reduction in total effective dose equivalent. This metric would be applied to both ingestion and inhalation radiotoxicity.

III.B.2 Transmutation Effectiveness Characterization

The metric developed for the transmutation effectiveness was based on the basic characteristics of radionuclides. This metric is a measure of the integral effect of the basic characteristics of the discharged fission product of interest. In order to derive the metric, some parameters were defined.

Consider a fission product target, which can be left to decay over a certain period or is discharged after irradiation over a similar period. This target would consist of several nuclides, which were created during the decay or irradiation period. There is a contribution by each of the constituent nuclide to the characteristics of the target. Let there be n total nuclides in the cooled or discharged target and m total number of characteristics. Suppose we are only interested in a nuclide i, which is part of the target's constituent. Then the evaluation of characteristic j for the selected nuclide i can be represented by $P_{i,j}$. The total value of the j^{th} characteristic for all nuclides present in the target is represented by $P_{0,j}$. Hence $P_{0,j}$ can be expressed as:

$$P_{0,j} = \sum_{i=1}^{n} P_{i,j} \tag{32}$$

The parameters $P_{i,j}$ and $P_{0,j}$ can be evaluated in both decay-only and transmutation scenarios. In this case, superscripts D and T can be included in the parameters to indicate decay-only and transmutation scenarios respectively. Now an improvement factor, $C_{i,j}$ can be define as the ratio of $P_{i,j}$ in transmutation to $P_{i,j}$ in decay-only scenario. Similarly, an overall improvement factor $C_{0,j}$ is defined as the ratio of $P_{0,j}$ in transmutation to $P_{0,j}$ in decay-only scenario. The expressions for these parameters are provided in equations (33a) and (33b).

$$C_{i,j} = \frac{P_{i,j}^{T}}{P_{i,j}^{D}} \tag{33a}$$

$$C_{0,j} = \frac{P_{0,j}^{T}}{P_{0,j}^{D}} \tag{33b}$$

Ideally, it is desired to have the improvement factors less than unity and as close to zero as possible. An improvement factor value of 1 or greater indicates no advantage from the transmutation of the nuclide of interest. The closer the value is to zero, the better the advantage gained through transmutation.

Once the improvement factor is evaluated for each characteristic, the values can be integrated to determine a transmutation effectiveness factor. Equations (34a) and (34b) give the formulae for transmutation effectiveness:

$$x_i = \sum_{j=1}^{m} w_j C_{i,j} \Big/ \sum_{j=1}^{m} w_j \tag{34a}$$

$$x_0 = \sum_{j=1}^{m} w_j C_{0,j} \Big/ \sum_{j=1}^{m} w_j \tag{34b}$$

The parameter x_i is the transmutation effectiveness factor for nuclide i, while x_0 is the equivalent total transmutation effectiveness factor. The transmutation effectiveness factors can be interpreted based on the values. If the value is greater than one, this indicates that the transmutation scheme is not effective; it resulted in a worse waste-form compared to a decay-only approach. A transmutation effectiveness value of one indicates that the transmutation scheme has the same effects as a decay-only scheme. If the transmutation effectiveness value is less than one, then the transmutation scheme provides net improvement over the decay-only approach. A value of zero indicates a complete destruction of all radionuclides. This is an ideal result, which is impractical. Thus the closer the transmutation effectiveness factor gets to zero, the better the advantage gained by transmutation of the radionuclide of interest.

The effectiveness factors are weighted mean of the improvement factors. The weight w_j is an importance attribute of the j^{th} characteristic. The method to determine the weight for j^{th} characteristic is based on the ratio of the j^{th} improvement factor to the simple average, $\bar{C}$ of all improvement factors. Thus, w_j is determined as:

$$w_j = \begin{cases} \chi_{i,j} & if: \quad \chi_{i,j} > 1.2 \\ 1 & if: \ 0.2 \le \chi_{i,j} \le 1.2 \\ 0.5 & if: \quad \chi_{i,j} < 0.2 \end{cases} \ ; \ \chi_{i,j} = C_{i,j} \Big/ \frac{1}{\mathrm{m}} \sum_{j=1}^{m} C_{i,j} \qquad (35)$$

The logic behind the weighting approach is the identification of outlying improvement factors around the mean value. Outliers around a mean value tend to distort the effects of the values that are reasonably close to the mean. In this case, consider an improvement factor $C_{i,small}$, which is very small compared with the average of all improvement factors. Then $C_{i,small}$ has the effect of reducing the average of all $C_{i,j}$s. If $C_{i,small}$ is

isolated from the other improvement factors, the average of the remaining $C_{i,j}$s would be a remarkable increase from the previous average. For the purpose of this research, isolation of any characteristic is not desired, hence the need to reduce the effect of such $C_{i,small}$. The effect is reduced by attributing a small weight $(w_j = 0.5)$ to the characteristic with the small $C_{i,j}$. The result is a conservative evaluation of the transmutation effectiveness since the average is increased due to the small weight. On the other hand, if a very large improvement factor $C_{i,large}$ exists, it has the effect of increasing the average of all improvement factors. Since a large $C_{i,j}$ is indicative of low transmutation effectiveness on the j^{th} characteristic, a conservative approach will seek to amplify the effect of the large improvement factor. Hence, a weight greater than unity is attributed to the $C_{i,j}$. Other improvement factors that are not in the categories of $C_{i,small}$ and $C_{i,large}$ are assigned a weight equal to one.

Once the weights are determined, they can be applied to equations (34a) and (34b) in the evaluation of the transmutation effectiveness factor. The result will be conservative evaluations of the transmutation effective factors.

CHAPTER IV

FISSION PRODUCT TRANSMUTATION IN VHTR SYSTEMS

This chapter discusses the modeling of the fission product transmutation strategy. A description of the VHTR employed in the transmutation strategy is presented. A detailed model of the VHTR is described in section IV.A. The transmutation strategy was based on an equilibrium cycle for the VHTR. The method through which the equilibrium cycle was determined is also described section IV.B. The results from the equilibrium cycle are also presented.

Reaction rates at different locations in the VHTR were calculated based on the equilibrium cycle. The results of this are discussed in section IV. C. The last section of this chapter discusses the simulation of the fission product irradiation in VHTR using ORIGEN-S code. Figure 17 shows the summary of this chapter.

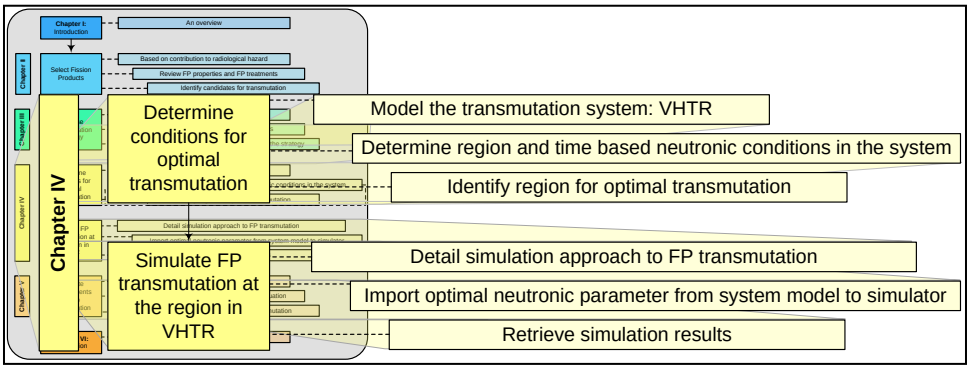

Fig. 17. Key focus of Chapter IV.

IV.A VHTR MODEL

The VHTR model was developed for simulations with MCNP5 code, release 1.51. The model takes into account fuel assembly blocks, control rod blocks, replaceable

reflectors and a permanent outer reflector. The fuel assembly blocks were based on HTTR fuel block configuration [55]. The HTTR fuel block was adapted into the VHTR power core model. Table XIII provides the major specification of the VHTR core.

Table XIII. VHTR core specifications.

Parameter	**Value**
Thermal Power (MW)	600
Power Density (MW/MTHM)	103
Coolant	Helium
Coolant Pressure (MPa)	4
Average Outlet Temperature (°C)	950
- Reflector material	Graphite
Core height (m)	10.44
Active core height (m)	7.54
Core diameter (m)	6.80
Core layout	
Radial arrangement	
- Fuel columns	Annular - 3 rings
- Number of Fuel Columns	66
- Center reflector	5 rings
- Outer reflector	Replaceable - 2 rings; Permanent
Axial arrangement	
- Number of fuel block layers	13
- Number of top reflector layers	2
- Number of bottom reflector layers	3
Fuel block	
- Number of fuel blocks	858
- Number of fuel elements per block	31
- Fuel element	TRISO particle in annular compact
- Fuel matrix	Graphite
- Fuel block height (cm)	58

IV.A.1 Fuel Block

The fuel assembly block consists of fuel elements, burnable poison rod, coolant channels and hexagonal graphite block. The graphite block is 36 cm across flats. It has 31 vertical borings of diameter 4.1 cm to accommodate the fuel elements. There are 3 vertical holes representing burnable poison locations. In the VHTR model, burnable poisons are loaded in 2 holes, while the third is reserved. The block has a handling hole in the center. The coolant channels are the gaps between fuel bores and fuel elements. The fuel assembly block model is provided in Figure 18.

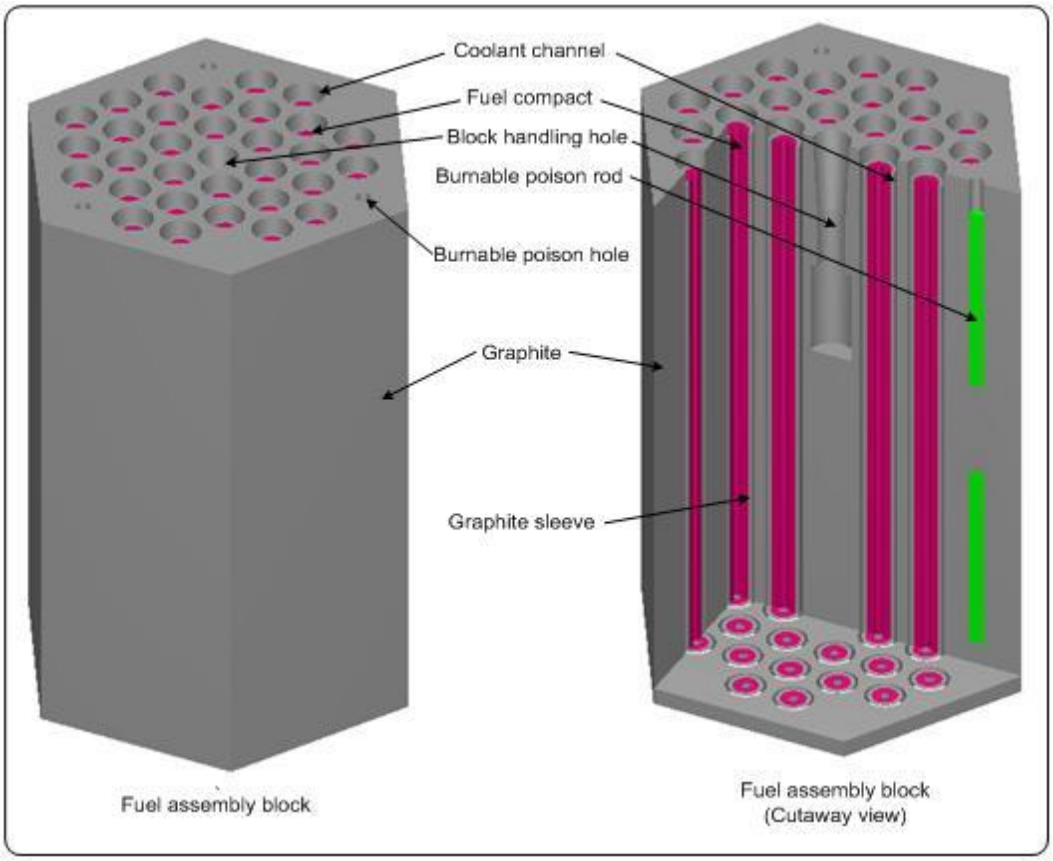

Fig. 18. Fuel assembly block.

The fuel assembly block specification is provided in Table XIV. Low concentration of natural boron was included in the fuel block model to account for impurities in graphite. Figure 19 provides the layout and dimensions of the fuel block.

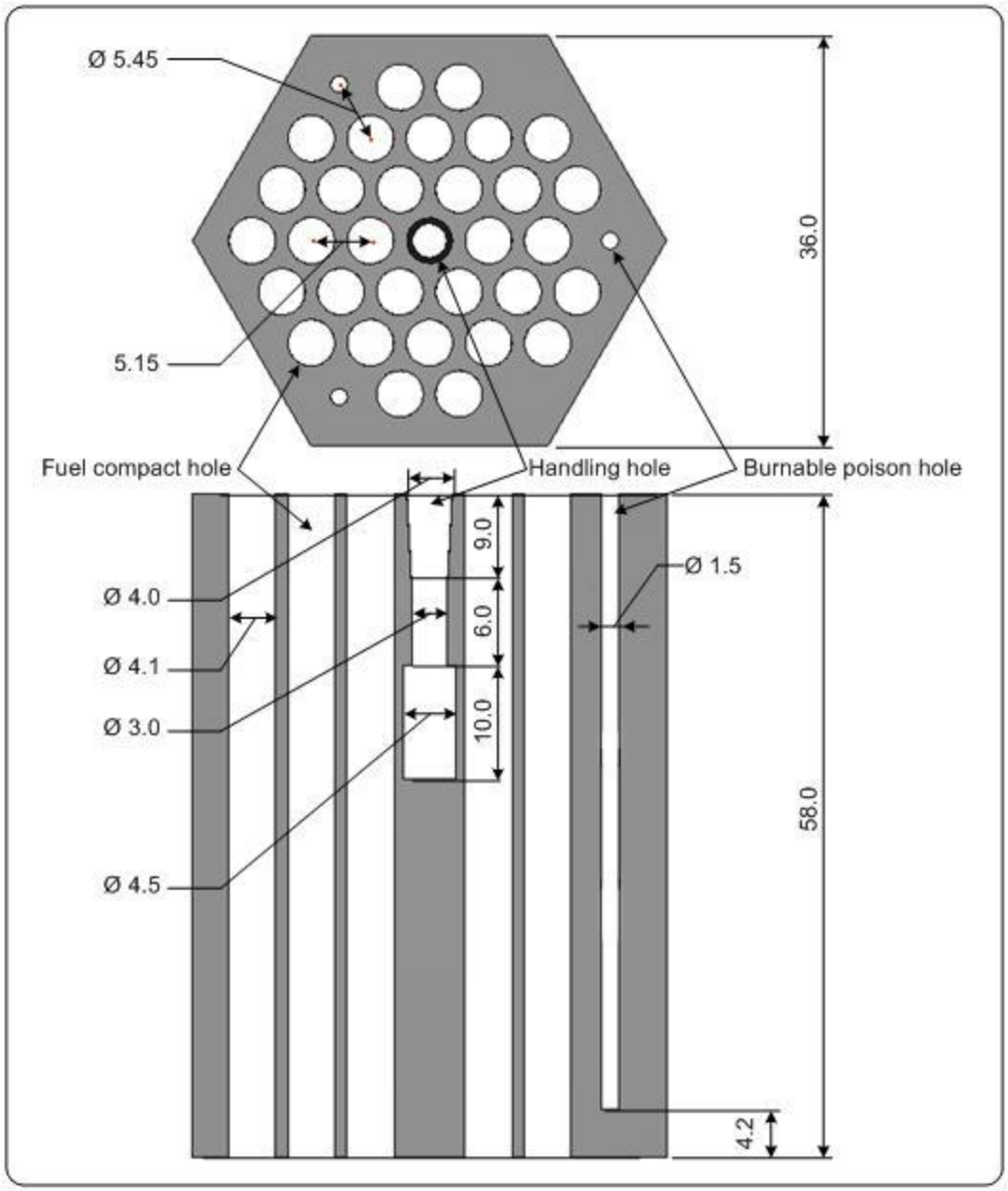

Fig. 19. Fuel assembly block dimensions (all values in cm).

Table XIV. Fuel assembly block specifications.

Parameter	Value
Assembly type	Pin-in-block
Block configuration	Hexagonal Prism
Material	Graphite
Density (g/cc)	1.770
Impurity (ppm B_{nat})	0.40
Height (cm)	58.0
Width across flats (cm)	36.0
Number of fuel holes	31
Fuel hole diameter (cm)	4.1
Fuel hole height (cm)	58.0
Number of burnable poison holes	3
Burnable poison hole diameter (cm)	1.5
Burnable poison hole height (cm)	53.8

The fuel element consists of 14 vertically stacked annular fuel compacts in graphite sleeve. The inner and outer diameters of the sleeve are 2.6 cm and 3.4 cm respectively. The graphite sleeve model included natural boron to account for impurities. The fuel compact has inner and outer diameters of 1.0 cm and 2.6 cm respectively. Each fuel compact is 3.9 cm in height. It consists of TRISO coated fuel particles at 0.3 volume fraction. The particles are embedded in graphite matrix with low concentrations of natural boron to account for impurities. Each fuel compact contains about 12,567 particles. The fuel element specifications are provided in Table XV.

Table XV. Fuel element specifications.

Fuel Compact	
Parameter	**Value**
Volume fraction of fuel grains	0.2
Number of fuel grains per fuel compact	8405
Number of compacts per fuel element	14
Inner diameter (cm)	1.0
Outer diameter (cm)	2.6
Compact height (cm)	3.9
Graphite matrix density (g/cc)	1.690
Matrix Impurity (ppm B_{nat})	0.82

Graphite Sleeve	
Parameter	**Value**
Material	Graphite
Density (g/cc)	1.770
Impurity (ppm B_{nat})	0.37
Inner diameter (cm)	2.6
Outer diameter (cm)	3.4
Height (cm)	54.6

The TRISO coated particles are composed of a spherical fuel kernel of diameter 0.6 mm. The kernel composition is uranium oxide at 15% ^{235}U enrichment. The kernel model neglects ^{234}U content in the uranium oxide fuel. The oxygen is modeled as 100% ^{16}O. The particle structure is provided in Figure 20. The first coating is a layer of low density porous carbon. The second coating is high density pyrolytic carbon, followed by silicon carbide layer. The outermost layer is also high density pyrolytic carbon. Table XVI provides the material and dimensions of the TRISO particle. The 4 layers of coatings were explicitly described in the computational model.

Table XVI. TRISO particle specifications.

	material	**density (g/cc)**	**diameter (cm)**
Fuel kernel	UO_2	10.41	0.0600
1st coating	Porous carbon	1.14	0.0718
2nd coating	Pyrolytic carbon	1.89	0.0780
3rd coating	Silicon carbide	3.20	0.0838
4th coating	Pyrolytic carbon	1.87	0.0930

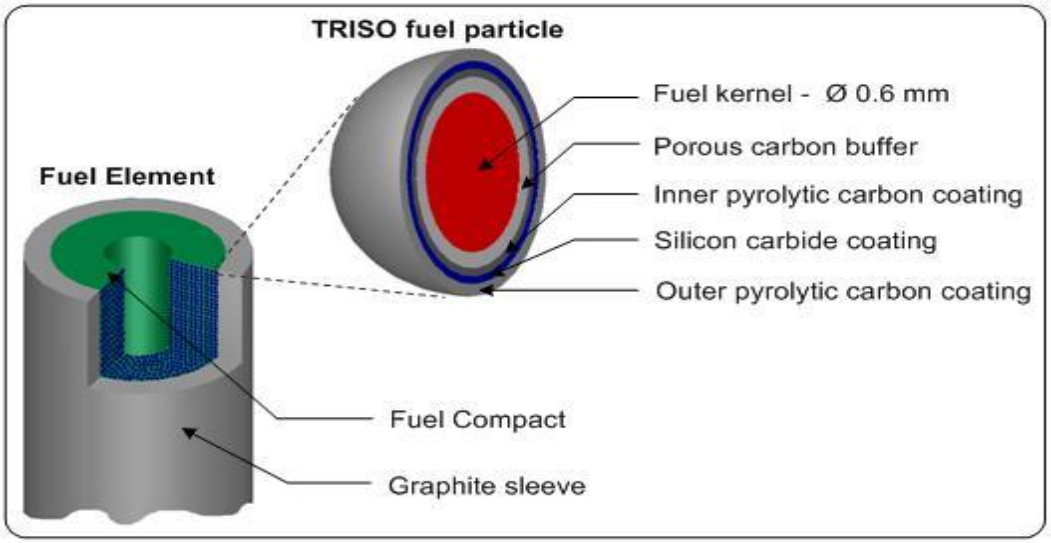

Fig. 20. TRISO fuel structure.

The burnable poison rod consists of 2 boron carbide/carbon sections with graphite middle section (see Fig. 18). The diameter of the rod is 1.5 cm and 50 cm height. The boron carbide/carbon sections have heights of 20 cm, while the graphite section is 10 cm. Table XVII provides the burnable poison specifications.

Table XVII. Burnable poison rod specifications.

Parameter	**Value**
Absorber section material	B_4C-C
Density (g/cc)	1.82
Natural boron concentration (wt.%)	2.74
Diameter (cm)	1.50
Height (cm)	20
B-10 abundance ratio (wt.%)	18.7
Graphite section - Density (g/cc)	1.77
- Diameter (cm)	1.50
- Height (cm)	10

IV.A.2 Replaceable Reflector Blocks

The replaceable reflector blocks are hexagonal prisms (similar to the fuel block). There are two types of reflector blocks: graphite reflector blocks with coolant channels, and solid graphite blocks. Both types have handling hole in the center. Figure 21 provides images of the replaceable reflector blocks. The blocks are 36 cm across flats and 58 cm in height. Table XVIII provides addition details of the blocks with coolant channels.

Table XVIII. Specification of replaceable reflector block with coolant channels.

Parameter	**Value**
Material	Graphite
Density (g/cc)	1.760
Impurity (ppm B_{nat})	0.37
Height (cm)	58.0
Width across flats (cm)	36.0
Number of coolant holes	31
Coolant hole diameter (cm)	4.1
Coolant hole height (cm)	58.0

The blocks with coolant channels are stacked directly above and below the fuel assembly blocks. They are arranged such that the fuel columns in the core have 18 blocks: 2 top and 3 bottom layers of replaceable reflector blocks, with 13 middle layers of fuel assembly blocks. The holes in the fuel assembly blocks and reflector blocks are aligned, creating passages for the coolant. The total number of in-core reflector blocks with coolant channels is 330.

The solid reflector blocks represent the central reflector column (61 block columns) and outer replaceable reflectors (102 columns). The blocks maintain the same dimensions and external form as the fuel block. The difference is the absence of holes

other than the handling hole. The total number of solid reflector blocks is 2,934. Table XIX provides addition details of the solid reflector blocks.

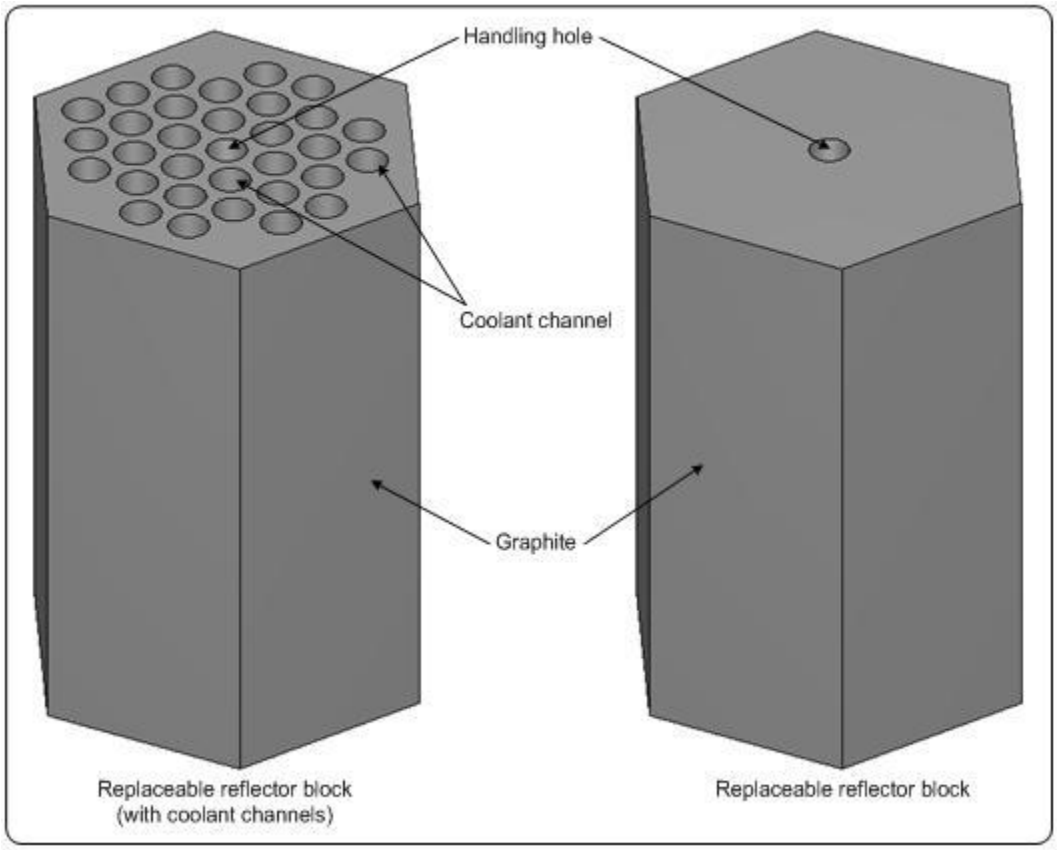

Fig. 21. Reflector blocks.

Table XIX. Solid reflector block specifications.

Parameter	Value
Material	Graphite
Density (g/cc)	1.760
Impurity (ppm B_{nat})	0.37
Height (cm)	58.0
Width across flats (cm)	36.0
Number of reflector columns	163
Number of blocks per column	18

IV.A.3 Control Rod Block

The control rod block consists of 3 vertical borings, each being 21.3 cm in diameter. The block is a hexagonal graphite prism with similar external form to the fuel block. It is 36 cm across flats and has a height of 58 cm. Figure 22 provides dimensions of the block. There are 36 columns of control rod blocks in the core. Each column consists of 18 blocks stacked one on another. Table XX provides the control rod block specification.

Table XX. Control rod block specification.

Parameter	Value
Material	Graphite
Density (g/cc)	1.770
Impurity (ppm B_{nat})	0.40
Height (cm)	58.0
Width across flats (cm)	36.0
Number of control rod holes in block	3
Control rod hole diameter (cm)	12.3
Control rod hole height (cm)	58.0

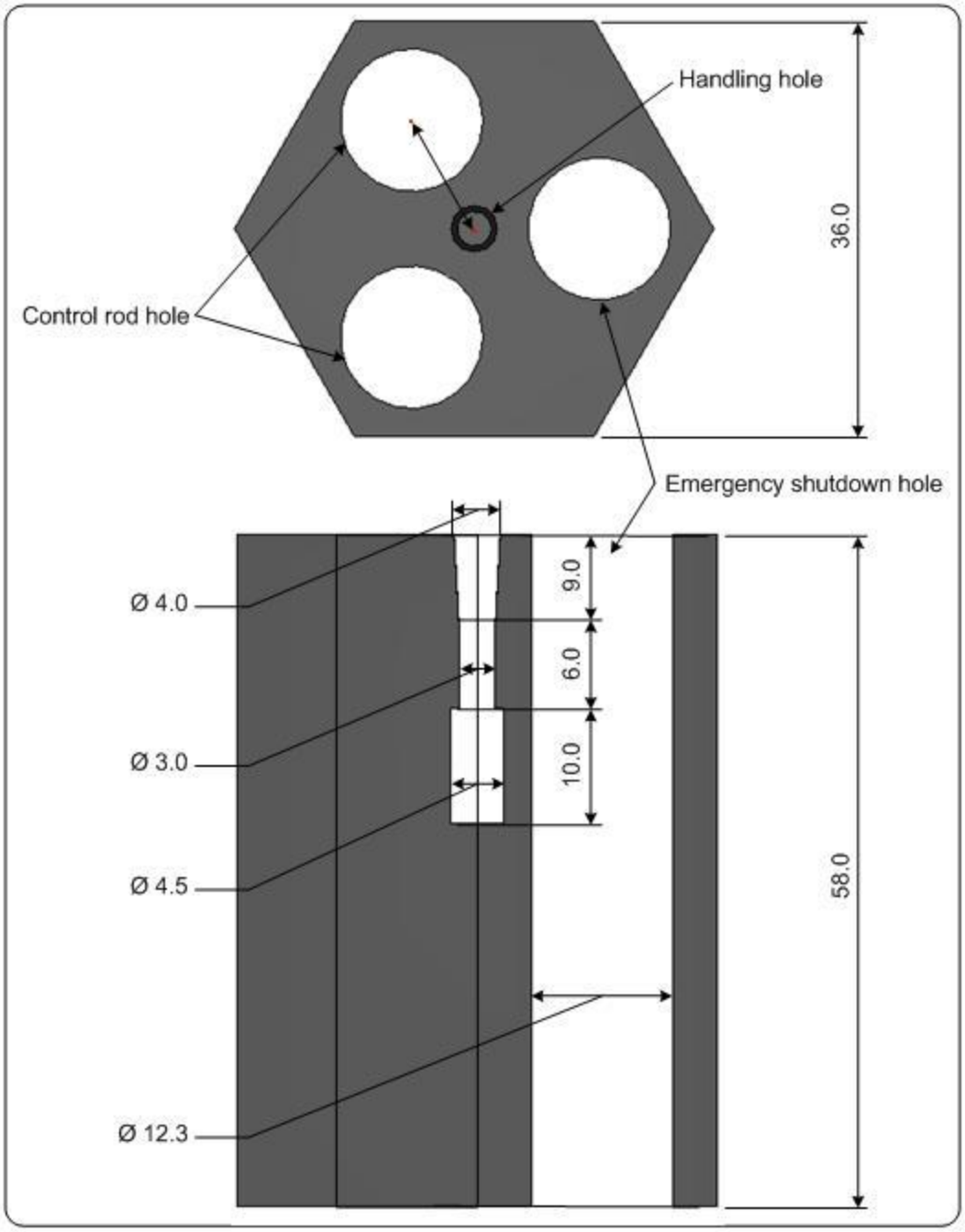

Fig. 22. Control rod block dimensions (all values in cm).

IV.A.4 3-D Whole Core VHTR Model

The 3-D whole core VHTR model is provided in Figure 23. The core was built by stacking the fuel assembly blocks, replaceable reflector blocks and control rod blocks in the cavity formed by the permanent graphite reflector structures. The control rod blocks and solid replaceable reflector blocks are stacked in columns to form the core assembly. The core height is 10.44 m. It has a diameter of 6.80 m. The active core height is 7.54 m, consisting of 13 fuel assembly blocks per column. The top and bottom axial reflectors are located above and below the active core. The axial reflector assembly is similar to the active core assembly. The difference is the presence of replaceable reflector blocks with coolant channels in place of the fuel assembly block.

The solid replaceable reflectors are arranged side-to-side to form the central reflector column. There are 61 columns of solid replaceable reflectors representing the central reflector. The solid reflectors form 2 additional rings of outer radial reflector for the core. There are 102 columns in the outer reflector. The permanent graphite reflector forms a radial outer boundary for the core. A cross sectional view of the active core can be seen in Figure 23. The whole core was explicitly modeled in MCNP5/MCNPX. All calculations where performed at system temperature of 1200K, except when otherwise stated.

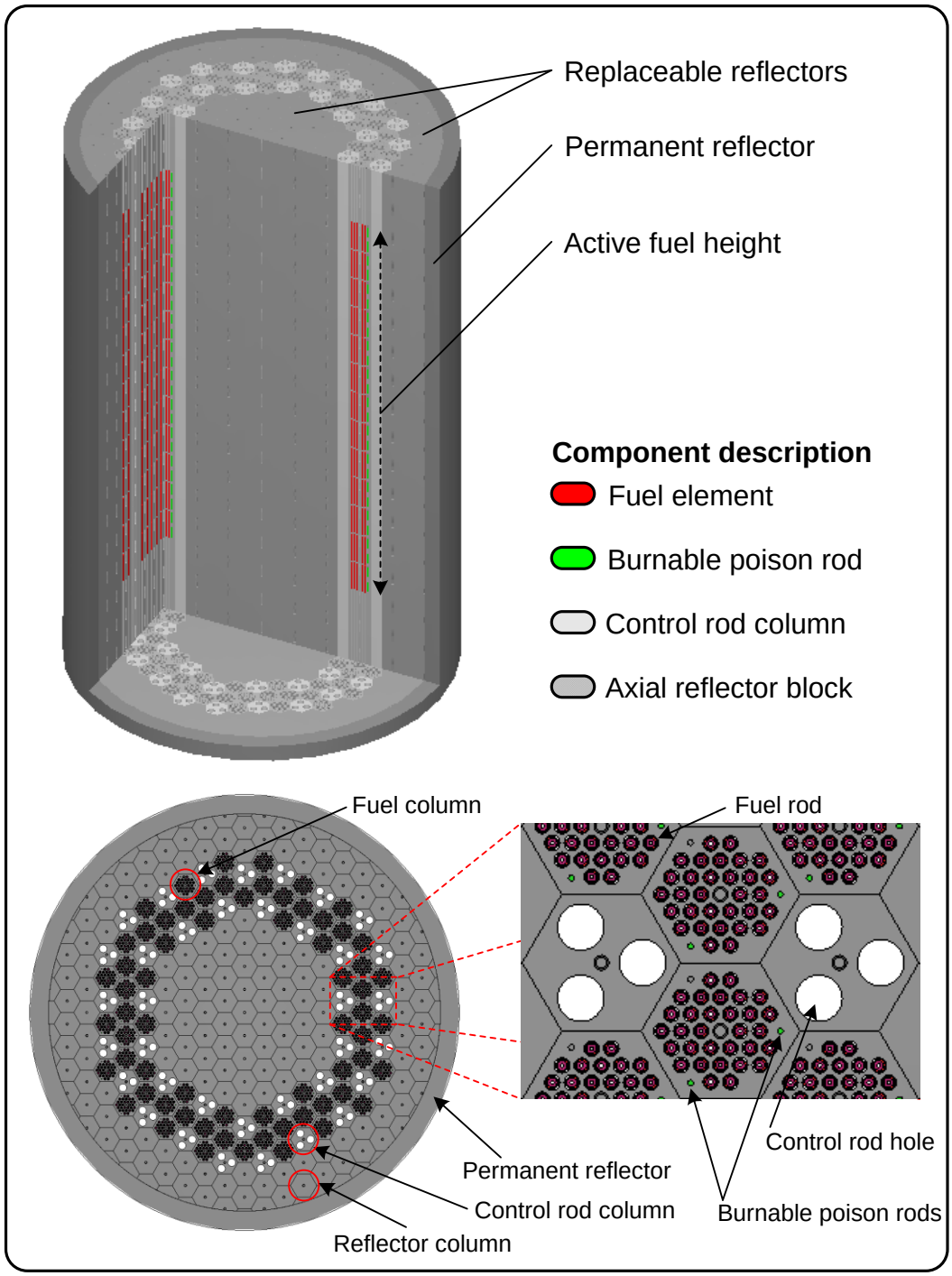

Fig. 23. 3-D whole-core VHTR model with horizontal cross-section view.

IV.A.5 Safety Considerations

Before continuing with the analysis of VHTR used in transmutation strategy, it is important to establish safety parameters. A power reactor configuration that cannot be shutdown is not desirable. Other criteria like reactivity feedback and temperature coefficients of reactivity are equally important indicator of reactor safety. Hence, these safety parameters were calculated to establish a basis for the continuation of use of the VHTR model.

The shutdown k-effective was calculated by modeling full insertion of control rods in 2 of the 3 control rod holes in each control rod block. The modeling assumes a third of the control rod locations is reserved for emergency shutdown. The control rod was modeled as described for the HTTR core components. The shutdown k-effective calculated for the UO_2 fueled VHTR is 0.7288 ± 0.0020. A shutdown k-effective of 0.8464 ± 0.0014 was calculated for a TRU-fueled VHTR. This was done to evaluated the shutdown possibility for a UO_2 fueled VHTR at a later stage of its cycle, when TRUs are already created in the core. The fuel composition used to estimate the stage is the TRU vector from PWR spent fuel at 45GWd/MTU and 85% load factor. The calculated coefficients of reactivity are all negative. The reactivity inserted by the coolant is also negative; an indication that loss of coolant will not increase reactivity in the core. Table XXI summarizes the safety parameters calculated for the VHTR.

Table XXI. Safety parameters of the VHTR.

Safety Parameter	Value
Shutdown k-effective: UO_2 kernel	0.7288
Shutdown k-effective: TRU kernel	0.8464
Isothermal temperature coefficient of reactivity ($\delta k/k\text{-}\delta T$)	-3.15×10^{-5}
Fuel temperature coefficient of reactivity ($\delta k/k\text{-}\delta T$)	-1.95×10^{-5}
Moderator temperature coefficient of reactivity ($\delta k/k\text{-}\delta T$)	-7.03×10^{-6}
Coolant temperature coefficient of reactivity ($\delta k/k\text{-}\delta T$)	-2.77×10^{-6}
Boron reactivity worth of burnable poison ($\Delta\rho_{B4C}$)	-0.0932
Coolant reactivity insertion of Helium ($\Delta\rho_{He}$)	-4.074×10^{-4}

IV.B EQUILIBRIUM CYCLE

In order to establish the VHTR equilibrium fuel cycle, the following were considered: number of fuel cycles leading to the equilibrium cycle and the core layout. It is also assumed that refueling process is continuous. The number of fuel cycles leading to the equilibrium cycle was set at 3. This essentially implies that a third of the core is discharged after each cycle. The active core layout is provided in Figure 24. There are a total of 66 columns of fuel blocks in the core. The fuel block assemblies are arranged in 3 rings: inner zone (15 fuel columns), middle zone (33 fuel columns) and outer zone (18 fuel columns). There are 36 control rod columns with 15 columns in the inner zone, 3 columns in the middle zone and 18 columns in the outer zone.

The approach to the discharge of a third of the core involved selection of a third of fuel blocks in each fuel zone. Close to uniform distribution of the discharged fuel columns is desired. Hence a constraint is imposed such that no more than a cluster of 2 adjacent fuel columns can be discharged in any cycle. The result of this approach is the refueling pattern shown in Fig. 24. The fuel columns labeled "1" are discharged after the first cycle, columns "2" are discharged after the 2nd cycle and columns "3" after the third.

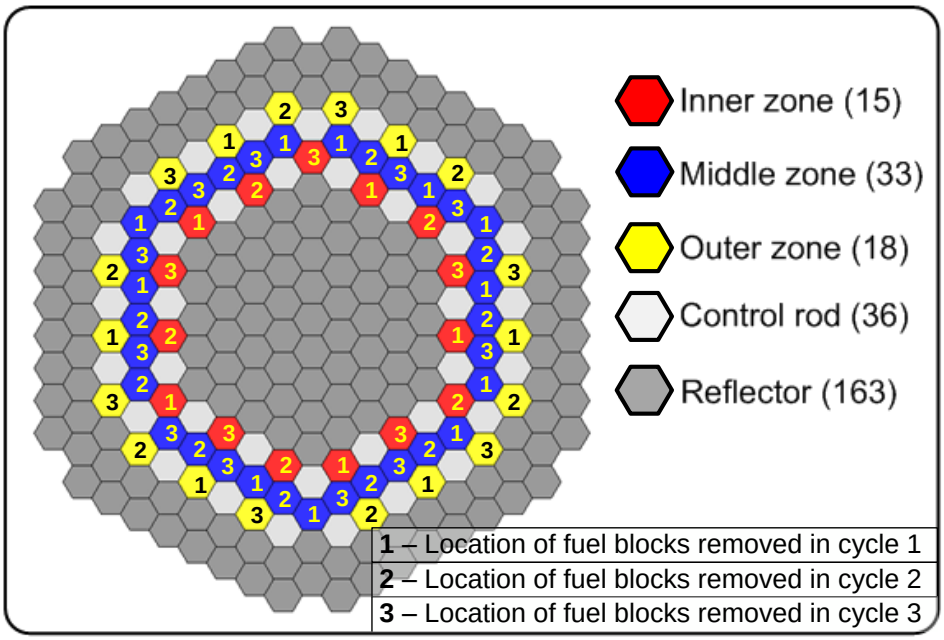

Fig. 24. Active core map including refueling pattern.

Figure 25 shows the process through which the equilibrium cycle is established. At the beginning of cycle (BOC) 1, the VHTR with core loading of 66 fresh fuel columns is operated until k-effective drops to 1. This cycle is stopped and the first one-third of the core (see Fig. 24) is removed, ending the first cycle. The discharged fuels are replaced with 22 columns of fresh fuel. The fresh fuels and 44 columns of fuels depleted over 1 cycle fill the core to start the second cycle. At the end of the second cycle, the core consists of one-third fuel depleted over 1 cycle and two-thirds fuel burnt over 2 cycles. Half of the 2 cycle burnt fuel is removed and replaced with another 22 columns of fresh fuel to start the next cycle. Hence cycle 3 starts with core loading of a third each of fresh fuels, fuels depleted over 1 cycle and fuels depleted over 2 cycles. At the end of the 3rd cycle, the core composition becomes one-third fuel depleted over 1 cycle, one-third fuel depleted over 2 cycles and one-third fuel depleted over 3 cycles. The fuels depleted over

3 cycles are the last of the initial fresh fuels loaded at BOC 1. These fuels are removed from the core and replaced by another set of fresh fuels. This is the beginning of the equilibrium cycle (BOEC). The cycle operated next is the equilibrium fuel cycle (EFC).

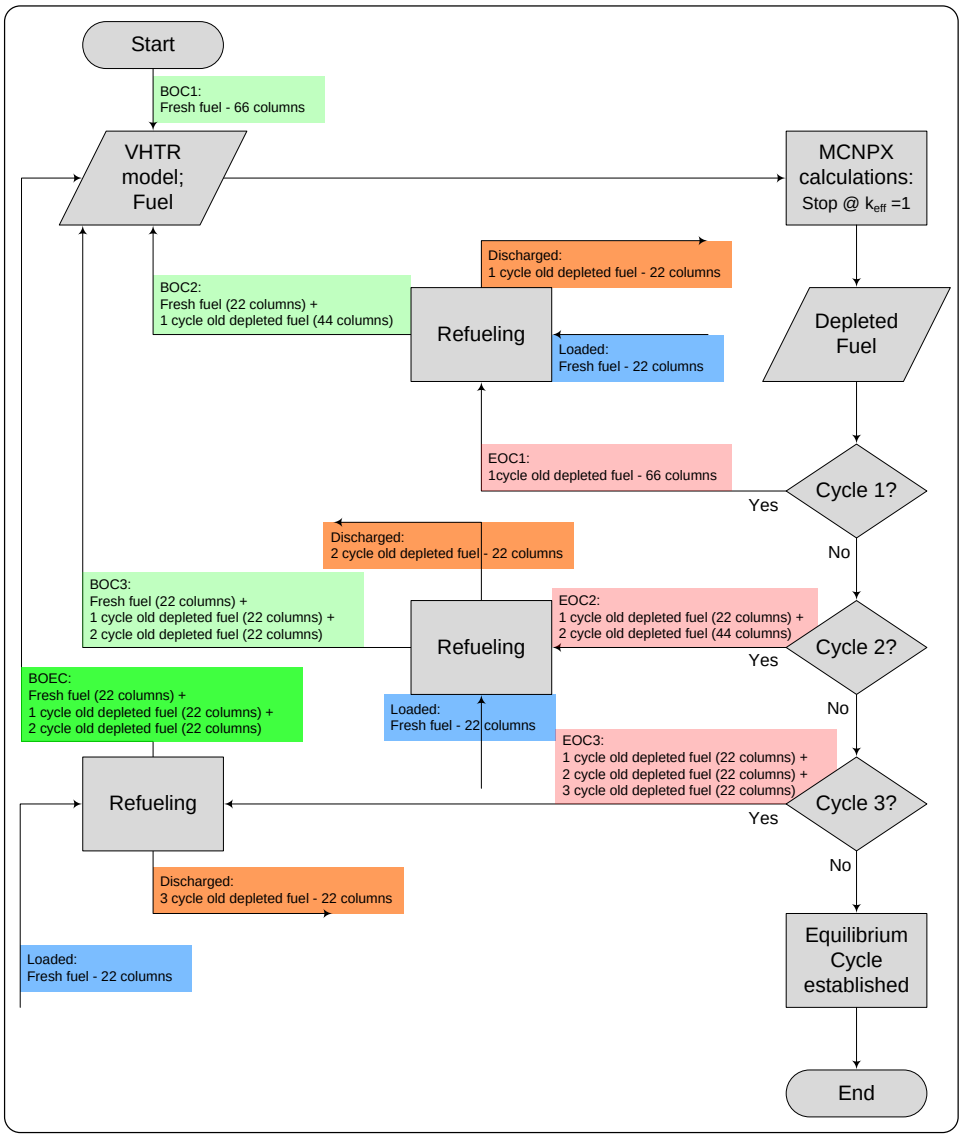

Fig. 25. Flowchart of the equilibrium fuel cycle approach.

Through the approach above, an EFC length of 405 day (approx. 14 months) is established for the VHTR fuel cycle. Figure 26 shows the k-effective over time from the start of the VHTR fuel cycle to the end of the first EFC. The first cycle lasts 910 days. This is equivalent to the length of a once-through-and-out cycle (OTOC) in the VHTR. A fresh fuel batch loaded into the core at BOEC will go through 3 EFCs before it is discharged from the core. Thus the effective full power days experienced by the batch is 1215 days. This is 34% improvement in the core lifetime of fresh fuel batches. This ensures deeper burn of the fuel loaded in the reactor system. In addition there are increased flux levels in the core under EFC. This potentially provides more neutrons to increase reaction rates for the transmutation of fission products. Table XXII provides the comparison of fuel cycle parameters between OTOC and EFC.

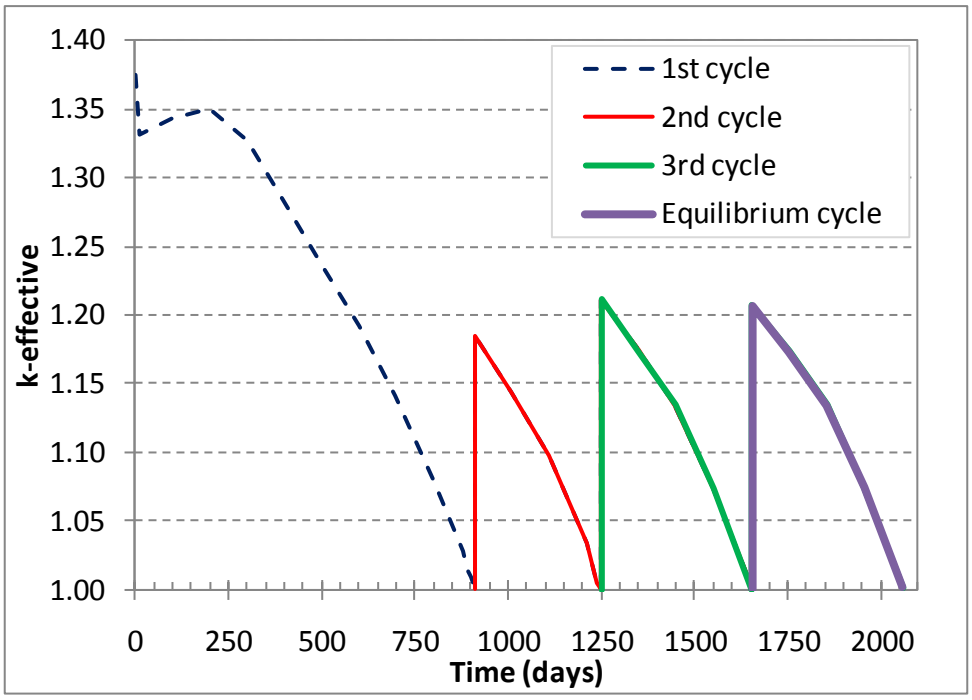

Fig. 26. K-effective vs. time leading to equilibrium fuel cycle.

Table XXII. VHTR fuel cycle parameters under OTOC and EFC.

Fuel cycle parameters	**OTOC**	**EFC**
starting k_{eff}	1.37477	1.20657
Average ν @ BOC	2.438	2.495
BOC flux (n/cm^2-s)	1.386E+14	1.993E+14
EOC flux/BOC flux	2.063	1.505
Effective lifetime of fuel batch (days)	910	1215
Average BU @ discharge of fuel (GWd/MTHM)	109	154

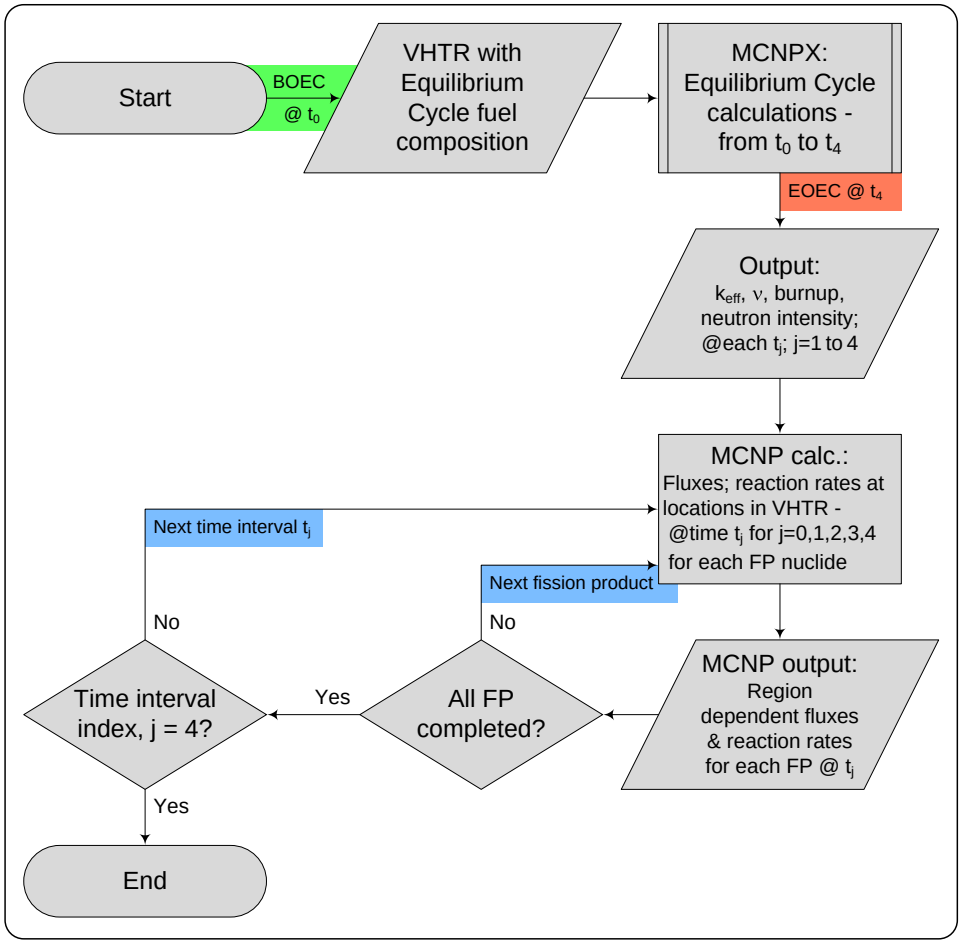

Fig. 27. Flowchart of the equilibrium fuel cycle.

IV.C DETERMINATION OF TRANSMUTATION REGIONS IN THE VHTR

Figure 27 provides the flowchart of the technique for the determination of various reaction rates in the VHTR during EFC. The neutronics parameters from the EFC simulation is performed with MCNPX over 4 time intervals between BOEC and EOEC. The stop criterion for the EOEC is at k-effective equals 1. Table XXIII summarizes the data for each time step.

Table XXIII. Neutronic parameters from the VHTR's EFC in 4 time steps.

Time step, t_j	time (days)	k-effective	flux (n/cm^2-s)	source intensity (n/s)
0	0.0	1.20657 ± 0.00101	1.993E+14	4.622E+19
1	100.0	1.17368 ± 0.00106	2.181E+14	4.654E+19
2	200.0	1.13439 ± 0.00099	2.378E+14	4.679E+19
3	300.0	1.07446 ± 0.00093	2.634E+14	4.705E+19
4	405.0	1.00116 ± 0.00103	2.999E+14	4.736E+19

The VHTR core model has radial and axial discretization. This is accomplished through the use of MCNP5's cylindrical mesh capability. Figure 28 shows the radial discretization. The discretization ensures each of the fuel zones are to a large extent, represented by a discrete region. Each radial region is made to represent a layer in the core's hexagonal array. For instance, there are 5 layers of reflector block forming the central reflector column. Hence 5 radial regions are imposed such that each region mostly represents each layer of the central reflector column. The dimensions of the radial discretization are thus determined to attain the conditions set above. Region 1 has a radius of 20.784cm. Regions 2 – 10 have thicknesses of 31.177cm each.

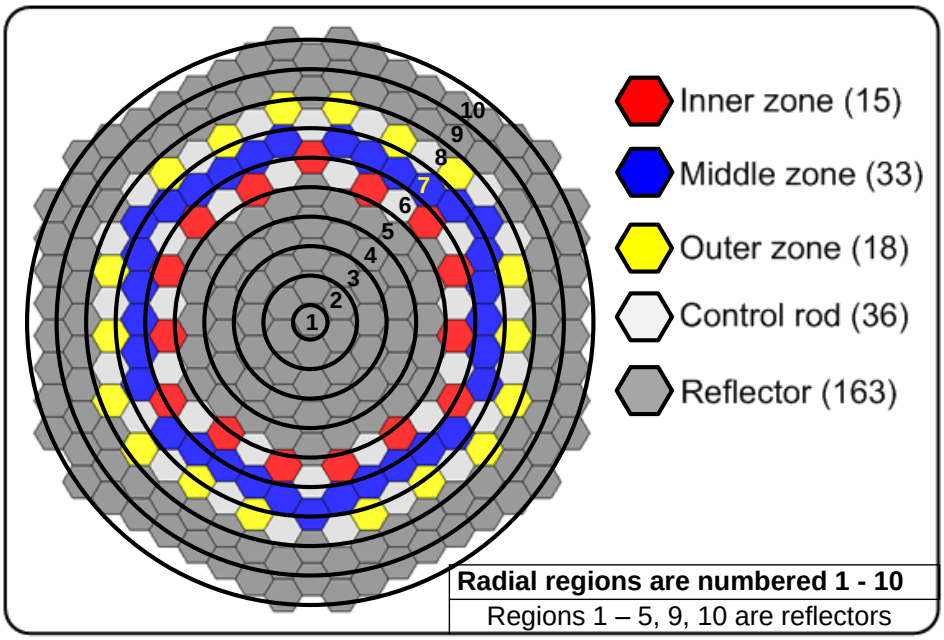

Fig. 28. VHTR core map with radial discretization.

The VHTR core configuration has its intrinsic axial regions. Hence the axial discretization of the core was chosen based on the height of the fuel and reflector blocks. This makes each axial region have a height of 58 cm. The 18 axial regions are labeled from bottom to the top. Axial regions 1 – 3 are the bottom reflectors. Regions 4 – 16 are the active core layers, while regions 17 and 18 are the top reflectors.

IV.C.1 Flux and Reaction Rates in the VHTR Core

Overall, there are 180 discrete regions in the VHTR. At each time t_j, the parameters from the EFC including depleted fuel composition are passed onto the MCNP5 model of the VHTR. Special tallies for scalar fluxes, energy-dependent fluxes and reaction rates for each FP nuclide are included in the MCNP calculations. These calculations are made for each discrete region of the VHTR.

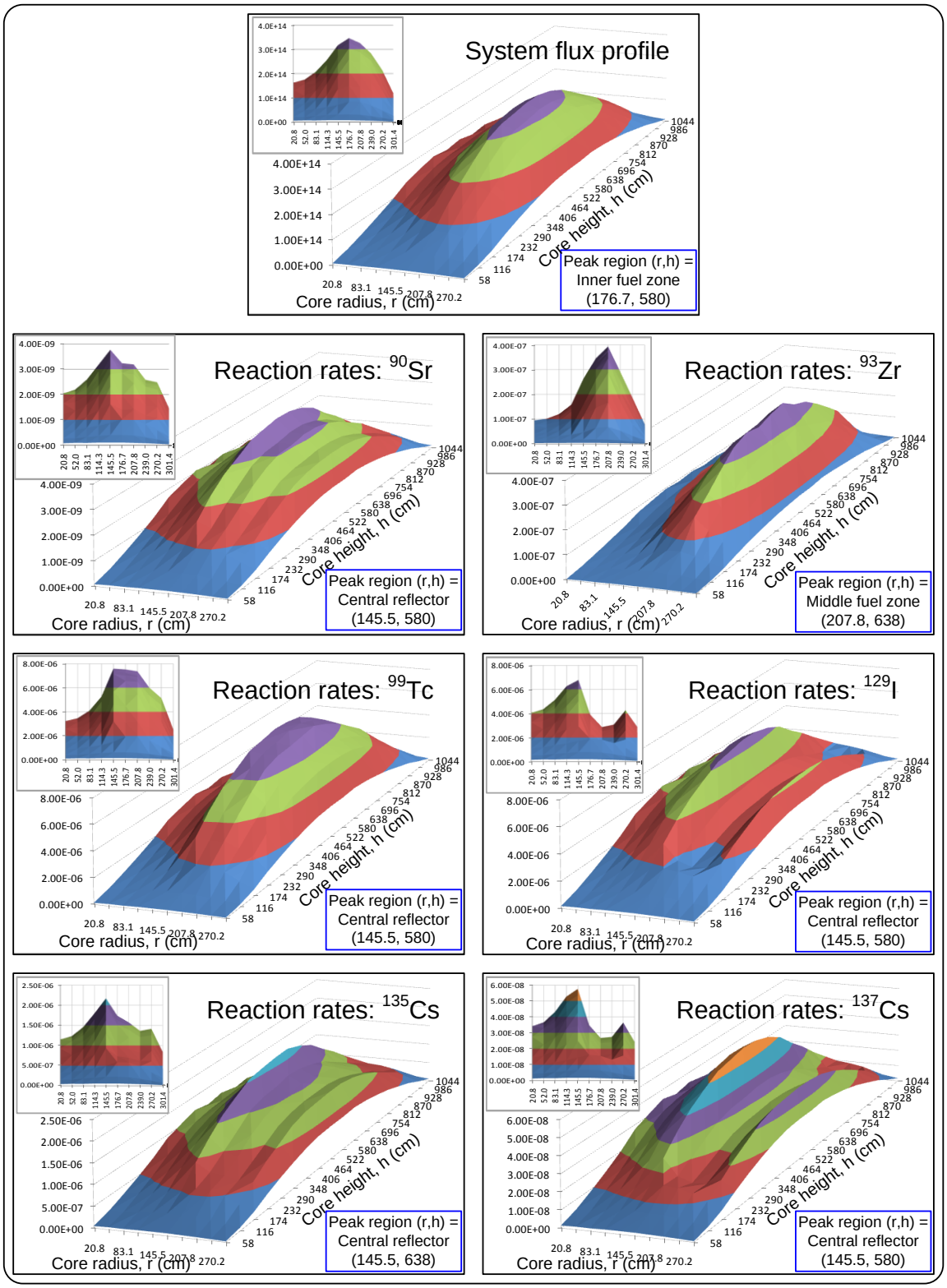

Fig. 29. Flux and reaction rate profiles in VHTR core at time t_0.

Figure 29 shows the scalar flux profile and reaction rates in the VHTR core at time t_0. The insert plot in each profile shown is the same profile viewed from the radial perspective. The peak flux is at the region defined by radial reference 6 and axial reference 10. This is the inner fuel zone at 7th axial layer of active fuel. This region bounds the central reflector, which facilitates increase in thermalized and reflected neutrons. Hence, a high neutron population and flux is expected in the region bounded by the central reflector.

The calculated FP reaction rates in the regions at time t_0 (see Fig. 29) indicate a shift in the location of peak reaction rate compared with the system flux. The peak reaction rate for ^{90}Sr, ^{99}Tc, ^{129}I and ^{137}Cs are at the region defined by the outer layer of the central reflector at the 7th axial layer of the active core. This region comprises of reflector blocks of the central column bounding the inner fuel zone. The peak ^{93}Zr reaction rate is at the middle fuel zone of the 8th axial layer of active fuel. The peak ^{135}Cs reaction rate is at the region defined by the outer layer of the central reflector at the 8th axial layer of the active core. These results confirm the theories presented in sections III.A.2 and III.A.3, which provide that the region of peak flux is not necessarily the region of peak reaction rate. The energy-dependent flux profiles in the fuel zones and the bounding reflector regions are provided in Figure 30. The energy profile in the region of peak ^{135}Cs reaction rate is similar to the profile at the peak reaction rate region for ^{90}Sr, ^{99}Tc, ^{129}I and ^{137}Cs. The central reflector region corresponding to the peak reaction rate region for ^{90}Sr et al. has the highest thermal neutron peak and the least contributions from resonance energy and fast neutrons. In contrast, the flux spectrum in the region of peak

^{93}Zr reaction rate – the middle fuel zone – has the highest resonance and fast neutron peak, and the lowest thermal neutron peak. The resonance integral capture cross section of ^{93}Zr is about 15 times its thermal neutron capture cross section (refer to Table IV), thus explaining the reason for its peak reaction rate in this region. It should be noted that region of peak ^{93}Zr reaction rate provides the worst reaction rates for ^{129}I and ^{137}Cs. This is evident in the dip on the reaction rate profiles for these nuclides at the middle fuel zone (see Fig. 29). The flux and reaction rate profiles in the core at time t_0 are similar to the profiles at other time instances t_1 to t_4. The differences in one time instance to another are the changes in regions of peak values, changes in absolute values of fluxes and reaction rates, and shifts in energy spectra over time as fuel composition changes in the core.

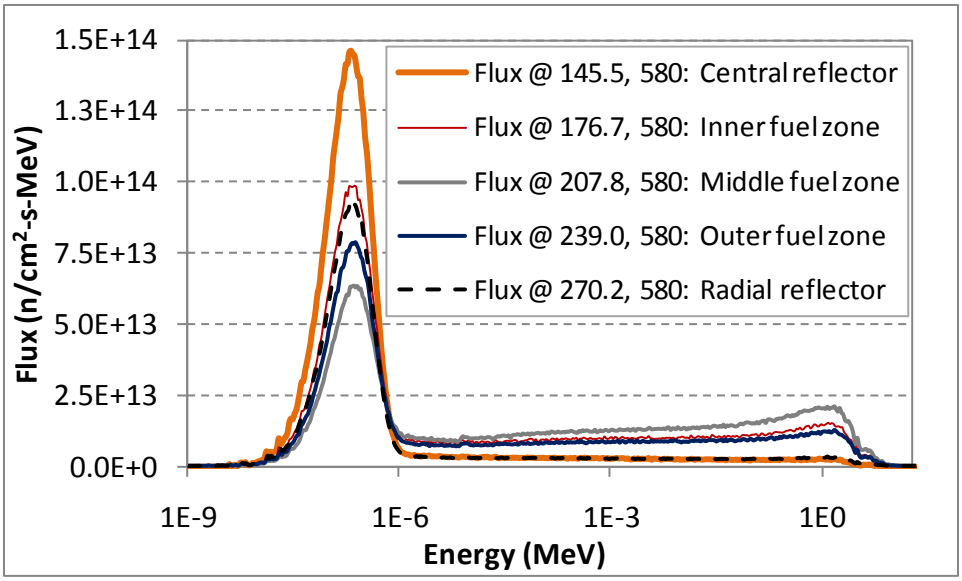

Fig. 30. Energy spectra in selected regions of VHTR core at time t_0.

IV.C.2 EFC-Integrated Reaction Rates

The reaction rates for each FP nuclide are calculated at 5 time instances t_0, t_1, t_2, t_3 and t_4 during the equilibrium fuel cycle. These are 0days, 100days, 200days, 300days and 405days of the EFC respectively. Table XXIV provides the coordinates of the regions of peak reaction rate for each radionuclide and at each time instance. Nuclides ^{93}Zr, ^{99}Tc and ^{135}Cs have shifts in regions of peak reaction rates. The peak ^{93}Zr reaction rate changes region at every time step except during the period between t_2 and t_3. The shift in peak ^{99}Tc reaction rate region starts after the first 200 days, while ^{135}Cs peak shift occurs after the first 100 days. However, ^{90}Sr, ^{129}I and ^{137}Cs maintain the same peak reaction rate location throughout the fuel cycle. All shifts in peak region are in the axial direction. Location of peak reaction rates are maintained in the radial direction.

Table XXIV. Regions of peak reaction rates for selected nuclides.

Nuclide	Locations [r(cm),h(cm)]				
	t_0 = 0days	t_1 = 100days	t_2 = 200days	t_3 = 300days	t_4 = 405days
^{90}Sr	145.5, 580	145.5, 580	145.5, 580	145.5, 580	145.5, 580
^{93}Zr	207.8, 638	207.8, 580	207.8, 522	207.8, 522	207.8, 580
^{99}Tc	145.5, 580	145.5, 580	145.5, 580	145.5, 522	145.5, 580
^{129}I	145.5, 580	145.5, 580	145.5, 580	145.5, 580	145.5, 580
^{135}Cs	145.5, 638	145.5, 580	145.5, 580	145.5, 580	145.5, 580
^{137}Cs	145.5, 580	145.5, 580	145.5, 580	145.5, 580	145.5, 580

The reaction rates at time instances t_0, t_1, t_2, t_3 and t_4 of the EFC are not individually sufficient in the evaluation of the best core location to achieve the highest transmutation. An integral value of reaction rates is a better determining factor. Recall equations (26) and (27) from section III.A.4, which provides the driver for maximum transmutation in the core. These equations are of the form:

$$N_{minimum\ after\ transmutation\ over\ time\ t} = N_0 \exp\left[\frac{-1}{N_0}F(t)\right] \tag{36}$$

It is assumed that there is no core shuffling between BOEC and EOEC, which makes equation (26) more appropriate for the conditions in the VHTR. Thus $F(t)$ for the VHTR is:

$$F(t) = \max_{1 \le i \le n} \sum_{j=1}^{4} \int_{t_{j-1}}^{t_j} R_{i,j}\, dt \tag{37}$$

$F(t)$ can also be written in terms of average reaction rates over a period from t_0 to t_4. This is given in equation (38).

$$F(t) = \max_{1 \le i \le n} R_{i,Ave}(t_4 - t_0) \tag{38}$$

A numeric approximation of equation (37) is obtained by setting the reaction rate $R_{i,j}$ at the time step between t_j and t_{j-1} as the average of the reaction rates at t_j and t_{j-1}. Also, dt is determined as $(t_j - t_{j-1})$. Hence equation (37) becomes:

$$F(t) = \max_{1 \le i \le n} \sum_{j=1}^{4} \frac{1}{2}\left(R_{i,j} + R_{i,j-1}\right)\left(t_j - t_{j-1}\right) \tag{39}$$

Thus from equation (38) and (39), the average reaction rate in the i^{th} region of the VHTR over the lifetime of the EFC can be written as:

$$R_{i,Ave} = \frac{1}{(t_4 - t_0)} \sum_{j=1}^{4} \frac{1}{2}\left(R_{i,j} + R_{i,j-1}\right)\left(t_j - t_{j-1}\right) \tag{40}$$

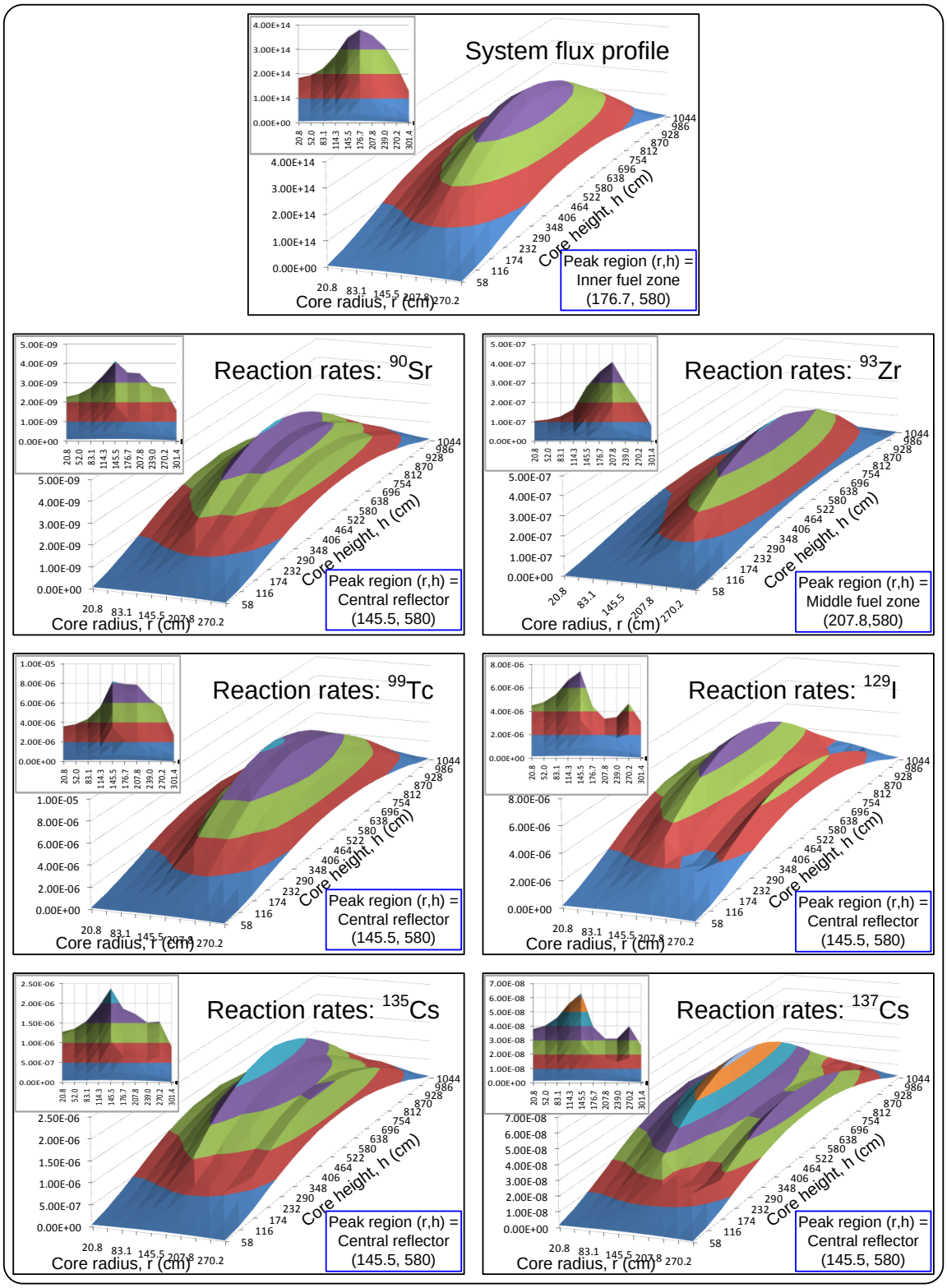

Fig. 31. Average flux and reaction rates profiles in VHTR core during EFC.

Equation (40) is applied to the reaction rates calculate by MCNP and the resultant average rate profile is shown in Figure 31. The location of the peak average reaction rates for each nuclide is the same as the peak location at time t_4. Table XXV provides the summary of the peak reaction rates, locations and transmutation potential. The ratio $\lambda/\sigma_c\phi$ for each nuclide indicates that each nuclide are transmutable in the VHTR. The region of peak reaction rate provides the maximum transmutation possible in the VHTR. The $\lambda/\sigma_c\phi$ ratios at the peak reaction rate locations are less than 1, which indicate that nuclide transformation by neutron capture dominates the transmutation process for each nuclide.

Table XXV. Summary of integrated reaction rates.

Nuclide	Peak location	$T_{1/2}$ (yrs)	λ	$R_{i,ave}$, ($\sigma_c\phi$)	$\lambda/(\sigma_c\phi)$
^{90}Sr	145.5, 580	28.9	7.60E-10	4.11E-09	0.1848
^{93}Zr	207.8, 580	1,500,000	1.46E-14	4.08E-07	3.59E-08
^{99}Tc	145.5, 580	213,000	1.03E-13	8.19E-06	1.26E-08
^{129}I	145.5, 580	15,700,000	1.40E-15	7.41E-06	1.89E-10
^{135}Cs	145.5, 580	2,300,000	9.55E-15	2.37E-06	4.03E-09
^{137}Cs	145.5, 580	30.07	7.30E-10	6.30E-08	0.0116

IV.D FP TRANSMUTATION

The analyses so far have shown that the selected FP can be successfully transmuted in VHTR core. The region of the VHTR at which maximum transmutation of each nuclide can be attained has been identified. The next task is the simulation of the FP transmutation. The goal at this stage is the evaluation of the transmutation impact over a long period. Since most reactors currently operating are licensed for about 40 years, a similar operating life appears reasonable for a VHTR. For this purpose, a 30 year

irradiation period is selected together with 10 year post-irradiation cooling for the FP targets. There are 27 EFCs in a 30 year period for a cycle of 405 effective full power days. For one EFC calculations performed with MCNPX, the computer labor time is 47.25 hours. This translates to a 53 day computer time for the completion of a 30 year FP irradiation calculations with MCNPX. Thus it is expensive to perform the simulation solely with MCNPX.

A faster approach to the simulation exists. Figure 32 shows the flowchart for the integrated simulation process employing MCNP and ORIGEN-S. This is done by supplying the MCNP calculated VHTR neutronic parameters during the EFC to ORIGEN-S for the simulation of multiple EFCs. The ORIGEN-S simulations also include a 10 year decay period after the 30 year irradiation. The ORIGEN-S calculations are less than 2 minutes each.

The advantage of this approach is in faster computation times. However there is a drawback to this approach. Cinder90, which is the depletion tool in MCNPX, performs depletion based on 63-group flux and 63-group cross sections [53]. This results in robust transmutation calculations. Unlike Cinder90, ORIGEN-S performs depletion calculations based on 3-group flux parameters and 3-group cross sections [54]. This is a less rigorous transmutation calculation than MCNPX's Cinder90. The result of this is that ORIGEN-S transmutation results could be less accurate than MCNPX's results. Nonetheless, ORIGEN-S has been extensively verified and validated thus making results from the code acceptable with proper recognition of inherent limitations.

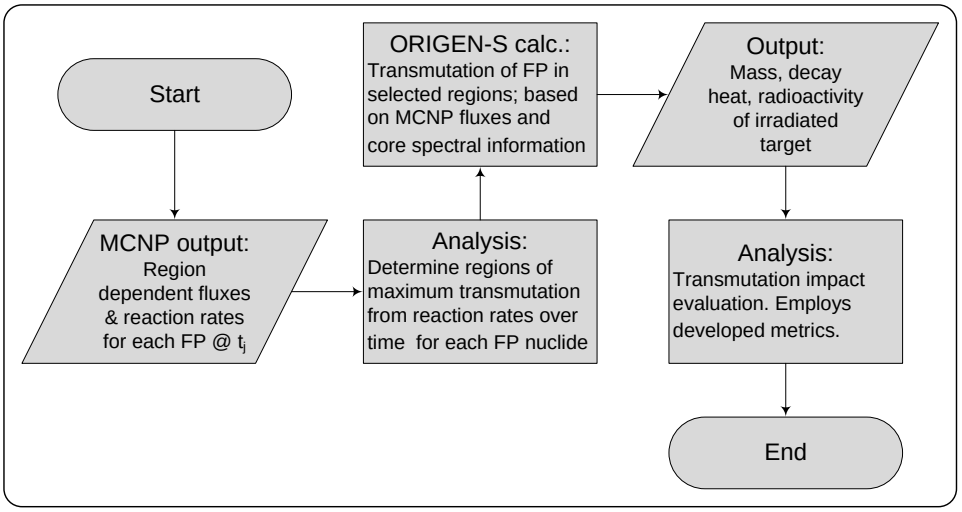

Fig. 32. Flowchart of the integrated simulation approach for FP transmutation evaluations.

In addition, the simulation procedure assumes transmutation of elemental targets. This implies that each target radionuclide is not separated from its other isotopes present in spent nuclear fuels. For instance, in the transmutation of ^{90}Sr, it is assumed that the target consists of ^{87}Sr, ^{88}Sr and ^{90}Sr. The percentage abundance of each nuclide is adopted from its ^{235}U fission yield. The mass basis for each target is 1 kg. It should be noted that ^{95}Zr is included in the zirconium composition. In practical situations, the nuclide would be completely decayed off before the zirconium stream is fabricated into targets. In this analysis, ^{95}Zr is included since it is part of the initial zirconium yield from fission reaction. The inclusion of the nuclide would not have any effect on the transmutation of ^{93}Zr since it is a heavier isotope. Table XXVI provides the yield data for all selected radionuclides and their stable and/or long lived isotopes.

The ORIGEN-S simulations employ the ENDF/B-VI.8 cross sections. The results from the simulations are analyzed with the metrics developed in section III.B. The

analyses are used to evaluate the radiotoxicity impact of the FP transmutation strategy. This is discussed in Chapter V.

Table XXVI. Yields of significant fission products from ^{235}U and ^{239}Pu

Nuclide	U235	Pu239
Sr86	0.000%	0.004%
Sr87	21.483%	22.621%
Sr88	29.998%	29.964%
Sr90	48.519%	47.411%
Total	100.000%	100.000%

Nuclide	U235	Pu239
Zr90	13.356%	8.276%
Zr91	13.462%	9.779%
Zr92	13.909%	11.834%
Zr93	14.659%	14.935%
Zr94	14.950%	16.997%
Zr95	15.021%	18.947%
Zr96	14.643%	19.232%
Total	100.000%	100.000%

Nuclide	U235	Pu239
Tc99	100.000%	100.000%

Nuclide	U235	Pu239
I127	22.413%	26.961%
I129	77.587%	73.039%
Total	100.000%	100.000%

Nuclide	U235	Pu239
Cs133	34.484%	33.025%
Cs134	0.000%	0.003%
Cs135	33.660%	35.871%
Cs137	31.855%	31.101%
Total	100.000%	100.000%

CHAPTER V

FP RADIOTOXICITY EVALUATION

This chapter discusses the results of the FP transmutation strategy. Analyses of the inventories after 30 years of irradiation and 10 year cooling are presented. The 30 year irradiation and 10 year cooling transmutation approach is subsequently referred to as 30+10 scenario. The results of the transmutation of each FP target are discussed. For the transmutation scenario, the inventories of newly created nuclides, their contribution to the radioactivity and decay heat generation are analyzed. The results are compared with decay-only scenarios for each FP. The inventory, radioactivity and decay heat values are obtained directly from ORIGEN-S output. The dose values are calculated from the radioactivity values based on the ICRP effective dose coefficients for ingestion. Further analyses using the metrics developed (see section III.B) are presented. Figure 33 shows the summary of this chapter.

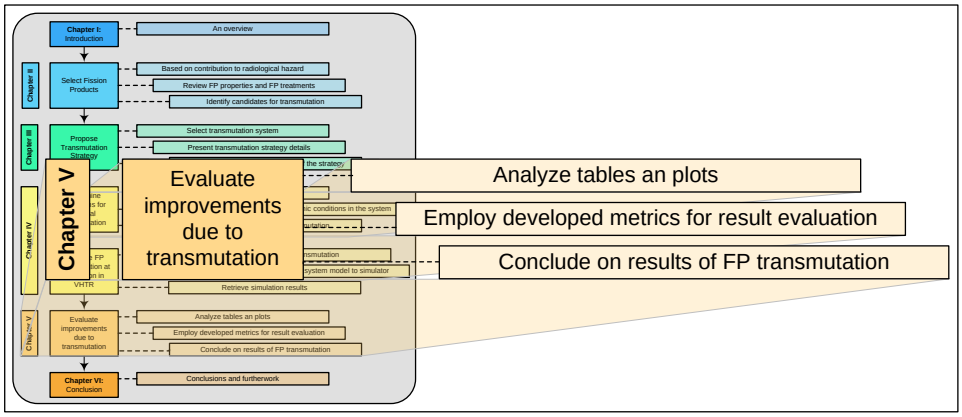

Fig. 33. Key focus of Chapter V.

V.A STRONTIUM TRANSMUTATION

Figure 34 shows the results of the transmutation strategy on strontium vector in comparison with decay only scenario. The initial composition of the strontium is 214.8g, 300g and 485.2g of ^{87}Sr, ^{88}Sr and ^{90}Sr respectively. The inventory after 30 year irradiation is shown in Fig. 34(a). There is no buildup of ^{90}Sr from lighter isotopes since the total combined inventory of ^{87}Sr and ^{88}Sr is not significantly changed over the irradiation period. The neutron capture link between ^{88}Sr and ^{90}Sr is ^{89}Sr, which is not a naturally occurring isotope. The thermal and epithermal capture cross sections of ^{88}Sr are about 2 orders of magnitude lower than the corresponding ^{89}Sr cross sections. Hence, there is no significant production of ^{89}Sr that can lead to additional ^{90}Sr. There is improvement in inventory reduction through the transmutation strategy. The initial ^{90}Sr content is reduced to 203.9g. The same initial ^{90}Sr inventory reduces to 232.1g in a 30 year decay-only scenario. This represents additional 5.8% reduction in the initial inventory during the 30 year irradiation period. It should be noted that 0.04g of ^{93}Zr was produced by the end of the irradiation period. However, the ^{93}Zr does not significantly add to the radiotoxicity of the discharged vector.

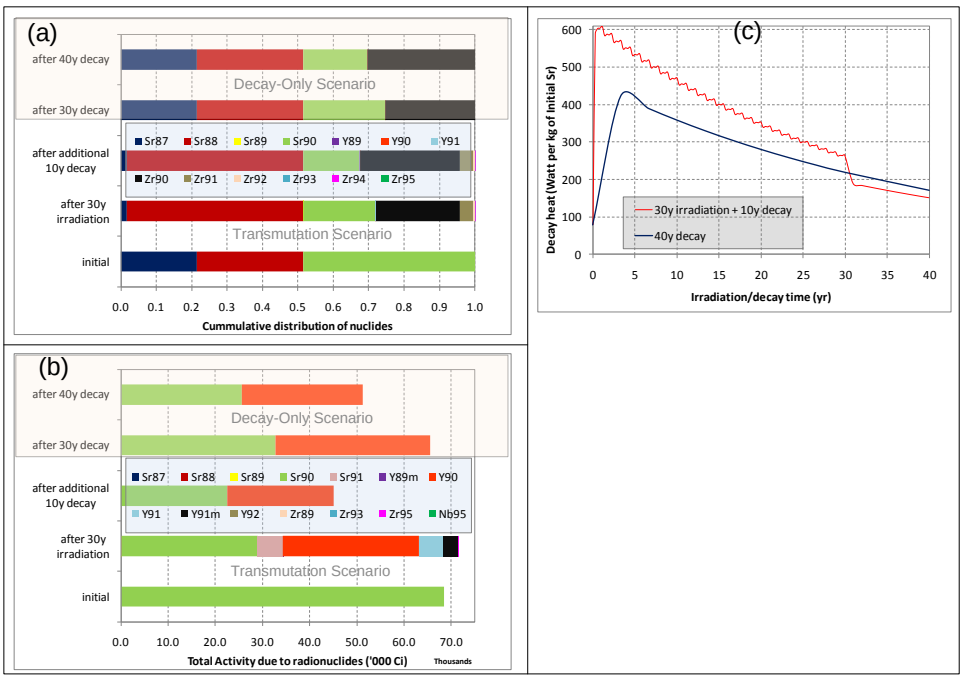

Fig. 34. Transmutation scenario vs. decay-only scenario for strontium vector. (a) inventories; (b) radioactivity; (c) decay heat.

The radioactivity of the vector at discharge is slightly higher than that of a 30 year decay-only scenario. However, after additional 10 year cooling, the radioactivity of the vector under transmutation scenario is lower than that of a similar vector in 40 year decay-only scenario (see Fig. 34(b)). The reduction in radioactivity is largely due to the decay of ^{91}Sr, ^{91m}Y and ^{91}Y with half-lives of 9.5 hrs, 49.7 minutes and 58.5 days respectively. The activity at the 40 year mark is only due to the residual ^{90}Sr and its daughter, ^{90}Y.

The decay heat profiles from the vector under both decay-only and transmutation scenarios are shown in Figure 34(c). During the 30 year irradiation, the heat generated in transmutation scenario is higher than the heat from decay-only scenario. However, 10 year post irradiation decay results in the reduction of decay heat below the level expected

in decay only scenario. The reduction in decay heat is largely due to the decay of ^{91}Sr, ^{91m}Y and ^{91}Y. The residual decay heat generation is from ^{90}Sr and ^{90}Y.

Table XXVII. Ingestion dose equivalent from strontium vector.

Nuclide	Ingestion Equivalent Dose (mrem)		
	initial	30yr irradiation + 10yr decay	40yr decay
Sr90	191.77	63.17	71.74
Y90	0	6.09	6.92
Y91	0	2.04E-19	0
Zr93	0	3.03E-09	0
Zr95	0	4.38E-24	0
Nb94	0	4.12E-14	0
Nb95	0	6.57E-24	0
Nb95m	0	3.28E-26	0
Nb93m	0	4.54E-10	0
Total	**191.77**	**69.26**	**78.66**

Table XXVII provides the ingestion dose equivalent for the vector. The total dose equivalent in the transmutation scenario is lower than the dose from the decay-only scenario. ^{90}Sr and ^{90}Y are responsible for the dose equivalent of the residuals in both transmutation and decay-only scenarios. The dose equivalent contributed by the additional radionuclides created during irradiation is insignificant after the addition 10 year of cooling has passed.

Table XXVIII provides the evaluation of transmutation strategy on ^{90}Sr. Overall, there is improvement in the reduction in ^{90}Sr parameters under transmutation scenario compared to decay-only scenario. The initial ^{90}Sr inventory was reduced by 67.1%. In a decay-only scenario, this is 62.6%. The residual ^{90}Sr contributes 50% of the vector's radioactivity. The other 50% is from ^{90}Y, which is in transient equilibrium with ^{90}Sr. Most of the decay heat is contributed by ^{90}Y; however, ^{90}Sr is responsible for 91.2% of the equivalent ingestion dose. The transmutation effectiveness factor is less than one for

both ^{90}Sr and the strontium vector as whole. This indicates that there is little advantage gained in the transmutation of ^{90}Sr.

Table XXVIII. Summary of metrics on strontium target in 30+10 scenario.

Metric	Value
Fraction of ^{90}Sr transmuted $f_{i = Sr90}$	0.671
Fraction of total radioactivity contributed to FP target $f_{A,iout}$	0.500
Fraction of total decay heat contributed to FP target $f_{Q,iout}$	0.173
Fraction of effective dose contributed to FP target $f_{D,iout}$	0.912
Transmutation Effectiveness Factor for ^{90}Sr, $x_{i = Sr90}$	0.880
Transmutation Effectiveness Factor for the target, x_{Target}	0.910

V.B ZIRCONIUM TRANSMUTATION

Figure 35 shows the results of the transmutation strategy on zirconium vector in comparison with decay only scenario. The initial composition of the zirconium is 146.6g, and 150.2g of ^{93}Zr and ^{95}Zr respectively. The stable zirconium isotopes make up the rest of the 1 kg initial zirconium loading. The inventory after 30 year irradiation is shown in Fig. 35(a). The combined inventory of ^{90}Zr to ^{94}Zr is not significantly changed over the irradiation period. This indicates that there is no significant transmutation of lighter isotopes to ^{95}Zr. Similarly, the combined inventory of ^{90}Zr, ^{91}Zr and ^{92}Zr is not significantly changed; an indication that there is no buildup of ^{93}Zr from lighter isotopes. The main transformation in the zirconium vector is the transmutation of ^{93}Zr to stable ^{94}Zr. This supports the behavior and results expected in the transmutation of elemental zirconium (see section II.B.2). All zirconium isotopes have small capture cross sections. However, ^{93}Zr capture cross section is much higher than those of other isotopes (see Table IV). It should be noted that 19.2g of the initial 146.4g of ^{96}Zr is transmuted to

higher elements. The transformation of the initial ^{95}Zr also created higher elements. Most of the higher elements created are stable isotopes of molybdenum and ruthenium. The most important radionuclide created from the higher elements is 0.4g of ^{99}Tc, which does not significantly add to the radiotoxicity of the discharged vector.

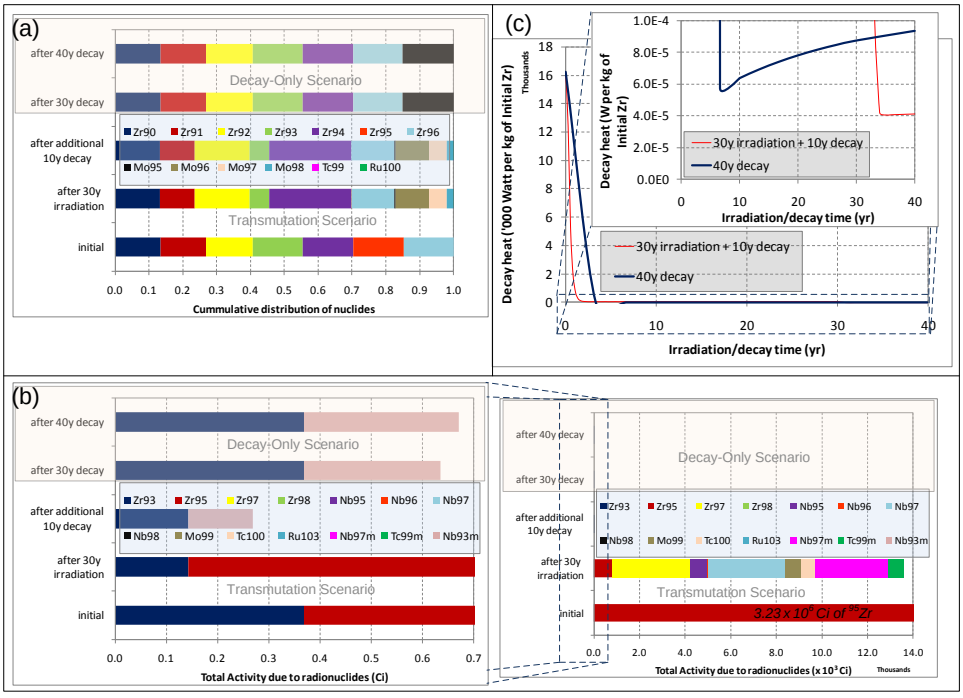

Fig. 35. Transmutation scenario vs. decay-only scenario for zirconium vector. (a) inventories; (b) radioactivity; (c) decay heat.

The initial radioactivity is largely due to the presence of ^{95}Zr. The contribution of ^{95}Zr to the radioactivity is completely lost in the first 2 years of irradiation and/or decay. Figure 35(b) shows that the radioactivity of the vector at discharge is much higher than that of a 30 year decay-only scenario. However, after additional 10 year cooling, the radioactivity of the vector under transmutation scenario is lower than that of a similar vector in 40 year decay-only scenario (see Fig. 35(b)). The reduction in radioactivity during the additional 10 year cooling is largely due to the decay of residual ^{95}Zr, ^{97}Zr,

^{95}Nb, ^{97m}Nb, ^{97}Nb, ^{99}Mo, ^{99m}Tc and ^{100}Tc. The radionuclides are also responsible for the post irradiation decay heat load. After the cooling period, the activity is only due to the residual ^{93}Zr and its daughter, ^{93m}Nb.

The decay heat profiles from the vector under both decay-only and transmutation scenarios are shown in Figure 35(c). The initial decay heat is largely due to the ^{95}Zr. This is lost after the complete transformation of ^{95}Zr. During the 30 year irradiation, the heat generated in transmutation scenario is higher than the heat from decay-only scenario. However, 10 year post irradiation decay of the nuclides listed above results in the reduction of decay heat below the level expected in decay-only scenario. The residual decay heat generation is from ^{93}Zr and ^{93m}Nb.

Table XXIX. Ingestion dose equivalent from zirconium vector.

Nuclide	Ingestion Equivalent Dose (mrem)		
	initial	30yr irradiation + 10yr decay	40yr decay
Zr93	1.03E-05	3.99E-06	1.03E-05
Zr95	283.89	4.74E-19	0
Nb93m	0	1.52E-06	3.63E-06
Nb94	0	2.22E-09	0
Nb95	0	7.11E-19	0
Nb95m	0	3.55E-21	0
Tc99	0	5.18E-07	0
Ru103	0	2.26E-32	0
Total	**283.89**	**6.03E-06**	**1.39E-05**

Table XXIX provides the ingestion dose equivalent for the zirconium vector. The total dose equivalent in the transmutation scenario is lower than the dose from the decay-only scenario. This indicates less radiotoxicity of the zirconium vector from the 30+10 transmutation scenario. ^{93}Zr and ^{93m}Nb are responsible for the dose equivalent of the residuals in both transmutation and decay-only scenarios. ^{99}Tc contributes 8.6% of the

equivalent dose from the transmutation vector. After the post irradiation period, the dose equivalent contributed by the additional radionuclides created during irradiation is insignificant.

Unlike the transmutation scenario, there is no significant reduction in the zirconium parameters under decay-only scenario. Table XXX provides the evaluation of transmutation strategy on ^{93}Zr. The transmutation scenario shows improvement in the reduction in ^{93}Zr parameters compared to decay-only scenario. The initial ^{93}Zr inventory was reduced by 61.3%. The residual ^{93}Zr contributes 51.7% of the vector's radioactivity and 38.9% of the decay heat. ^{93}Zr is responsible for 66.2% of the ingestion dose equivalent. The transmutation effectiveness factor is less than one for both ^{93}Zr and the zirconium vector. The transmutation effectiveness factor for ^{93}Zr indicates that there is significant advantage gained by transmuting the radionuclide. The transmutation effectiveness factor for the zirconium vector indicates less radiological hazard from the transmutation vector compared with decay-only zirconium vector.

Table XXX. Summary of metrics on zirconium target in 30+10 scenario.

Metric	Value
Fraction of ^{93}Zr transmuted $f_{i = Zr93}$	0.613
Fraction of total radioactivity contributed to FP target $f_{A,iout}$	0.517
Fraction of total decay heat contributed to FP target $f_{Q,iout}$	0.389
Fraction of effective dose contributed to FP target $f_{D,iout}$	0.662
Transmutation Effectiveness Factor for ^{93}Zr, $x_{i = Zr93}$	0.387
Transmutation Effectiveness Factor for the target, x_{Target}	0.571

V.C TECHNETIUM TRANSMUTATION

Figure 36 shows the results of the transmutation strategy on technetium vector in comparison with decay only scenario. The initial technetium composition is 1 kg of ^{99}Tc. There is no appreciable ^{99}Tc inventory decrease in the decay-only scenario (see Fig. 36(a)). The inventory after 30 year irradiation is shown in Fig. 36(a). After transmutation, the ^{99}Tc content is 32.9g. The significant nuclides of the discharged vector are ^{99}Tc, ^{100}Ru, ^{101}Ru and ^{102}Ru. The nuclides represent 993.1g of the discharged vector. All the nuclides except ^{99}Tc are stable. The highly radioactive nuclides of the discharged vector are ^{100}Tc, ^{103}Ru and ^{104}Rh, which represent 0.12g of the discharged inventory.

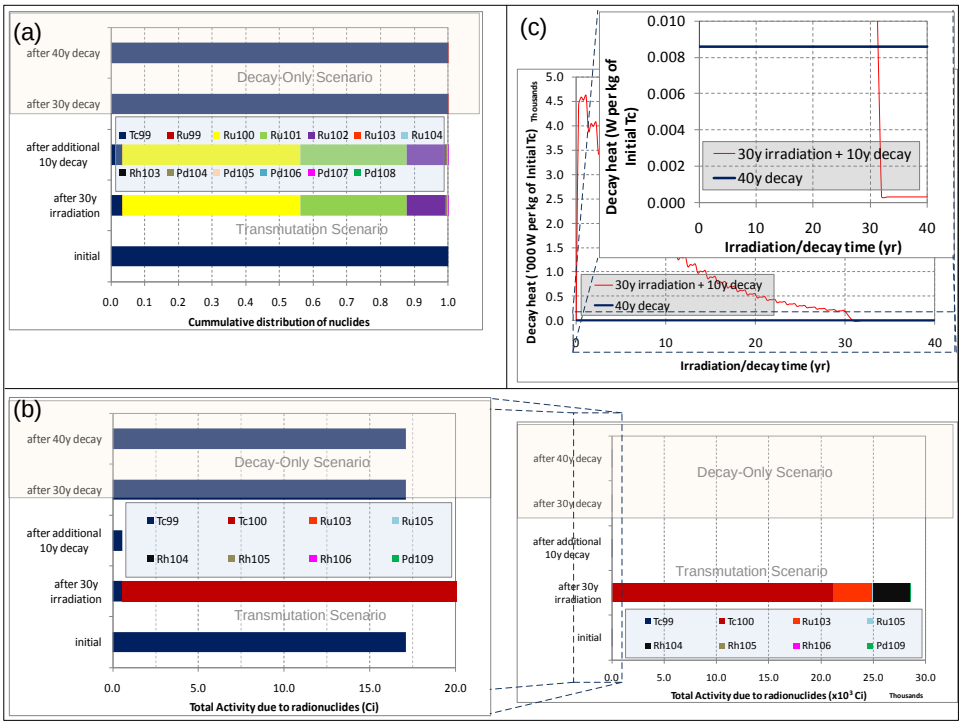

Fig. 36. Transmutation scenario vs. decay-only scenario for technetium vector. (a) inventories; (b) radioactivity; (c) decay heat.

Figure 36(b) shows the radioactivity of the transmutation vector. The initial radioactivity is due to ^{99}Tc. The radioactivity of the vector at discharge is much higher than that of a 30 year decay-only scenario (see Fig. 36(b)). However, after additional 10 year cooling, the total decay of ^{100}Tc, ^{103}Ru and ^{104}Rh reduce the radioactivity below that of a similar vector in 40 year decay-only scenario (see Fig. 36(b)). The radionuclides are also responsible for the post irradiation decay heat load. After the cooling period, the activity is only due to the residual ^{99}Tc.

The decay heat profiles from the vector under both decay-only and transmutation scenarios are shown in Figure 36(c). The initial decay heat is only due to ^{99}Tc. During the 30 year irradiation, the heat generated in transmutation scenario is higher than the heat from decay-only scenario. However, the decay heat is reduced below the level expected in decay-only scenario after the post irradiation decay period. The residual decay heat generation is from ^{99}Tc.

Table XXXI. Ingestion dose equivalent from technetium vector.

Nuclide	Ingestion Equivalent Dose (mrem)		
	initial	30yr irradiation + 10yr decay	40yr decay
Tc99	1.33E-03	4.46E-05	1.33E-03
Ru103	0	2.74E-29	0
Ru106	0	8.26E-13	0
Pd107	0	1.59E-12	0
Total	**1.33E-03**	**4.46E-05**	**1.33E-03**

Table XXXI provides the ingestion dose equivalent for the technetium vector. The total dose equivalent in the transmutation scenario is lower than the dose from the decay-only scenario. This indicates less radiotoxicity of the residual vector from the 30+10 transmutation scenario. ^{99}Tc is responsible for the dose equivalent of the residual

vector in both transmutation and decay-only scenarios. After the post irradiation decay period, there is no significant contribution to dose equivalent by the radionuclides created during irradiation period.

The decay-only scenario does not provide significant reduction in the technetium parameters. The transmutation scenario indicates appreciable reductions in the parameters. Table XXXII provides the evaluation of transmutation strategy on ^{99}Tc. The initial ^{93}Zr inventory was reduced by 96.7%. The residual ^{99}Tc is responsible for 100% of the residual vector's radioactivity, decay heat and dose equivalent. The transmutation effectiveness factor is less than one for both ^{99}Tc and the residual vector. The transmutation effectiveness factor for ^{99}Tc indicates that there is significant advantage gained by transmuting the radionuclide. The transmutation effectiveness factor for the zirconium vector indicates less radiological hazard from the transmutation vector compared with decay-only vector.

Table XXXII. Summary of metrics on technetium target in 30+10 scenario.

Metric	Value
Fraction of ^{99}Tc transmuted $f_{i = Tc99}$	0.967
Fraction of total radioactivity contributed to FP target $f_{A,iout}$	1.000
Fraction of total decay heat contributed to FP target $f_{Q,iout}$	1.000
Fraction of effective dose contributed to FP target $f_{D,iout}$	1.000
Transmutation Effectiveness Factor for ^{99}Tc, $x_{i = Tc99}$	0.033
Transmutation Effectiveness Factor for the target, x_{Target}	0.275

V.D IODINE TRANSMUTATION

Figure 37 shows the results of the transmutation strategy on iodine vector in comparison with decay only scenario. The initial composition of the iodine is 224.1g, and 775.9g of ^{127}I and ^{129}I respectively. The inventory after 30 year irradiation is shown in Fig. 37(a). After transmutation, the ^{129}I content is 16.2g. The xenon content of the discharged vector is 901.1g, which consists of isotopes ^{128}Xe to ^{132}Xe, and ^{134}Xe. This includes 0.6g of ^{131m}Xe, which is the only significant radioactive isotope of xenon in the discharged vector. Other radionuclides of notable quantity in the discharged vector include 0.6g of ^{134}Cs, 2.8g of ^{135}Cs, 0.02g of ^{133}Xe, 0.01g of ^{136}Cs and 0.004g of ^{130}I.

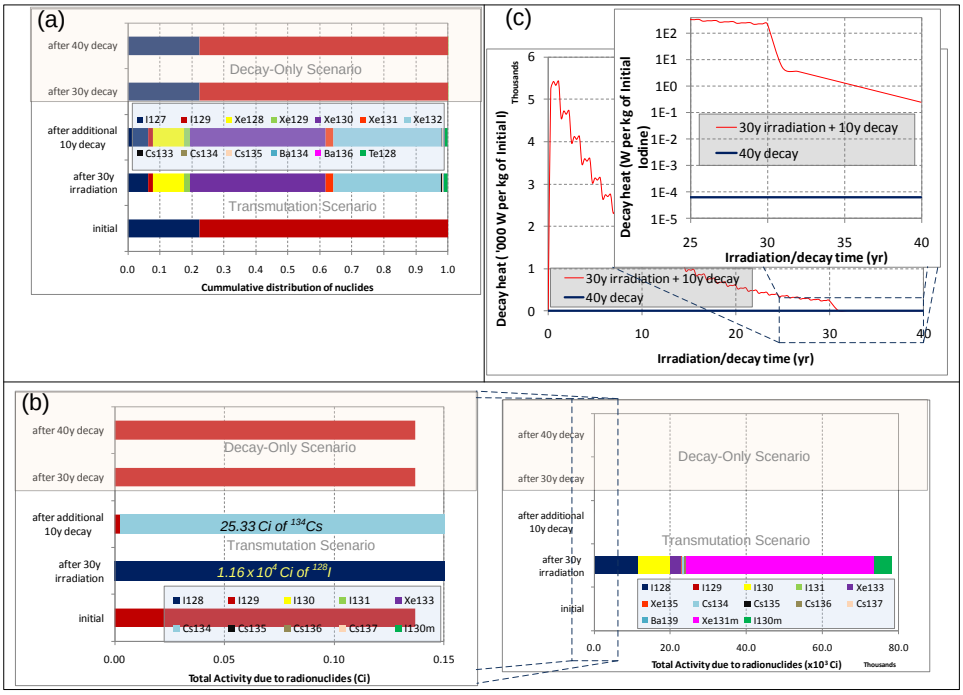

Fig. 37. Transmutation scenario vs. decay-only scenario for iodine vector. (a) inventories; (b) radioactivity; (c) decay heat.

Figure 37(b) shows that the radioactivity of the transmutation vector. The initial radioactivity is only due to ^{129}I. The radioactivity of the vector at discharge is

7.829×10^4 Ci, which is much higher than that of a 30 year decay-only scenario (see Fig. 37(b)). However, after additional 10 year cooling, the total decay of ^{128}I, ^{130m}I, ^{130}I, ^{131m}Xe, ^{133}Xe and ^{136}Cs reduces the radioactivity to 25.4 Ci. This is still higher than that of iodine vector in 40 year decay-only scenario (see Fig. 37(b)). Almost all of the residual activity is from ^{134}Cs. Additional 16 years of cooling is required to reduce the total activity below the level from a decay-only scenario.

The radionuclides listed above are responsible for the post irradiation decay heat of the discharged vector. The decay heat profiles from the vector under both decay-only and transmutation scenarios are shown in Figure 37(c). The initial decay heat is only due to ^{129}I. During the 30 year irradiation, the heat generated in transmutation scenario is higher than the heat from decay-only scenario. A 10 year post irradiation cooling period is not sufficient to reduce the decay heat to comparable level as the decay-only scenario. Since the bulk of the decay heat generated after the cooling period is from ^{134}Cs, additional cooling of up to 20 years (about 10 half-lives of ^{134}Cs) will result in the reduction of decay heat below the level expected in decay-only scenario.

Table XXXIII. Ingestion dose equivalent from iodine vector.

Nuclide	Ingestion Equivalent Dose (mrem)		
	initial	30yr irradiation + 10yr decay	40yr decay
I129	1.51E-03	3.18E-05	1.51E-03
Cs134	0	0.05	0
Cs135	0	6.41E-07	0
Cs137	0	3.36E-05	0
Total	**1.51E-03**	**0.05**	**1.51E-03**

Table XXXIII provides the ingestion dose equivalent for the iodine vector. The total dose equivalent in the transmutation scenario is higher than the dose from the decay-

only scenario. The total ingestion dose equivalent is almost exclusively due to ^{134}Cs in the discharged vector. The contribution of ^{129}I to the dose equivalent is very small. The other long-lived radionuclide (^{135}Cs) has negligible contribution to the dose. The higher equivalent dose from the transmutation scenario is not a desired result. Given adequate extra time for the complete decay of ^{134}Cs, the vector from the transmutation scenario will become less radiotoxic.

The transmutation scenario does not provide significant reduction in all parameters of iodine. Table XXXIV provides the evaluation of transmutation strategy on ^{129}I. The initial ^{129}I inventory was reduced by 97.9%. The residual ^{129}I has negligible contribution to the residual vector's radioactivity, decay heat and dose equivalent. This indicates that other radionuclides created during irradiation have significant contributions to the radioactivity, decay heat and dose equivalent of the discharged vector. The transmutation effectiveness factor for ^{129}I indicates that there is significant advantage gained by transmuting the radionuclide by itself. However, the transmutation effectiveness factor for the iodine vector is greater than unity. This indicates higher radiological hazard from the transmutation vector compared with decay-only vector. It should be noted that the overall transmutation effectiveness will be less than unity if more cooling time is provided for the discharged vector.

Table XXXIV. Summary of metrics on iodine target in 30+10 scenario.

Metric	Value
Fraction of ^{129}I transmuted $f_{i = I129}$	0.979
Fraction of total radioactivity contributed to FP target $f_{A,iout}$	1.140E-04
Fraction of total decay heat contributed to FP target $f_{Q,iout}$	5.236E-06
Fraction of effective dose contributed to FP target $f_{D,iout}$	0.001
Transmutation Effectiveness Factor for ^{129}I, $x_{i = I129}$	0.021
Transmutation Effectiveness Factor for the target, x_{Target}	1062.790

V.E CESIUM TRANSMUTATION

Figure 38 shows the results of the transmutation strategy on cesium vector in comparison with decay only scenario. The initial composition of the cesium is 344.9g, 336.6g and 318.5g of ^{133}Cs, ^{135}Cs and ^{137}Cs respectively. Let's consider the change in ^{137}Cs inventory. There is no obvious advantage in inventory reduction in transmutation scenario over the decay-only scenario. After 30 year decay, the ^{137}Cs inventory is 159.5g, while the discharged ^{137}Cs inventory after 30 year irradiation is 155.9g. Two things contribute to the low transmutation gain. Of all significant cesium isotopes, ^{137}Cs has the lowest neutron capture cross sections at thermal and epithermal energies (see Table XI). Its capture cross section at less than 1 barn in the thermal and epithermal energy range results in little capture reaction rate. Secondly, any loss achieved through transmutation is negated by the production of ^{137}Cs from lighter isotopes. In particular, radiative capture reaction of ^{136}Cs, which is created from the irradiation of ^{135}Cs, results in the production of ^{137}Cs.

Unlike ^{137}Cs, there is appreciable decrease of ^{135}Cs inventory in the transmutation scenario when compare with the decay-only scenario. The discharge ^{135}Cs inventory is 176.9g, which represents 52.6% of the initial ^{135}Cs loading. It is conceivable that there is higher efficiency in the transmutation of ^{135}Cs. This may have been negated by the production of ^{135}Cs from lighter cesium isotopes. This is notable in the loss of 99.3% of the initial ^{133}Cs inventory. Radiative capture in ^{133}Cs produces ^{134}Cs, which is the neutron link to ^{135}Cs. The half-live of ^{135}Cs is 2.07 years and it has the capture cross section that is significantly higher than those of other cesium isotopes (see Table XI). Hence, some of the ^{134}Cs may be transmuted to ^{135}Cs before it effectively decays off.

Other than cesium isotopes, the significant nuclides of the discharged vector are ^{134}Ba, ^{135}Ba, ^{136}Ba, ^{137}Ba, ^{138}Ba, ^{139}La and ^{140}Ce. All the nuclides are stable and they represent 665.3g of the discharged vector. Radionuclides of notable quantity in the discharged vector include 0.49g of ^{134}Cs and 0.43g of ^{136}Cs. Other radionuclides like ^{138}Cs, ^{136m}Ba, ^{137m}Ba, ^{139}Ba and ^{140}La represent about 0.3 milligram of the discharged vector.

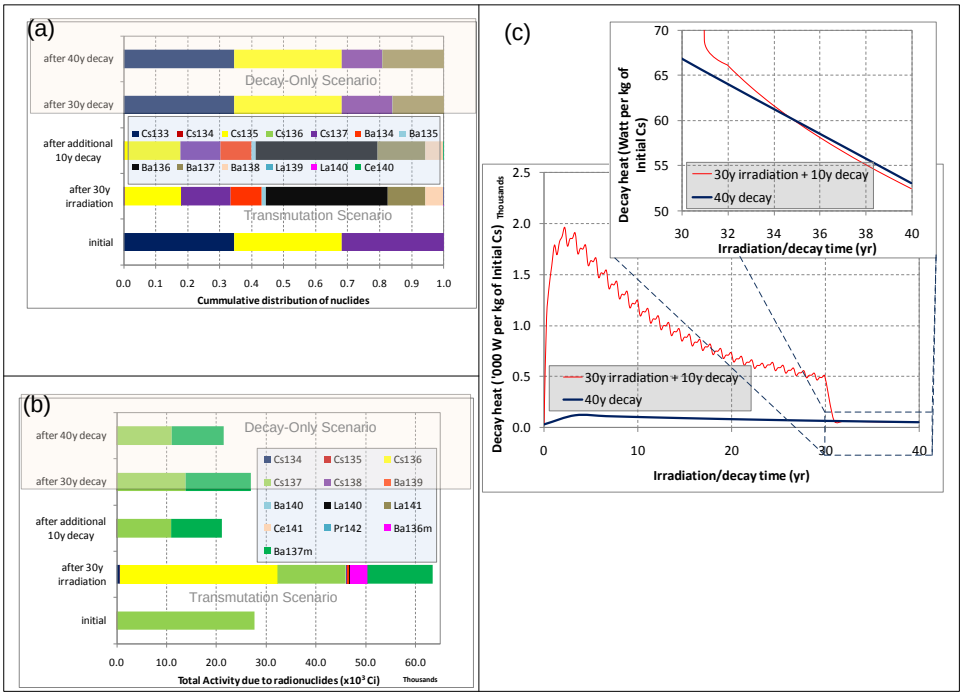

Fig. 38. Transmutation scenario vs. decay-only scenario for cesium vector. (a) inventories; (b) radioactivity; (c) decay heat.

Figure 38(b) shows the radioactivity of the transmutation vector. The initial radioactivity is almost all due to ^{137}Cs. The radioactivity of the vector at discharge is much higher than that of a 30 year decay-only scenario (see Fig. 38(b)). However, after additional 10 year cooling, the total decay of all short lived radionuclides reduces the radioactivity below that of a similar vector in 40 year decay-only scenario (see

Fig. 38(b)). However, the radioactivity level attained after the cooling period is not appreciably lower than the level in 40 year decay-only scenario. The residual activity at this point is mostly due to ^{137}Cs and its daughter, ^{137m}Ba.

The decay heat profiles from the vector under both decay-only and transmutation scenarios are shown in Figure 38(c). The initial decay heat is due to ^{137}Cs. The contribution of ^{135}Cs to the decay heat load is negligible. The decay heat generated after the 30 year irradiation is higher than the heat from decay-only scenario. In a similar trend to the radioactivity of the discharged vector, the decay heat is reduced slightly below the level expected in decay-only scenario after the post irradiation decay period. The residual decay heat is generated by ^{137}Cs and ^{137m}Ba.

Table XXXV. Ingestion dose equivalent from cesium vector.

Nuclide	Ingestion Equivalent Dose (mrem)		
	initial	30yr irradiation + 10yr decay	40yr decay
Cs134	0	0.04	0
Cs135	7.75E-05	4.08E-05	7.75E-05
Cs137	36.04	14.09	14.33
Ce141	0	3.23E-37	0
Ce144	0	1.66E-14	0
Pr144	0	1.59E-16	0
Total	**36.04**	**14.13**	**14.33**

Table XXXV provides the ingestion dose equivalent for the cesium vector. The total dose equivalent in the transmutation scenario is slightly lower than the dose from the decay-only scenario. The total ingestion dose equivalent is almost exclusively due to ^{137}Cs in both scenarios. The contribution of ^{135}Cs and other radionuclides to the dose equivalent is negligible. The transmutation scenario does not provide appreciable reduction in the radiotoxicity of the cesium vector.

Table XXXVI provides the evaluation of transmutation strategy on ^{135}Cs and ^{137}Cs. The initial ^{135}Cs inventory was reduced by 47.4%, which is a significant improvement since no significant reduction in ^{135}Cs inventory is noted in decay-only scenario. There is 60.9% reduction in ^{137}Cs inventory, which is not a significant improvement over the decay-only scenario. In decay-only scenario, 60.3% inventory reduction is attained over a similar time frame. The residual ^{135}Cs has negligible contribution to the residual vector's radioactivity, decay heat and dose equivalent. ^{137}Cs contributes 51.4% of the residual activity, 23% of the residual decay heat and 99.7% of the residual dose equivalent. The transmutation effectiveness factor for ^{135}Cs indicates that there is significant advantage gained by transmuting the radionuclide by itself. On the other hand, the transmutation effectiveness factor for ^{137}Cs indicates that there is no appreciable advantage gained from its transmutation. Since ^{137}Cs is the dominant nuclide in all parameters evaluated for cesium, the transmutation effectiveness factor for the cesium vector explicably indicates slight advantage gained through the transmutation of cesium isotopes.

Table XXXVI. Summary of metrics on cesium target in 30+10 scenario.

Metric	i = ^{135}Cs	i = ^{137}Cs
Fraction of nuclide *i* transmuted f_i	0.474	0.609
Fraction of total radioactivity contributed to target $f_{A,iout}$	9.66E-6	0.514
Fraction of total decay heat contributed to target $f_{O,iout}$	1.30E-6	0.230
Fraction of effective dose contributed to target $f_{D,iout}$	2.88E-6	0.997
Transmutation Effectiveness Factor, x_i	0.526	0.984
Transmutation Effectiveness Factor – target, x_{Target}	0.990	0.990

CHAPTER VI

CONCLUSIONS AND RECOMMENDATIONS

In this dissertation, the potential advantage of a comprehensive closed nuclear cycle, which involves recycling of reusable materials and minimization of material inventories to be discarded, has been demonstrated. The argument has been made that fission products deserve attention since they are responsible for radiological concerns at disposal sites. The compelling rationale is: in a closed fuel cycle, assuming all TRU are completely incinerated, fission products become the only source of radiological hazard concerns. It has been demonstrated that fission products are significant contributors to the radiotoxicity concerns in the first 300 – 500 years in a geological repository and their impact can be efficiently reduced via in-reactor retention scenarios. It is established that long-lived fission products are significant contributors to the long-term radiological concerns at a repository. In current P&T schemes, the management approach for fission products is focused on disposal in geological repositories. Some researches focused on possible transmutation of the fission products have been acknowledged. The proposed transmutation strategy takes advantage of the neutronics conditions in an advanced nuclear system for the effective transmutation of fission products.

The theories supporting the transmutation strategy has been discussed. Detailed equations and concepts have been provided to support the theories put forth. Some FP nuclides have been identified as candidates for the transmutation strategy. The radiotoxicity potential of fission products have been analyzed as the basis of the candidate selection made. We have also analyzed neutronic properties of the candidates to establish the best reactor conditions for their transmutation. Their chemical properties

have been analyzed in order to identify possible waste-form for each candidate. The reduction of fission product inventory is a primary metric of the transmutation strategy. The strategy also considers the effect of the reduction on radioactivity, decay heat and radiotoxicity of the residual. Metrics have been developed to evaluate these parameters.

The reactor system for the implementation of the transmutation strategy is the VHTR. The rationale for the selection of the VHTR has been discussed. The VHTR configuration, model and safety considerations are also presented. The transmutation strategy has been simulated, assuming a VHTR operation at equilibrium fuel cycle. The equilibrium fuel cycle has been determined based on the refueling of a third of the VHTR core after every cycle. The region of the VHTR with the highest scalar flux has been determined at the inner fuel zone of the 7^{th} layer of the VHTR's active core. In addition, the regions of the VHTR, which provides the highest transmutation for each candidate nuclide has been determined. The result indicates that the axial reference corresponding to the optimal transmutation region for all candidate nuclides is the 7^{th} layer of the VHTR's active core. The central reflector region bounding the inner fuel zone is the radial location for optimal transmutation of all candidate nuclides except ^{93}Zr. The middle fuel zone represents the radial region for the optimal transmutation of ^{93}Zr. The key difference between the 2 radial regions of optimal transmutation is their energy spectra, which are different from the energy spectrum at the location of peak scalar flux. The central reflector region is rich in thermal neutron and has little contribution to the scalar flux from epithermal and fast energy neutrons. On the other hand, the middle fuel zone has the least thermal neutron contribution to its scalar flux; and the highest contributions by epithermal and fast neutrons. The region of peak scalar flux has less

thermal spectrum than the central reflector region, but provides a more thermal energy profile than the middle fuel zone. This is indicative that ^{93}Zr is best transmuted in regions of high epithermal and fast flux contributions, while other candidate nuclides are best suited for thermal neutron transmutation.

The quantitative analysis of the developed transmutation strategy demonstrates reductions in the inventories of the irradiated samples. The effect of the transmutation strategy on radiological parameters of the irradiated samples differs based on the classification of the candidate nuclide. For the long-lived fission products, there is no significant effect of newly created radionuclides on the radiotoxicity of the transmuted fission product vector. There is significant reduction in the radiological parameters of this class of fission products. The relatively short-lived candidates (^{90}Sr and ^{137}Cs) show insignificant reduction in their radiological parameters.

Since the transmutation strategy assumes no separation of the candidate nuclide from its isotopes and isomers, the simulation involves transmutation targets, which consists of the candidate nuclide and its entire isotopes present in the fission product stream. In the transmutation of ^{90}Sr, the target vector includes ^{87}Sr, ^{88}Sr and ^{90}Sr. The improvement achieved in the transmutation of ^{90}Sr over a decay-only approach was minimal. It may not be significant enough to make it an attractive approach for ^{90}Sr reduction. However, the minimal advantage gained through the transmutation strategy, coupled with the virtual storage provide for the strontium waste stream while in-core make the transmutation of ^{90}Sr in VHTR makes it strategy worth deploying.

The transmutation of ^{93}Zr in elemental zirconium stream results in a significant reduction in the inventory and radiological parameter of the nuclide. The overall

transmutation effectiveness for the zirconium target indicates that the radiological hazards associated with the geological disposal of ^{93}Zr are significantly reduced through the transmutation strategy. The same conclusion is drawn in the transmutation of ^{99}Tc. About 96.7% of the initial ^{99}Tc inventory was transmuted. This is particularly a great result since ^{99}Tc is one of the fission products that pose the greater concerns with post-closure issues at a repository due to its mobility in geological environments.

The other important nuclide in post-closure issues is ^{129}I, which has the highest transmutation effectiveness. About 97.9% of the initial inventory was transmuted. The main concern with iodine transmutation is the containment of the xenon gases created in vector. Xenon isotopes and isomers represent about 90.1% of the discharged mass. In the transmutation of iodine involving physical targets, it will be imperative to include a gas plenum and/or fabricate gas pours in the target in order to create room for the xenon created over time. An addition consideration in the transmutation of iodine vector is the creation of ^{134}Cs in quantities large enough to have significant contribution to the radiotoxicity of the discharge vector. Unlike the other candidate nuclides in which 10 year post-irradiation cooling is sufficient to achieve a lowered radiotoxicity contribution from the transmutation target compared with decay-only scenario, iodine transmutation requires a longer post irradiation cooling period to be effective. The quantity of ^{134}Cs produced increases the required post irradiation cooling time to about 26 years.

For the transmutation of elemental cesium, significant advantages are noted for ^{135}Cs, while the transmutation of ^{137}Cs provides marginal advantages. The ^{135}Cs of the cesium vector experiences significant reduction of its inventory – an impossible result in decay-only strategy over the same time period. The transmutation effectiveness factor

for ^{135}Cs indicates that radiotoxicity contribution from the nuclide is reducible through the transmutation strategy. Furthermore, assuming isotopic separation of cesium nuclides, higher transmutation effectiveness can be derived for ^{135}Cs since the creation of addition ^{135}Cs from lighter isotopes will be avoided. On the other hand, the transmutation of ^{137}Cs does not indicate the levels of advantage gained in the transmutation of ^{135}Cs. The fraction of ^{137}Cs transmuted is 60.9%, which is an insignificant gain over the 60.3% loss of the same nuclide in decay-only scenario over similar time frame. The transmutation effectiveness factor for ^{137}Cs indicates minimal reduction in radiological parameters from the transmutation strategy. It is not clear if irradiation of ^{137}Cs alone will significantly improve the transmutation of the nuclide. The small capture cross section of ^{137}Cs may make it practically difficult to achieve higher transmutation efficiency. Due to the dominance of ^{137}Cs in the cesium vector, the overall transmutation effectiveness for the cesium target is comparable to that of ^{137}Cs. This indicates that the transmutation of cesium vector containing ^{137}Cs is unlikely to yield a significant improvement in the reduction of radiological parameters when compared to a decay-only scenario. However, the little improvement derived via transmutation coupled with the virtual storage provided in the VHTR makes the transmutation strategy a positive scheme in the management of radioactive cesium waste stream.

Overall, the transmutation strategy has been proven to be a viable approach in the reduction of fission products' contribution to radiological hazard in a final geological repository. This has been made possible due to the capability of the VHTR to supply different energy spectra in various locations of the reactor core. In addition, minimal

parasitic neutron absorption in the graphite-moderated, helium-cooled reactor provides improved neutron economy to support the implementation of the strategy.

Combined with the in-core incineration options for TRU, the developed transmutation strategy leads to potential achievability of engineering time scales in the comprehensive nuclear waste management.

REFERENCES

1. "The Report to the President and the Congress by the Secretary of Energy on the Need for a Second Repository," DOE/RW-0595, Office of Civilian Radioactive Waste Management, USDOE (December 2008).

2. M. HOLT, "Nuclear Waste Disposal: Alternatives to Yucca Mountain," R40202, Congressional Research Service (February 2009).

3. "Final Supplemental Environmental Impact Statement for a Geologic Repository for the Disposal of Spent Nuclear Fuel and High-Level Radioactive Waste at Yucca Mountain, Nye County, Nevada: Summary," DOE/EIS-0250F-S1, Office of Civilian Radioactive Waste Management, USDOE (June 2008).

4. B. C. GITLIN, "EPA's Final Health and Safety Standard for Yucca Mountain," RL34698, Resources, Science, and Industry Division, Congressional Research Service (October 2008).

5. "Standards," Subpart A of: "Environmental Radiation Protection Standards for Management and Disposal of Spent Nuclear Fuel, High-Level and Transuranic Radioactive Wastes," in: *"Title 40: Code of Federal Regulations," Revised Ed.*, 40CFR191.03, U.S. Government Printing Office, USA (July 2009).

6. H. OIGAWA, K. NISHIHARA, S. NAKAYAMA and Y. MORITA, "Concept of Waste Management and Geological Disposal Incorporating Partitioning and Transmutation Technology," 10th Information Exchange Meeting on Partitioning and Transmutation, Mito, Japan, NEA-OECD (October 2008).

7. V. BHATNAGAR, "EU Strategy in Partitioning & Transmutation and its Implementation within the EURATOM Framework Programmes," 10th Information Exchange Meeting on Partitioning and Transmutation, Mito, Japan, NEA-OECD (October 2008).

8. E. M. GONZALEZ, "Summary of RED-IMPACT results on the Impact of P&T on the High Level Waste Management," 10th Information Exchange Meeting on Partitioning and Transmutation, Mito, Japan, NEA-OECD (October 2008).

9. M. SAITO, V. APSE, V. ARTISYUK and A. CHMELEV, "Transmutation of Elemental Cesium by a Fusion Neutron Source," *Nuclear Technology*, **133**, 229-241 (2001).

10. J. C. BRESEE, J. J LAIDLER and K. W. THOMAS, "Recovery and Transmutation of Iodine-129 in an Accelerator-Driven Transmutation System," Waste Management Conference, Tucson, Arizona (February 2001).

11. E. ICHIMURA, N. TAKAKI, R. P. C. SCHRAM, R. KLEIN MEULEKAMP and K. BAKKER, "Iodine Transmutation Studies Using Metal Iodide Targets," *Journal of Nuclear Materials*, **334**, 149-158 (2004).

12. J. M. BONNEROT, V. BROUDIC, M. PHELIP, C. JEGOU, F. VARAINE et al., "Transmutation in Reactor and Aqueous Corrosion Resistance of Technetium Metal," *Journal of Nuclear and Radiochemical Sciences*, **6**, 287-290 (2005).

13. T. AOYAMA, S. SHIGETAKA, Y. MAEDA and S. SUZUKI, "Transmutation of Technetium in the Experimental Fast Reactor "JOYO"," *Journal of Nuclear and Radiochemical Sciences*, **6**, 279-282 (2005).

14. K. MINATO, T. IKEGAMI and T. INOUE, "Recent Research and Development Activities on Partitioning and Transmutation of Radioactive Nuclides in Japan," 8th Information Exchange Meeting on Partitioning and Transmutation, Las Vegas, Nevada, (November 2004)

15. C. RODRIGUEZ and A. BAXTER, "Transmutation of Nuclear Waste Using Gas-Cooled Reactor Technologies", 8th International Conference on Nuclear Engineering, Baltimore, Maryland (April 2000).

16. "Report to Congress on Advanced Fuel Cycle Initiative: The Future Path for Advanced Spent Fuel Treatment and Transmutation Research," 03-GA50439-06, Office of Nuclear Energy, Science, and Technology, USDOE (January 2003).

17. "Current Status and Future Development of Modular High Temperature Gas-cooled Reactor Technology," IAEA-TECDOC-1198, International Atomic Energy Agency, Vienna, Austria (February 2001).

18. P. E. MCDONALD, "Next Generation Nuclear Plant (NGNP): A Very High Temperature Gas-cooled Reactor (VHTR)," USDOE Advanced Reactor, Fuel Cycle, and Energy Products Workshop for Universities, Gaithersburg, Maryland, USDOE (March 2004).

19. "Evaluation of High Temperature Gas-cooled Reactor Performance: Benchmark Analysis Related to Initial Testing of the HTTR and HTR-10," IAEA-TECDOC-1382, International Atomic Energy Agency, Vienna, Austria (2003).

20. C. RODRIGUEZ, A. BAXTER, D. MCEACHERN, M. FIKANI and F. VENNERI, "Deep-Burn: Making Nuclear Waste Transmutation Practical," *Nuclear Engineering and Design*, **222**, 299-317 (2003).

21. P. V. TSVETKOV, D. E. AMES II, A. B. ALAJO, T. G. LEWIS, "Spectrum Shifting as a Mechanism to Improve Performance of VHTRs with Advanced Actinide Fuels," *Nuclear Engineering and Design*, **238**, 1958-1964 (2008).

22. P. V. TSVETKOV, A. B. ALAJO, T. G. LEWIS III, D. E. AMES II, "Out-of-Core Fuel Cycle Characteristics of VHTRs with No On-Site Refueling," *Proc. of the Intern. Congr. Adv. Nucl. Power Plants (ICAPP 08)*, Anaheim, California, ANS Annual Meeting, paper 8233, pp. 298 - 302, ANS (2008).

23. G. ALIBERTI, G. PALMIOTTI, M. SALVATORES, T. K. KIM, T. A. TAIWO et al., "Nuclear data sensitivity, uncertainty and target accuracy assessment for future nuclear systems," *Annals of Nuclear Energy*, **33**, 700-733 (2006).

24. Final Environmental Impact Statement for a Geologic Repository for the Disposal of Spent Nuclear Fuel and High-Level Radioactive Waste at Yucca Mountain, Nye County, Nevada, Vol. 2, Appendix A, "Inventory and Characteristics of Spent Nuclear Fuel, High-Level Radioactive Waste, and Other Materials," DOE/EIS-0250, U.S. DOE (2002).

25. A. B. ALAJO, "Impact of PWR Spent Fuel Variations on TRU-Fueled VHTRs," M.S. Thesis, Department of Nuclear Engineering, Texas A&M University, College Station, Texas (December 2007).

26. "Atomic Masses and Abundances," in D. R. LIDE, Ed., *CRC Handbook of Chemistry and Physics, 90th Ed.*, CRC Press, Boca Raton, Florida (2009).

27. C. R. HAMMOND, "The Elements," in D. R. LIDE, Ed., *CRC Handbook of Chemistry and Physics, 90th Ed.*, CRC Press, Boca Raton, Florida (2009).

28. N. E. HOLDEN, "Table of the Isotopes," in D. R. LIDE, Ed., *CRC Handbook of Chemistry and Physics, 90th Ed.*, CRC Press, Boca Raton, Florida (2009).

29. "Melting, Boiling, Triple, and Critical Point Temperatures of the Elements," in D. R. LIDE, Ed., *CRC Handbook of Chemistry and Physics, 90th Ed.*, CRC Press, Boca Raton, Florida (2009).

30. "Physical Constants of Inorganic Compounds," in D. R. LIDE, Ed., *CRC Handbook of Chemistry and Physics, 90th Ed.*, CRC Press, Boca Raton, Florida (2009).

31. "Thermal and Physical Properties of Pure Metals," in D. R. LIDE, Ed., *CRC Handbook of Chemistry and Physics, 90th Ed.*, CRC Press, Boca Raton, Florida (2009).

32. "Evaluated Nuclear Data File Version B," Release VII.0, National Nuclear Data Center, Brookhaven National Laboratory, Upton New York (2006).

33. "Evaluated Nuclear Data File Version B," Release VI.8, National Nuclear Data Center, Brookhaven National Laboratory, Upton New York (2001).

34. E. M. BAUM, H. D. KNOX and T. R. MILLER, Eds., *Nuclides and Isotopes: Chart of the Nuclides,* 16th Ed., KAPL Inc., Schenectady New York (2002).

35. G. VASUDEVAMURTHY, T. W. KNIGHT, E. ROBERTS, T. M. ADAMS, "Laboratory Production of Zirconium Carbide Compacts for Use in Inert Matrix Fuels," *Journal of Nuclear Materials*, **374**, 241-247 (2008).

36. R. G. SHUMILOVA and T. Y. KOSOLAPOVA, "Production of Zirconium Carbide on a Pilot-Plant Scale," *Journal of Powder Metallurgy and Metal Ceramics*, **7**, 317-319 (1968).

37. R. ALBERTO, "High- and Low-Valency Organometallic Compounds of Technetium and Rhenium," in K YOSHIHARA and T OMORI, Eds., *Technetium and Rhenium: Their Chemistry and Its Applications,* Vol. 176, of Topics in Current Chemistry, Springer, Berlin, Germany (1996).

38. "Dose Coefficients for Intakes of Radionuclides by Workers," ICRP Publication 68 in: Annals of the ICRP, Vol. 24, #4, Elsevier Science Inc., Tarrytown, New York (1995).

39. "Advanced Nuclear Fuel Cycles and Radioactive Waste Management," OECD Nuclear Energy Agency, OECD Publishing, Paris, France (2006).

40. T. DUJARDIN, "Overview of NEA Activities in Actinide and Fission Product Partitioning and Transmutation," 10th Information Exchange Meeting on Partitioning and Transmutation, Mito, Japan, NEA-OECD (October 2008).

41. E. RUOKOLA, "Management of Spent Nuclear Fuel in Finland: Policy, Past and Present Practices, Plans for the Future," in NATO Science Series Vol. 215: "Scientific and Technical Issues in the Management of Spent Fuel of Decommissioned Nuclear Submarines," Springer, Dordrecht, The Netherlands (2006).

42. "Developing Multinational Radioactive Waste Repositories: Infrastructural Framework and Scenarios of Cooperation," IAEA-TECDOC-1413, International Atomic Energy Agency, Vienna, Austria (October 2004).

43. "Technical, Economic and Institutional Aspects of Regional Spent Fuel Storage Facilities," IAEA-TECDOC-1482, International Atomic Energy Agency, Vienna, Austria (November 2005).

44. J. WALLENIUS, "A Preface from Red Impact," *Progress in Nuclear Energy*, **49**, 567 (2007).

45. W. VON LENSA R. NABBI and M. ROSSBACH, "Impact of Partitioning, Transmutation and Waste Reduction Technologies on the Final Nuclear Waste Disposal (RED-IMPACT)," Forschungszentrum Jülich (2008)

46. J. B. CHOI, "Status of Fast Reactor and Pyroprocess Technology Development in Korea," International Conference on Fast Reactors and Related Fuel Cycles, Kyoto, Japan (December 2009).

47. E. H. KIM, G. I. PARK, I. T. KIM, H. LEE and S. W. PARK, "Partitioning of Fission Products and Waste Salt Minimization During Pyroprocess," 10th Information Exchange Meeting on Partitioning and Transmutation, Mito, Japan, NEA-OECD (October 2008).

48. "Updated Consolidated Report on Radioactive Waste Management in FNCA Countries," FNCA-RWM-R004, Radioactive Waste Management Project Group, Forum for Nuclear Cooperation in Asia (March 2007).

49. "Definitions," Subpart A of: "Disposal of High-Level Radioactive Wastes in Geologic Repositories," in: *"Title 10: Code of Federal Regulations,"* Revised Ed., 10CFR60.2, U.S. Government Printing Office, USA (2009).

50. "Waste Classification," Subpart D of: "Licensing Requirements for Land Disposal of Radioactive Waste," in: *"Title 10: Code of Federal Regulations,"* Revised Ed., 10CFR61.55, U.S. Government Printing Office, USA (2009).

51. MCNP User Manual, Version 5, LA-UR-03-1987, Vol. I, Los Alamos National Laboratory, Revised (2008).

52. MCNP User Manual, Version 5, LA-CP-03-0245, Vol. II, Los Alamos National Laboratory, Revised (2008).

53. D. B. PELOWITZ, Ed., MCNPX User's Manual, LA-CP-07-1473, Version 2.6.0, Los Alamos National Laboratory (April 2008).

54. I. C. GAULD, O. W. HERMANN and R. M. WESTFALL, "ORIGEN-S: SCALE System Module to Calculate Fuel Depletion, Actinide Transmutation, Fission Product Buildup and Decay, and Associated Radiation Source Terms," Vol. II, Sect. F7 of *SCALE: A Modular Code System for Performing Standardized Computer Analyses for Licensing Evaluation, Version 6*, ORNL/TM-2005/39, 3 Volumes (January 2009).

55. T. IYOKU, S. UETA, J. SUMITA, M. UMEDA and M. ISHIHARA, "Design of Core Components," *Nuclear Engineering and Design*, **233**, 71–79 (2004).

APPENDIX A

The energy-dependent capture cross sections of strontium, zirconium, iodine and cesium isotopes are shown below. The cross sections are from ENDF/B-VII.0

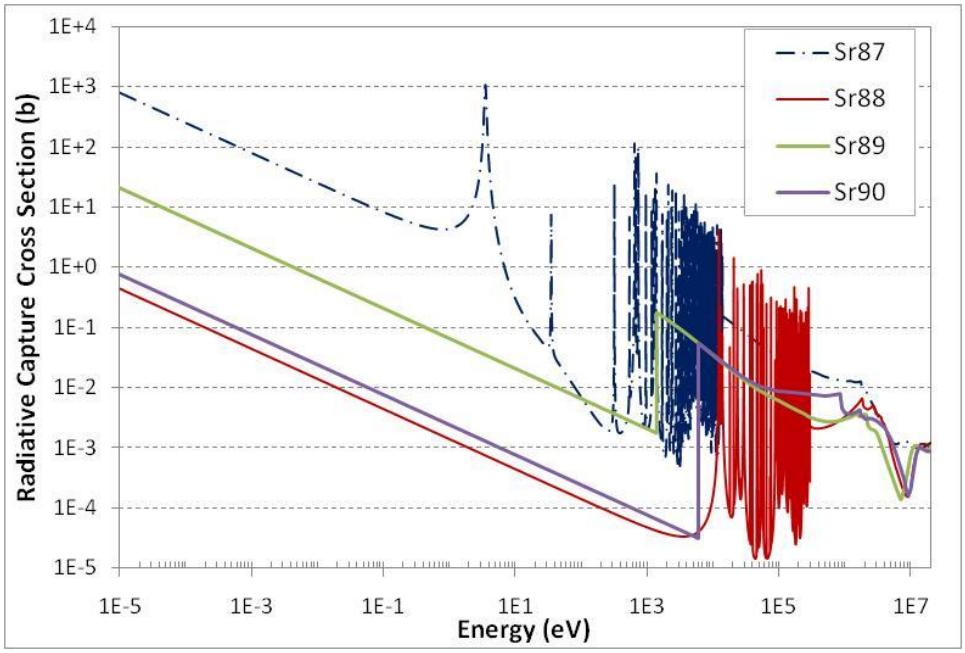

Fig. A1. Energy dependent radiative capture cross sections of strontium isotopes.

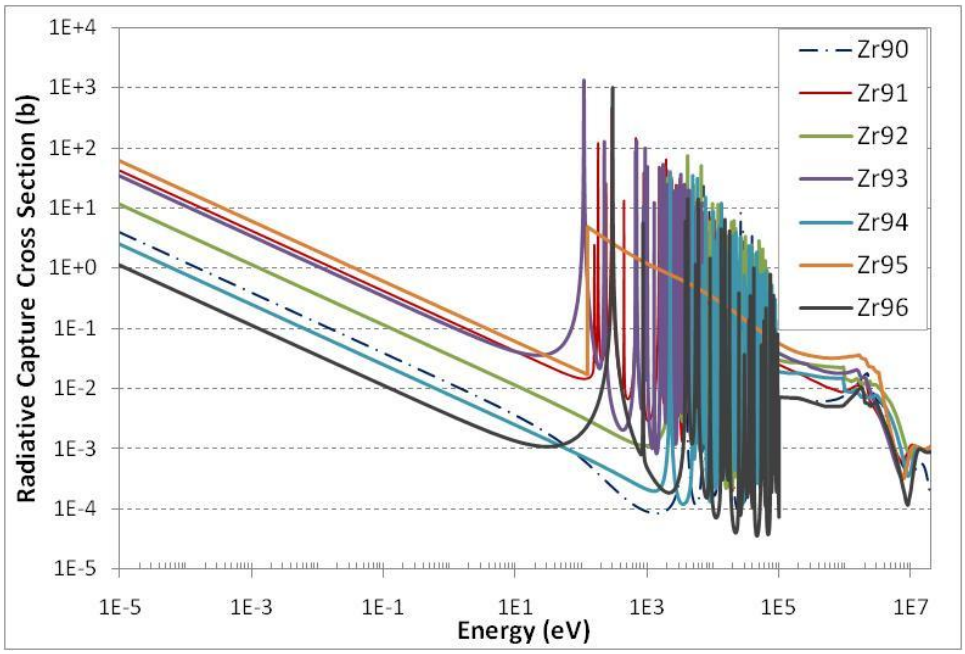

Fig. A2. Energy dependent radiative capture cross sections of zirconium isotopes.

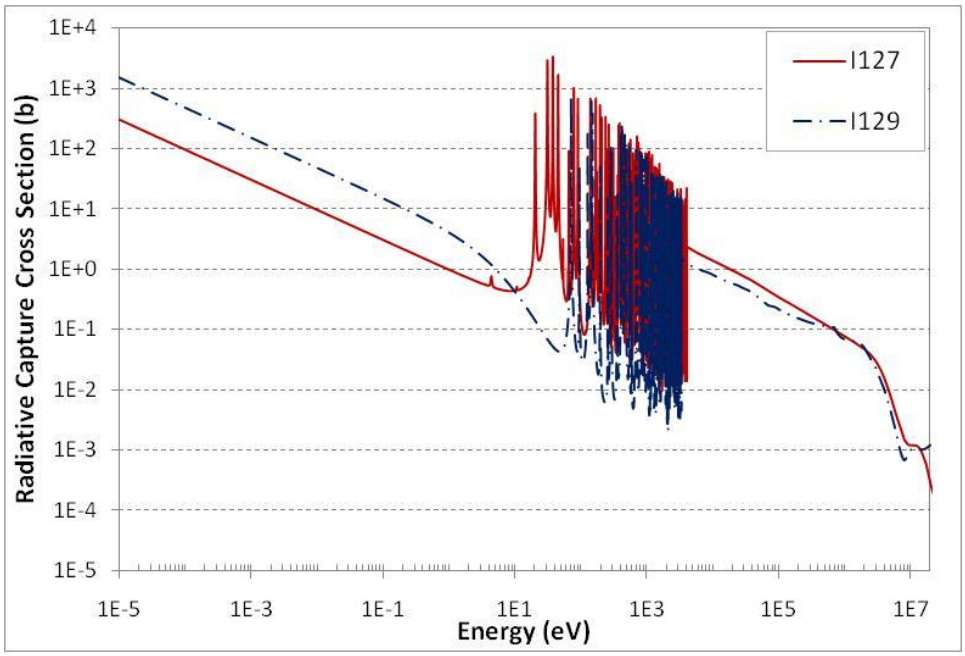

Fig. A1. Energy dependent radiative capture cross sections of iodine isotopes.

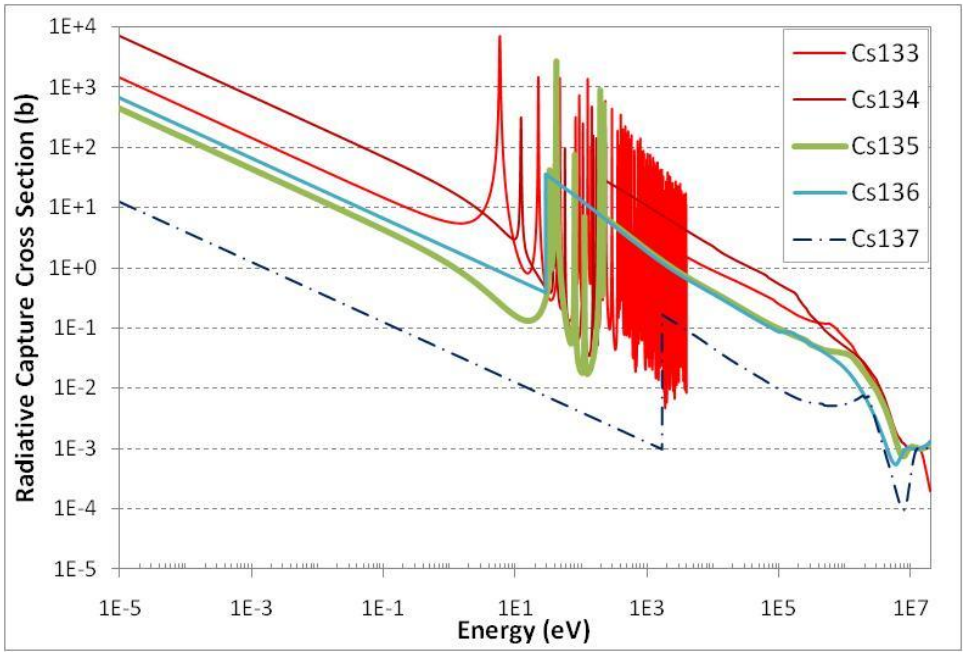

Fig. A1. Energy dependent radiative capture cross sections of cesium isotopes.

APPENDIX B

Flux and reaction rate profiles in VHTR core at time t_1 to t_4. Times t_1, t_2, t_3 and t_4 are 100 days, 200 days, 300 days and 405 days into the equilibrium cycle respectively.

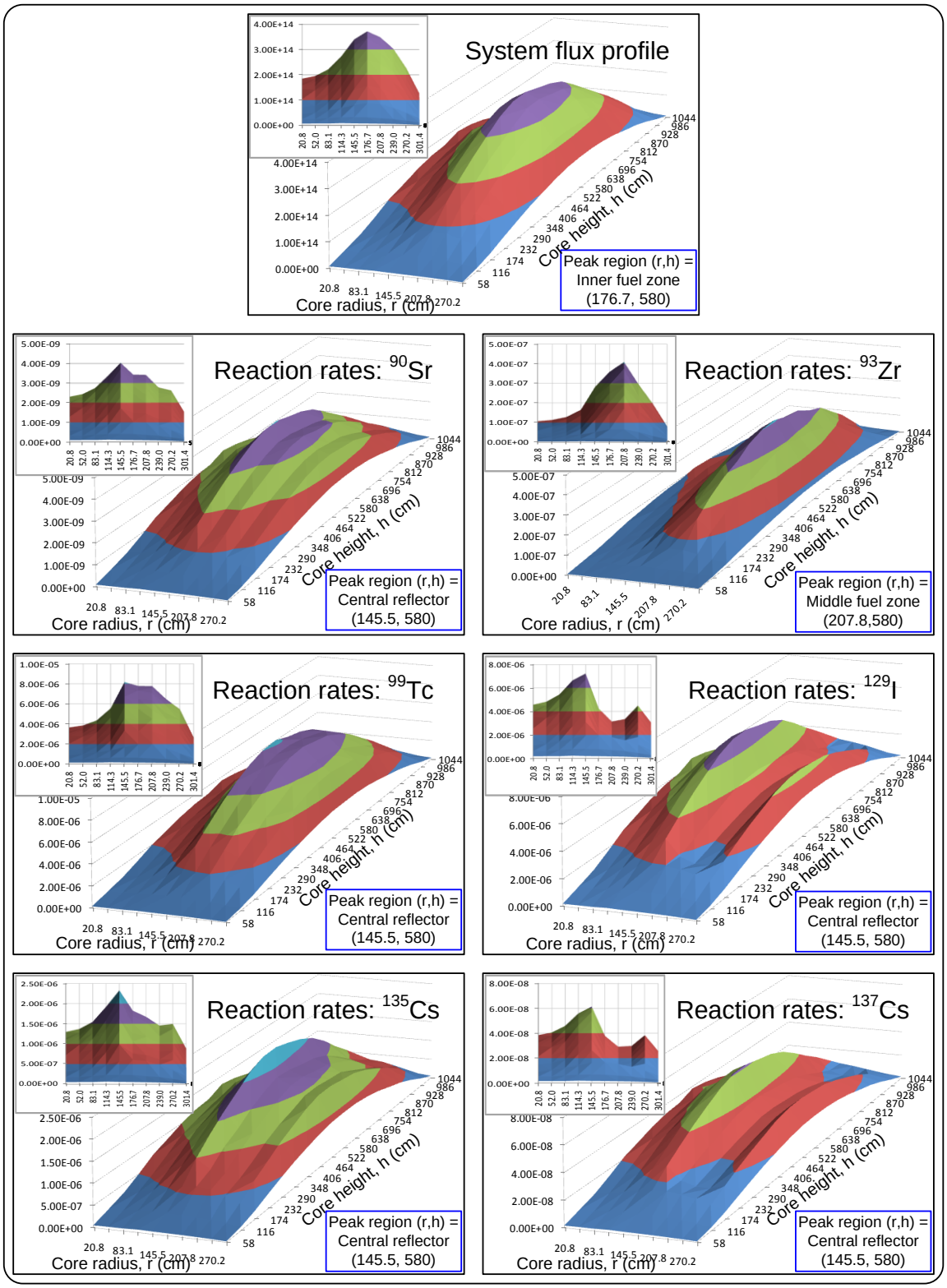

Fig. B1. Flux and reaction rate profiles in VHTR core at time t_1.

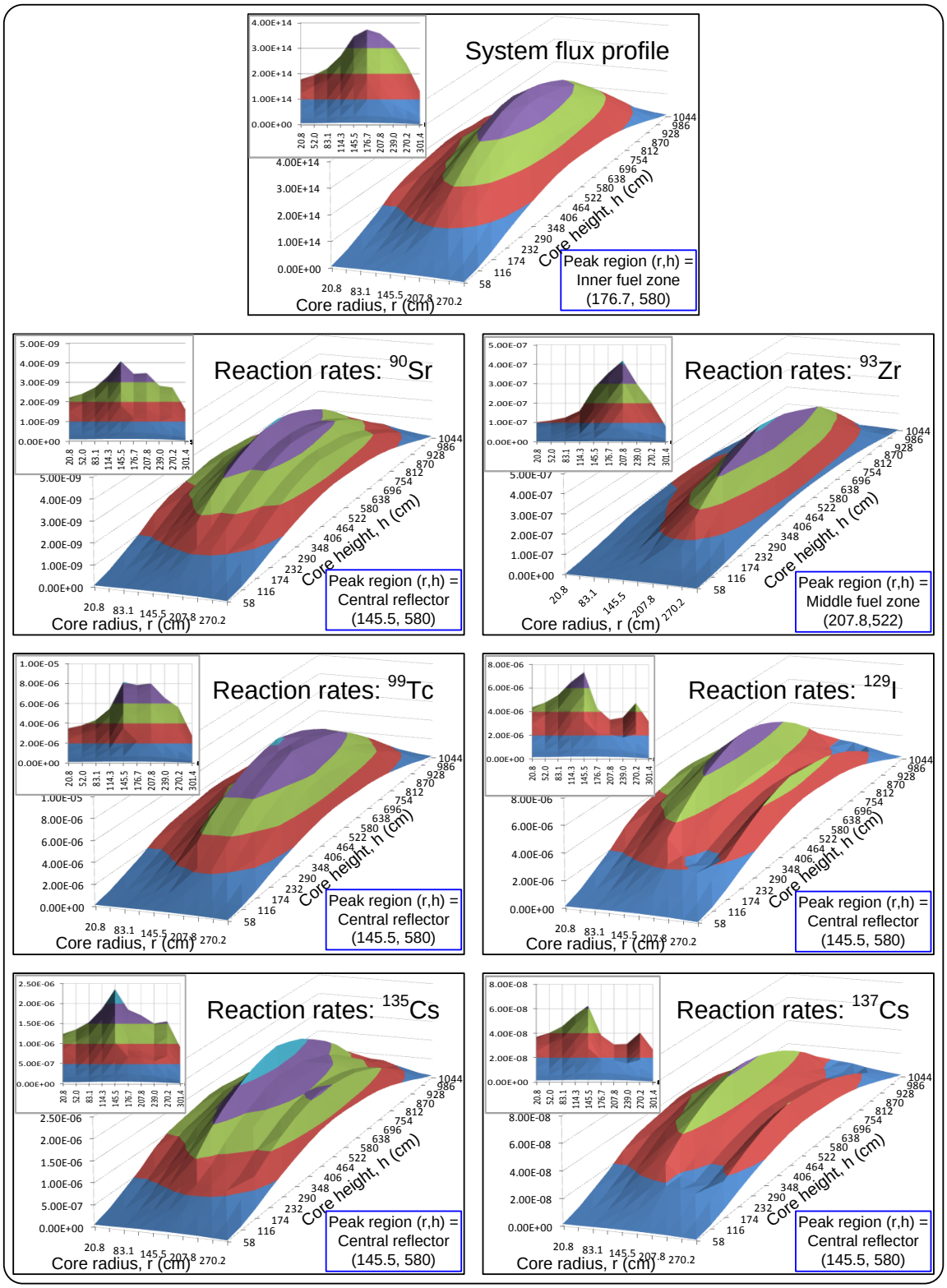

Fig. B2. Flux and reaction rate profiles in VHTR core at time t_2.

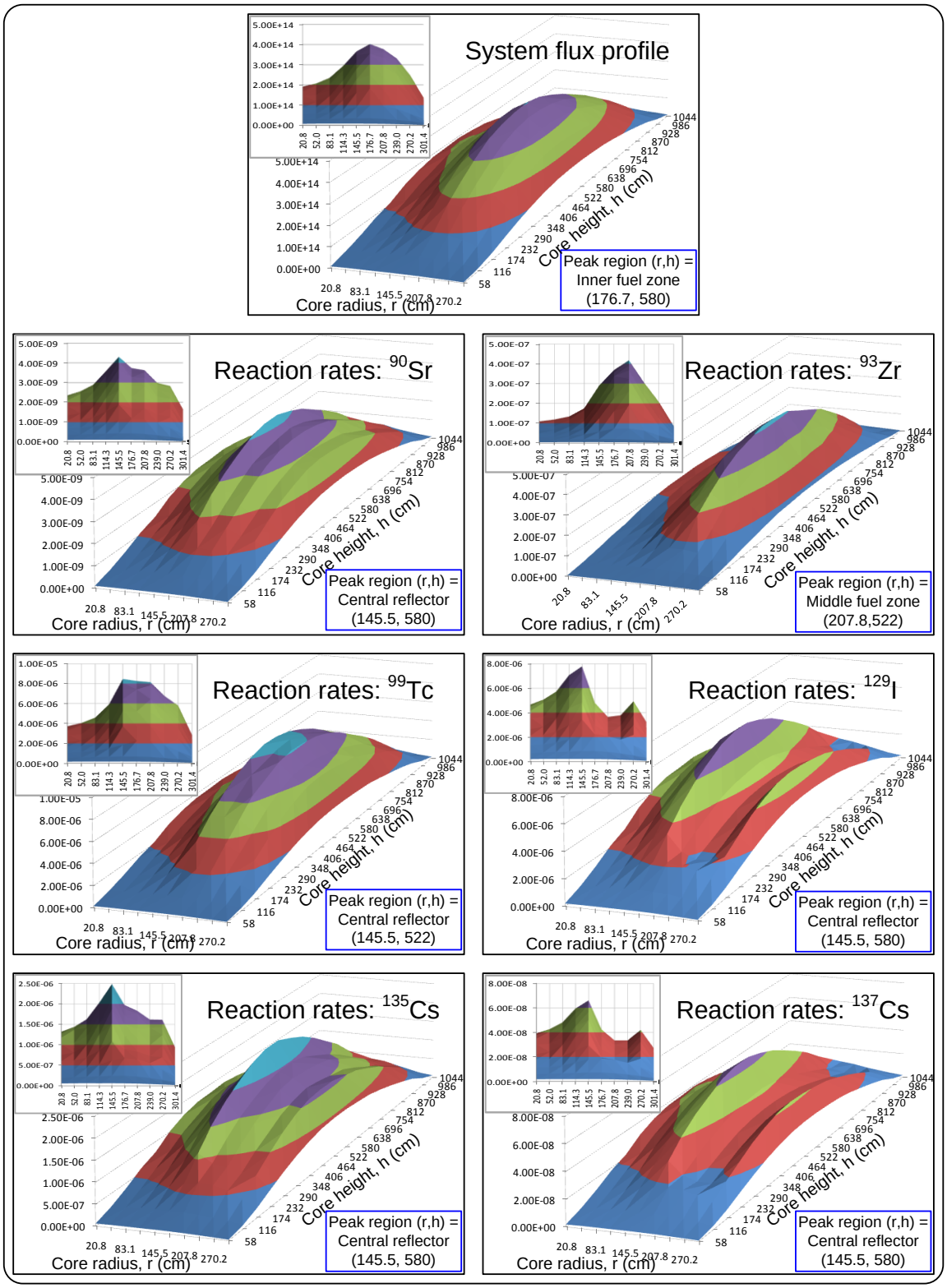

Fig. B3. Flux and reaction rate profiles in VHTR core at time t_3.

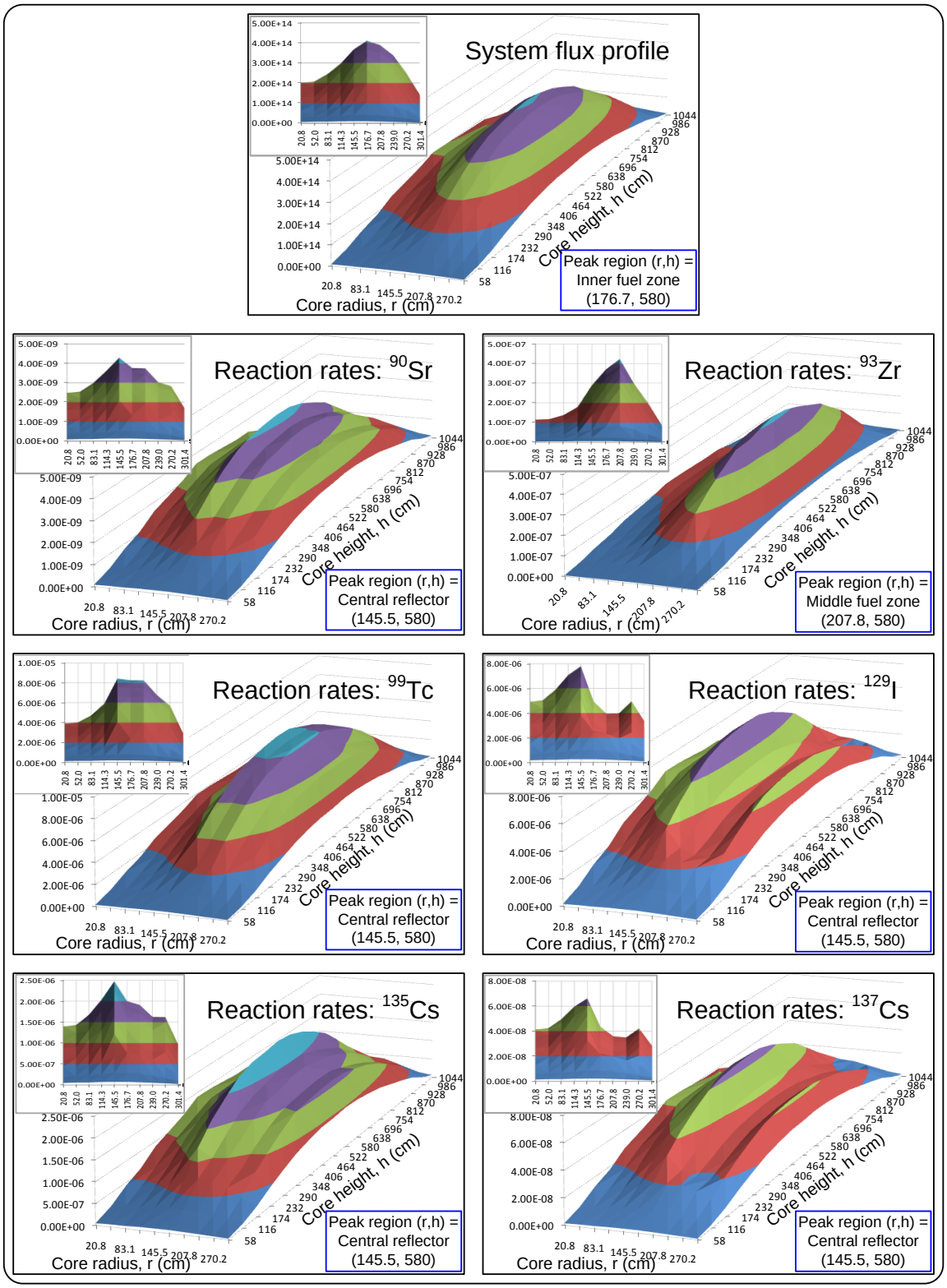

Fig. B4. Flux and reaction rate profiles in VHTR core at time t_4.

APPENDIX C

SAMPLE MCNP, MCNPX AND ORIGEN-S INPUT FILES

C-1: SAMPLE MCNP INPUT DECK.

```
VHTR Prismatic Power Core
c vhtr_leu15_3zn_endf6_cyc3 timestep0 with reaction rate tallies
c based on Japan's HTTR fuel and block design
c  -- Cell cards --
c  TRISO particle
c    Zone 1
1    11 6.982E-02  -10     u=10 imp:n=1 VOL=1.13097e-04 $ Fuel kernel
(15% u235 enrichment)
2    2  -1.14       10 -11 u=10 imp:n=1  $ Porous buffer
3    2  -1.89       11 -12 u=10 imp:n=1  $ IPyC
4    3  -3.2        12 -13 u=10 imp:n=1  $ SiC containment
5    2  -1.87       13 -14 u=10 imp:n=1  $ OPyC
6    6  -1.69       14     u=10 imp:n=1  $ Graphite matrix
c
c    Zone 2
7    21 6.982E-02  -10     u=11 imp:n=1 VOL=1.13097e-04 $ Fuel kernel
(15% enrichment)
8    2  -1.14       10 -11 u=11 imp:n=1  $ Porous buffer
9    2  -1.89       11 -12 u=11 imp:n=1  $ IPyC
10   3  -3.2        12 -13 u=11 imp:n=1  $ SiC containment
11   2  -1.87       13 -14 u=11 imp:n=1  $ OPyC
12   6  -1.69       14     u=11 imp:n=1  $ Graphite matrix
c
c    Zone 3
13   31 7.232E-02  -10     u=12 imp:n=1 VOL=1.13097e-04 $ Fuel kernel
(15% enrichment)
14   2  -1.14       10 -11 u=12 imp:n=1  $ Porous buffer
15   2  -1.89       11 -12 u=12 imp:n=1  $ IPyC
16   3  -3.2        12 -13 u=12 imp:n=1  $ SiC containment
17   2  -1.87       13 -14 u=12 imp:n=1  $ OPyC
18   6  -1.69       14     u=12 imp:n=1  $ Graphite matrix
c
19   0             -21 22 -23 24 -25 26 lat=1 u=15 fill=10 imp:n=1  $
Unit of compact lattice
20   0             -21 22 -23 24 -25 26 lat=1 u=16 fill=11 imp:n=1  $
Unit of compact lattice
21   0             -21 22 -23 24 -25 26 lat=1 u=17 fill=12 imp:n=1  $
Unit of compact lattice
c  Fuel compact
c    Zone 1
22   4  -0.001708   36 -37 -30      u=20         imp:n=1  $ Helium in
inner annulus
23   0              36 -37  30 -31  u=20 fill=15 imp:n=1  $ Fuel
compact annulus
24   8  -1.77       35 -38  31 -32  u=20         imp:n=1  $ Graphite
sleeve
```

```
25   4  -0.001708   35 -38  32 -33  u=20         imp:n=1  $ Coolant
channel
26   4  -0.001708  -35 -33          u=20         imp:n=1  $ Helium
below fuel rod
27   4  -0.001708   38 -33          u=20         imp:n=1  $ Helium
above fuel rod
28   8  -1.77       35 -36 -31      u=20         imp:n=1  $ Graphite
sleeve bottom-cap
29   8  -1.77       37 -38 -31      u=20         imp:n=1  $ Graphite
sleeve top-cap
30   7  -1.77       33              u=20         imp:n=1  $ Surrounding
Graphite
c
c    Zone 2
31   4  -0.001708   36 -37 -30      u=21         imp:n=1  $ Helium in
inner annulus
32   0              36 -37  30 -31  u=21 fill=16 imp:n=1  $ Fuel region
of rod
33   8  -1.77       35 -38  31 -32  u=21         imp:n=1  $ Graphite
sleeve
34   4  -0.001708   35 -38  32 -33  u=21         imp:n=1  $ Helium
coolant channel
35   4  -0.001708  -35 -33          u=21         imp:n=1  $ Helium
below fuel rod
36   4  -0.001708   38 -33          u=21         imp:n=1  $ Helium
above fuel rod
37   8  -1.77       35 -36 -31      u=21         imp:n=1  $ Graphite
sleeve bottom-cap
38   8  -1.77       37 -38 -31      u=21         imp:n=1  $ Graphite
sleeve top-cap
39   7  -1.77       33              u=21         imp:n=1  $ Surrounding
Graphite
c
c    Zone 3
40   4  -0.001708   36 -37 -30      u=22         imp:n=1  $ Helium in
inner annulus
41   0              36 -37  30 -31  u=22 fill=17 imp:n=1  $ Fuel region
of rod
42   8  -1.77       35 -38  31 -32  u=22         imp:n=1  $ Graphite
sleeve
43   4  -0.001708   35 -38  32 -33  u=22         imp:n=1  $ Helium
coolant channel
44   4  -0.001708  -35 -33          u=22         imp:n=1  $ Helium
below fuel rod
45   4  -0.001708   38 -33          u=22         imp:n=1  $ Helium
above fuel rod
46   8  -1.77       35 -36 -31      u=22         imp:n=1  $ Graphite
sleeve bottom-cap
47   8  -1.77       37 -38 -31      u=22         imp:n=1  $ Graphite
sleeve top-cap
48   7  -1.77       33              u=22         imp:n=1  $ Surrounding
Graphite
c
c  Burnable poison rod
c    Zone 1
49   15  9.147E-02  41 -42 -40      u=23 imp:n=1 VOL=35.3429 $ Lower
portion of BP rod
```

```
50   2  -1.77       42 -43 -40      u=23         imp:n=1  $ Middle
(graphite) portion of BP rod
51   15  9.147E-02  43 -44 -40      u=23 imp:n=1 VOL=35.3429 $ Upper
portion of BP rod
52   7  -1.77       40              u=23         imp:n=1  $ Surrounding
Graphite
53   7  -1.77       44 -40          u=23         imp:n=1  $ Graphite
above BP rod
54   7  -1.77      -41 -40          u=23         imp:n=1  $ Graphite
below BP rod
c
c    Zone 2
55   25  9.147E-02  41 -42 -40      u=24 imp:n=1 VOL=35.3429 $ Lower
portion of BP rod
56   2  -1.77       42 -43 -40      u=24         imp:n=1  $ Middle
(graphite) portion of BP rod
57   25  9.147E-02   43 -44 -40      u=24 imp:n=1 VOL=35.3429 $ Upper
portion of BP rod
58   7  -1.77       40              u=24         imp:n=1  $ Surrounding
Graphite
59   7  -1.77       44 -40          u=24         imp:n=1  $ Graphite
above BP rod
60   7  -1.77      -41 -40          u=24         imp:n=1  $ Graphite
below BP rod
c
c    Zone 3
61   35  9.151E-02  41 -42 -40      u=25 imp:n=1 VOL=35.3429 $ Lower
portion of BP rod
62   2  -1.77       42 -43 -40      u=25         imp:n=1  $ Middle
(graphite) portion of BP rod
63   35 -1.82       43 -44 -40      u=25 imp:n=1 VOL=35.3429 $ Upper
portion of BP rod
64   7  -1.77       40              u=25         imp:n=1  $ Surrounding
Graphite
65   7  -1.77       44 -40          u=25         imp:n=1  $ Graphite
above BP rod
66   7  -1.77      -41 -40          u=25         imp:n=1  $ Graphite
below BP rod
c
c  Empty BP location
67   4  -0.001708   41 -44 -40      u=27         imp:n=1
68   7  -1.77      #67              u=27         imp:n=1
c
c  Block handling hole
69   4  -0.001708   53 -54 -50      u=28         imp:n=1  $ Lower block
handling hole
70   4  -0.001708   54 -55 -51      u=28         imp:n=1  $ Middle
block handling hole
71   4  -0.001708   55 -52          u=28         imp:n=1  $ Upper block
handling hole
72   7  -1.77      #71 #70 #69      u=28         imp:n=1  $ Surrounding
graphite
c  Graphite part of fuel block
73   7  -1.77      -34              u=29         imp:n=1
c
c  Fuel block
c    Zone 1
```

```
74   0  -60 lat=2 imp:n=1 u=30 fill=-4:4 -4:4 0:0   $ Pitch = 5.15 cm
      29 29 29 29 29 29 29 29 29  $ROW 1
       29 29 29 29 27 20 20 20 29  $ROW 2
        29 29 29 20 20 20 20 20 29  $ROW 3
         29 29 20 20 20 20 20 20 29  $ROW 4
          29 20 20 20 28 20 20 23 29  $ROW 5
           29 20 20 20 20 20 20 29 29  $ROW 6
            29 20 20 20 20 20 29 29 29  $ROW 7
             29 23 20 20 20 29 29 29 29  $ROW 8
              29 29 29 29 29 29 29 29 29  $ROW 9
75   0  -61  fill=30 u=31 imp:n=1
76   0  #75          u=31 imp:n=0
c
c    Zone 2
77   0  -60 lat=2 imp:n=1 u=35 fill=-4:4 -4:4 0:0   $ Pitch = 5.15 cm
      29 29 29 29 29 29 29 29 29  $ROW 1
       29 29 29 29 27 21 21 21 29  $ROW 2
        29 29 29 21 21 21 21 21 29  $ROW 3
         29 29 21 21 21 21 21 21 29  $ROW 4
          29 21 21 21 28 21 21 24 29  $ROW 5
           29 21 21 21 21 21 21 29 29  $ROW 6
            29 21 21 21 21 21 29 29 29  $ROW 7
             29 24 21 21 21 29 29 29 29  $ROW 8
              29 29 29 29 29 29 29 29 29  $ROW 9
78   0  -61  fill=35 u=32 imp:n=1
79   0  #78          u=32 imp:n=0
c
c    Zone 3
80   0  -60 lat=2 imp:n=1 u=36 fill=-4:4 -4:4 0:0   $ Pitch = 5.15 cm
      29 29 29 29 29 29 29 29 29  $ROW 1
       29 29 29 29 27 22 22 22 29  $ROW 2
        29 29 29 22 22 22 22 22 29  $ROW 3
         29 29 22 22 22 22 22 22 29  $ROW 4
          29 22 22 22 28 22 22 25 29  $ROW 5
           29 22 22 22 22 22 22 29 29  $ROW 6
            29 22 22 22 22 22 29 29 29  $ROW 7
             29 25 22 22 22 29 29 29 29  $ROW 8
              29 29 29 29 29 29 29 29 29  $ROW 9
81   0  -61  fill=36 u=33 imp:n=1
82   0  #81          u=33 imp:n=0
c
c  Control rod block
83   4  -0.001708   53 -54 -50              u=38 imp:n=1  $ Lower block
handling hole
84   4  -0.001708   54 -55 -51              u=38 imp:n=1  $ Middle
block handling hole
85   4  -0.001708   55 -52                  u=38 imp:n=1  $ Upper block
handling hole
86   4  -0.001708  -70                      u=38 imp:n=1  $ Control rod
channel
87   4  -0.001708  -71                      u=38 imp:n=1  $ Control rod
channel
88   4  -0.001708  -72                      u=38 imp:n=1  $ Control rod
channel
89   7  -1.77      -61 70 71 72 #83 #84 #85 u=38 imp:n=1  $ Graphite
Control rod block
90   0              61  u=38    imp:n=0
```

```
c
c  Graphite Reflector block
91   4  -0.001708   53 -54 -50      u=39 imp:n=1  $ Lower block
handling hole
92   4  -0.001708   54 -55 -51      u=39 imp:n=1  $ Middle block
handling hole
93   4  -0.001708   55 -52          u=39 imp:n=1  $ Upper block
handling hole
94   7  -1.77      -61 #91 #92 #93  u=39 imp:n=1  $ Prismatic block
95   0              61              u=39 imp:n=0
c
c  Columns
96   0   80 -81 lat=1 imp:n=1 u=1 fill=31  $ Fuel block column - Zone 1
97   0   80 -81 lat=1 imp:n=1 u=2 fill=32  $ Fuel block column - Zone 2
98   0   80 -81 lat=1 imp:n=1 u=3 fill=33  $ Fuel block column - Zone 3
99   0   80 -81 lat=1 imp:n=1 u=8 fill=38  $ Control block column
100  0   80 -81 lat=1 imp:n=1 u=9 fill=39  $ Graphite block column
c
c  Core
101  0  -61 lat=2  imp:n=1 u=100  fill=-10:10 -10:10 0:0
      9 9 9 9 9 9 9 9 9 9 9 9 9 9 9 9 9 9 9 9 9 9 9  $ROW 1
       9 9 9 9 9 9 9 9 9 9 9 9 9 9 9 9 9 9 9 9 9 9 9  $ROW 2
        9 9 9 9 9 9 9 9 9 9 9 9 9 9 9 9 9 9 9 9 9 9 9  $ROW 3
         9 9 9 9 9 9 9 9 9 9 9 8 3 8 1 8 2 9 9 9 9  $ROW 4
          9 9 9 9 9 9 9 9 9 9 8 1 2 1 2 3 1 8 3 9 9 9  $ROW 5
           9 9 9 9 9 9 9 9 9 2 3 8 3 8 1 8 2 1 8 9 9 9  $ROW 6
            9 9 9 9 9 9 9 9 8 1 2 9 9 9 9 9 8 2 1 9 9 9  $ROW 7
             9 9 9 9 9 9 9 1 3 8 9 9 9 9 9 9 3 3 8 9 9 9  $ROW 8
              9 9 9 9 9 9 8 2 1 9 9 9 9 9 9 9 8 2 2 9 9 9  $ROW 9
               9 9 9 9 3 1 8 9 9 9 9 9 9 9 9 1 3 8 9 9 9  $ROW 10
                9 9 9 9 8 3 9 9 9 9 9 9 9 9 9 8 1 9 9 9 9  $ROW 11
                 9 9 9 2 1 8 9 9 9 9 9 9 9 9 2 2 8 9 9 9 9  $ROW 12
                  9 9 9 8 3 2 9 9 9 9 9 9 9 9 8 1 3 9 9 9 9 9  $ROW 13
                   9 9 9 1 2 8 9 9 9 9 9 9 3 3 8 9 9 9 9 9 9  $ROW 14
                    9 9 9 8 3 1 9 9 9 9 9 9 8 2 1 9 9 9 9 9 9 9  $ROW 15
                     9 9 9 3 2 8 3 8 2 8 1 3 8 9 9 9 9 9 9 9 9  $ROW 16
                      9 9 9 8 1 3 1 2 3 2 8 2 9 9 9 9 9 9 9 9 9  $ROW
17
                        9 9 9 9 8 2 8 1 8 3 9 9 9 9 9 9 9 9 9 9 9  $ROW
18
                         9 9 9 9 9 9 9 9 9 9 9 9 9 9 9 9 9 9 9 9 9 9 9  $ROW
19
                           9 9 9 9 9 9 9 9 9 9 9 9 9 9 9 9 9 9 9 9 9 9 9
$ROW 20
                            9 9 9 9 9 9 9 9 9 9 9 9 9 9 9 9 9 9 9 9 9 9 9
$ROW 21
102  0          -91  80 -93 fill=100 imp:n=1  $ Core
103  7  -1.77    91 -92 -93          imp:n=1  $ Upper reflector
104  7  -1.77   -80  90 -93          imp:n=1  $ Lower reflector
105  9  -1.732   90 -92  93 -94      imp:n=1  $ Outer reflector
106  0          #102 #103 #104 #105  imp:n=0

c  -- Surface Cards --
c    TRISO Particle surfaces
10   so 0.03     $ U kernel, diameter = 0.03cm
11   so 0.0359   $ Carbon buffer, thickness = 0.0059cm
12   so 0.039    $ IPyC, thickness = 0.0031cm
```

```
13   so 0.0419   $ SiC, thickness = 0.0029cm
14   so 0.0465   $ OPyC, thickness = 0.0046cm
c    TRISO lattice boundary, VF=0.3, side length=R[(4pi/3VF)^(1/3)]
21   pz  0.055986
22   pz -0.055986
23   px  0.055986
24   px -0.055986
25   py  0.055986
26   py -0.055986
c  Fuel compact surfaces
30   cz  0.5   $ Inner compact radius
31   cz  1.3   $ Outer compact radius
32   cz  1.7   $ Graphite sleeve, thickness = 0.4cm
33   cz  2.05  $ Helium coolant channel O/Dia.
34   cz  8.5   $ Graphite for remaining area
35   pz  0.15  $ Bottom plane - sleeve
36   pz  1.7   $ Bottom plane - compact
37   pz  56.3  $ Top plane - compact
38   pz  57.85 $ Top plane - sleeve
c  Burnable poison (BP) surfaces
40   cz  0.75  $ BP rod
41   pz  4.2   $ Bottom - lower part of BP rod
42   pz  24.2  $ Top - lower part of BP rod
43   pz  34.2  $ Bottom - upper part of BP rod
44   pz  54.2  $ Top - upper part of BP rod
c    Block handling hole surfaces
50   cz  2.25  $ Lower cylindrical section of handling hole
51   cz  1.5   $ Middle cylindrical section of handling hole
52   cz  2     $ Upper cylindrical section of handling hole
53   pz  33    $ Lower plane
54   pz  43    $ Middle plane
55   pz  49    $ Upper plane
c    Fuel element hexagonal surface
60   rhp 0 0 0  0 0 754  2.575 0 0   $ Pitch = 5.15 cm
c    Fuel/Reflector/Control block hexagonal surface
61   rhp 0 0 0  0 0 754  0 18 0      $ Pitch = 36 cm
c  Control rod channels
70   c/z -5.4   9.353 6.15
71   c/z -5.4  -9.353 6.15
72   c/z  10.8  0     6.15
c  Fuel/Control/Reflector block planes
80   pz   0     $ Bottom of active core
81   pz   58    $ Top of fuel/control block
c  Core and reflector
90   pz  -174   $ Lower plane of lower reflector
91   pz   754   $ Top plane of active core
92   pz   870   $ Top plane of upper reflector
93   cz   310   $ core
94   cz   340   $ outer reflector

c  Data cards
c  Criticality control cards
 kcode 2500 1.0 50 250
c USE SOURCE DISTRIBUTION IN FILE VHTR_3ZN_SRC
 sdef pos=0 0 0 rad=d1 axs=0 0 1 ext=d2
 si1 144 252
 si2 0  754
```

```
c
c  Material cards
m2   6000.73c   1               $ Carbon coatings
mt2  grph.17t
m3   14028.73c -0.64561         $ SiC coating
     14029.73c -0.03278
     14030.73c -0.02161
     6000.73c  -0.3
mt3  grph.17t
m4   2003.73c  -0.00000137      $ Helium coolant, density = 0.001708
g/cm3 (300K)
     2004.73c  -0.99999863
m6   6000.73c  -0.9999992       $ Graphite matrix (compact)
     5010.73c  -0.0000001631    $ B10 impurities
     5011.73c  -0.0000006569    $ B11 impurities
mt6  grph.17t
m7   6000.73c  -0.9999996       $ Graphite prismatic block
     5010.73c  -0.0000000796    $ B10 impurities
     5011.73c  -0.0000003204    $ B11 impurities
mt7  grph.17t
m8   6000.73c  -0.99999963      $ Graphite sleeve (rod)
     5010.73c  -0.0000000736    $ B10 impurities
     5011.73c  -0.0000002964    $ B11 impurities
mt8  grph.17t
m9   6000.73c  -0.999998        $ Graphite outer cylinder
     5010.73c  -0.000000398     $ B10 impurities
     5011.73c  -0.000001602     $ B11 impurities
mt9  grph.17t
c
m11  92235.73c  3.215E-04
     92238.73c  1.886E-02
     8016.73c   4.651E-02
     93237.73c  1.376E-05
     94238.73c  1.271E-05
     94239.73c  4.852E-05
     94240.73c  5.660E-05
     94241.73c  2.784E-05
     95241.73c  3.775E-07
     95242.73c  2.919E-09
     95243.73c  4.358E-06
     96242.73c  7.225E-07
     96243.73c  1.650E-08
     96244.73c  2.835E-06
     96245.73c  9.504E-08
     33074.73c  1.000E-36
     33075.73c  3.246E-08
     35079.73c  3.066E-11
     35081.73c  5.825E-06
     36078.73c  1.000E-36
     36080.73c  2.091E-11
     36082.73c  2.780E-07
     36083.73c  9.625E-06
     36084.73c  3.486E-05
     36086.73c  5.954E-05
     37085.73c  2.724E-05
     37087.73c  7.406E-05
     39089.73c  1.223E-04
```

```
40090.73c  4.843E-06
40091.73c  1.486E-04
40092.73c  1.743E-04
40093.73c  1.829E-04
40094.73c  2.002E-04
40096.73c  1.911E-04
41093.73c  1.000E-36
42095.73c  1.480E-04
43099.73c  1.655E-04
44101.73c  1.598E-04
44103.73c  4.553E-06
44105.73c  1.502E-08
46102.73c  1.000E-36
46104.73c  3.456E-05
46105.73c  4.614E-05
46106.73c  2.455E-05
46108.73c  1.353E-05
46110.73c  4.796E-06
47107.73c  1.000E-36
47109.73c  6.779E-06
48106.73c  1.000E-36
48108.73c  1.000E-36
48110.73c  3.486E-06
48111.73c  2.220E-06
48112.73c  1.196E-06
48113.73c  3.007E-09
50120.73c  3.789E-07
53127.73c  6.113E-06
53129.73c  1.964E-05
54124.73c  1.000E-36
54126.73c  1.000E-36
54128.73c  3.969E-07
54129.73c  4.891E-09
54130.73c  2.506E-06
54131.73c  6.022E-05
54132.73c  1.846E-04
54134.73c  2.588E-04
54135.73c  8.657E-09
54136.73c  3.749E-04
55133.73c  1.765E-04
55134.73c  2.286E-05
55135.73c  5.802E-05
55136.73c  1.105E-07
55137.73c  1.948E-04
56138.73c  2.178E-04
59141.73c  1.626E-04
60143.73c  8.408E-05
60145.73c  1.007E-04
60147.73c  6.161E-07
60148.73c  5.509E-05
60150.73c  2.248E-05
61147.73c  1.484E-05
61149.73c  1.228E-07
62147.73c  1.022E-05
62149.73c  9.499E-08
62150.73c  3.663E-05
62151.73c  1.116E-06
```

```
      62152.73c  1.427E-05
      63151.73c  3.057E-10
      63152.73c  5.769E-10
      63153.73c  1.371E-05
      63154.73c  1.681E-06
      63155.73c  3.784E-07
      64152.73c  1.419E-09
      64154.73c  1.886E-07
      64155.73c  2.181E-09
      64156.73c  1.334E-05
      64157.73c  8.427E-09
      64158.73c  2.161E-06
      64160.73c  7.683E-08
      67165.73c  3.381E-09
c
m15   1001.73c   1.000E-36
      1002.73c   1.000E-36
      1003.73c   1.220E-09
      2003.73c   1.000E-36
      2004.73c   1.857E-08
      3006.73c   1.000E-36
      3007.73c   2.332E-04
      4009.73c   5.366E-11
      5010.73c   1.000E-36
      5011.73c   1.943E-03
      6000.73c   8.929E-02
      6012       1.733E-08
      6013       1.000E-36
      7014.73c   1.000E-36
      7015.73c   1.000E-36
mt15  grph.17t
c
m21   92235.73c  3.532E-03
      92238.73c  1.976E-02
      8016.73c   4.653E-02
      93237.73c  1.000E-36
      94238.73c  1.000E-36
      94239.73c  1.000E-36
      94240.73c  1.000E-36
      94241.73c  1.000E-36
      95241.73c  1.000E-36
      95242.73c  1.000E-36
      95243.73c  1.000E-36
      96242.73c  1.000E-36
      96243.73c  1.000E-36
      96244.73c  1.000E-36
      96245.73c  1.000E-36
      33074.73c  1.000E-36
      33075.73c  1.000E-36
      35079.73c  1.000E-36
      35081.73c  1.000E-36
      36078.73c  1.000E-36
      36080.73c  1.000E-36
      36082.73c  1.000E-36
      36083.73c  1.000E-36
      36084.73c  1.000E-36
      36086.73c  1.000E-36
```

```
37085.73c  1.000E-36
37087.73c  1.000E-36
39089.73c  1.000E-36
40090.73c  1.000E-36
40091.73c  1.000E-36
40092.73c  1.000E-36
40093.73c  1.000E-36
40094.73c  1.000E-36
40096.73c  1.000E-36
41093.73c  1.000E-36
42095.73c  1.000E-36
43099.73c  1.000E-36
44101.73c  1.000E-36
44103.73c  1.000E-36
44105.73c  1.000E-36
46102.73c  1.000E-36
46104.73c  1.000E-36
46105.73c  1.000E-36
46106.73c  1.000E-36
46108.73c  1.000E-36
46110.73c  1.000E-36
47107.73c  1.000E-36
47109.73c  1.000E-36
48106.73c  1.000E-36
48108.73c  1.000E-36
48110.73c  1.000E-36
48111.73c  1.000E-36
48112.73c  1.000E-36
48113.73c  1.000E-36
50120.73c  1.000E-36
53127.73c  1.000E-36
53129.73c  1.000E-36
54124.73c  1.000E-36
54126.73c  1.000E-36
54128.73c  1.000E-36
54129.73c  1.000E-36
54130.73c  1.000E-36
54131.73c  1.000E-36
54132.73c  1.000E-36
54134.73c  1.000E-36
54135.73c  1.000E-36
54136.73c  1.000E-36
55133.73c  1.000E-36
55134.73c  1.000E-36
55135.73c  1.000E-36
55136.73c  1.000E-36
55137.73c  1.000E-36
56138.73c  1.000E-36
59141.73c  1.000E-36
60143.73c  1.000E-36
60145.73c  1.000E-36
60147.73c  1.000E-36
60148.73c  1.000E-36
60150.73c  1.000E-36
61147.73c  1.000E-36
61149.73c  1.000E-36
62147.73c  1.000E-36
```

```
      62149.73c  1.000E-36
      62150.73c  1.000E-36
      62151.73c  1.000E-36
      62152.73c  1.000E-36
      63151.73c  1.000E-36
      63152.73c  1.000E-36
      63153.73c  1.000E-36
      63154.73c  1.000E-36
      63155.73c  1.000E-36
      64152.73c  1.000E-36
      64154.73c  1.000E-36
      64155.73c  1.000E-36
      64156.73c  1.000E-36
      64157.73c  1.000E-36
      64158.73c  1.000E-36
      64160.73c  1.000E-36
      67165.73c  1.000E-36
c
m25   3006.73c   1.000E-36
      3007.73c   1.000E-36
      4009.73c   1.000E-36
      5010.73c   4.671E-04
      5011.73c   1.710E-03
      6000.73c   8.929E-02
      6012       1.000E-36
      6013       1.000E-36
      7014.73c   1.000E-36
      7015.73c   1.000E-36
mt25 grph.17t
c
m31   92235.73c  1.831E-03
      92238.73c  2.013E-02
      8016.73c   4.817E-02
      93237.73c  8.720E-06
      94238.73c  1.528E-06
      94239.73c  7.548E-05
      94240.73c  4.462E-05
      94241.73c  2.198E-05
      95241.73c  1.928E-07
      95242.73c  1.515E-09
      95243.73c  3.775E-07
      96242.73c  9.480E-08
      96243.73c  7.189E-10
      96244.73c  4.637E-08
      96245.73c  8.039E-10
      33074.73c  1.000E-36
      33075.73c  1.729E-08
      35079.73c  1.000E-36
      35081.73c  3.177E-06
      36078.73c  1.000E-36
      36080.73c  1.000E-36
      36082.73c  5.367E-08
      36083.73c  7.467E-06
      36084.73c  1.638E-05
      36086.73c  3.248E-05
      37085.73c  1.456E-05
      37087.73c  4.020E-05
```

```
39089.73c  5.817E-05
40090.73c  1.025E-06
40091.73c  6.862E-05
40092.73c  9.349E-05
40093.73c  9.881E-05
40094.73c  1.041E-04
40096.73c  1.003E-04
41093.73c  1.000E-36
42095.73c  6.037E-05
43099.73c  9.272E-05
44101.73c  8.280E-05
44103.73c  9.870E-06
44105.73c  2.399E-08
46102.73c  1.000E-36
46104.73c  6.721E-06
46105.73c  1.717E-05
46106.73c  5.856E-06
46108.73c  3.163E-06
46110.73c  1.111E-06
47107.73c  1.000E-36
47109.73c  1.841E-06
48106.73c  1.000E-36
48108.73c  1.000E-36
48110.73c  2.238E-07
48111.73c  5.421E-07
48112.73c  3.371E-07
48113.73c  5.435E-09
50120.73c  2.092E-07
53127.73c  2.728E-06
53129.73c  9.695E-06
54124.73c  1.000E-36
54126.73c  1.000E-36
54128.73c  5.578E-08
54129.73c  1.847E-10
54130.73c  3.107E-07
54131.73c  4.087E-05
54132.73c  7.862E-05
54134.73c  1.309E-04
54135.73c  3.107E-08
54136.73c  1.903E-04
55133.73c  1.009E-04
55134.73c  5.270E-06
55135.73c  2.428E-05
55136.73c  5.786E-08
55137.73c  1.012E-04
56138.73c  1.109E-04
59141.73c  7.963E-05
60143.73c  7.313E-05
60145.73c  5.926E-05
60147.73c  1.766E-06
60148.73c  2.801E-05
60150.73c  1.092E-05
61147.73c  2.091E-05
61149.73c  2.578E-07
62147.73c  2.687E-06
62149.73c  2.671E-07
62150.73c  1.941E-05
```

```
      62151.73c  1.511E-06
      62152.73c  8.493E-06
      63151.73c  5.133E-10
      63152.73c  1.083E-09
      63153.73c  4.913E-06
      63154.73c  5.568E-07
      63155.73c  1.353E-07
      64152.73c  1.045E-09
      64154.73c  1.409E-08
      64155.73c  7.182E-10
      64156.73c  1.483E-06
      64157.73c  5.257E-09
      64158.73c  4.265E-07
      64160.73c  1.871E-08
      67165.73c  6.291E-10
c
m35   1003.73c   1.000E-36
      2004.73c   1.000E-36
      3006.73c   1.000E-36
      3007.73c   2.332E-04
      4009.73c   4.184E-11
      5010.73c   2.166E-08
      5011.73c   1.944E-03
      6000.73c   8.933E-02
      6012       1.373E-08
      6013       1.000E-36
      7014.73c   1.000E-36
      7015.73c   1.000E-36
mt35 grph.17t
c
m40   38090.73c 1
m41   40093.73c 1
m42   43099.73c 1
m43   53129.73c 1
m44   55135.73c 1
m45   55137.73c 1
c
c  Tallies
fc4   Flux in the system
fmesh4:n geom=cyl origin=0 0 -174 axs=0 0 1 vec=1 0 0 &
          imesh=20.7846 301.3768 iints=1 9 jmesh=1044 jints=18 &
          kmesh=1 kints=1 &
          emesh=1.05000e-10 &
    1.00000e-9 1.05925e-9 1.12202e-9 1.18850e-9 1.25893e-9 &
    1.33352e-9 1.41254e-9 1.49624e-9 1.58489e-9 1.67880e-9 &
    1.77828e-9 1.88365e-9 1.99526e-9 2.11349e-9 2.23872e-9 &
    2.37137e-9 2.51189e-9 2.66073e-9 2.81838e-9 2.98538e-9 &
    3.16228e-9 3.34965e-9 3.54813e-9 3.75837e-9 3.98107e-9 &
    4.21697e-9 4.46684e-9 4.73151e-9 5.01187e-9 5.30884e-9 &
    5.62341e-9 5.95662e-9 6.30957e-9 6.68344e-9 7.07946e-9 &
    7.49894e-9 7.94328e-9 8.41395e-9 8.91251e-9 9.44061e-9 &
    1.00000e-8 1.05925e-8 1.12202e-8 1.18850e-8 1.25893e-8 &
    1.33352e-8 1.41254e-8 1.49624e-8 1.58489e-8 1.67880e-8 &
    1.77828e-8 1.88365e-8 1.99526e-8 2.11349e-8 2.23872e-8 &
    2.37137e-8 2.51189e-8 2.66073e-8 2.81838e-8 2.98538e-8 &
    3.16228e-8 3.34965e-8 3.54813e-8 3.75837e-8 3.98107e-8 &
    4.21697e-8 4.46684e-8 4.73151e-8 5.01187e-8 5.30884e-8 &
```

```
5.62341e-8 5.95662e-8 6.30957e-8 6.68344e-8 7.07946e-8 &
7.49894e-8 7.94328e-8 8.41395e-8 8.91251e-8 9.44061e-8 &
1.00000e-7 1.05925e-7 1.12202e-7 1.18850e-7 1.25893e-7 &
1.33352e-7 1.41254e-7 1.49624e-7 1.58489e-7 1.67880e-7 &
1.77828e-7 1.88365e-7 1.99526e-7 2.11349e-7 2.23872e-7 &
2.37137e-7 2.51189e-7 2.66073e-7 2.81838e-7 2.98538e-7 &
3.16228e-7 3.34965e-7 3.54813e-7 3.75837e-7 3.98107e-7 &
4.21697e-7 4.46684e-7 4.73151e-7 5.01187e-7 5.30884e-7 &
5.62341e-7 5.95662e-7 6.30957e-7 6.68344e-7 7.07946e-7 &
7.49894e-7 7.94328e-7 8.41395e-7 8.91251e-7 9.44061e-7 &
1.00000e-6 1.05925e-6 1.12202e-6 1.18850e-6 1.25893e-6 &
1.33352e-6 1.41254e-6 1.49624e-6 1.58489e-6 1.67880e-6 &
1.77828e-6 1.88365e-6 1.99526e-6 2.11349e-6 2.23872e-6 &
2.37137e-6 2.51189e-6 2.66073e-6 2.81838e-6 2.98538e-6 &
3.16228e-6 3.34965e-6 3.54813e-6 3.75837e-6 3.98107e-6 &
4.21697e-6 4.46684e-6 4.73151e-6 5.01187e-6 5.30884e-6 &
5.62341e-6 5.95662e-6 6.30957e-6 6.68344e-6 7.07946e-6 &
7.49894e-6 7.94328e-6 8.41395e-6 8.91251e-6 9.44061e-6 &
1.00000e-5 1.05925e-5 1.12202e-5 1.18850e-5 1.25893e-5 &
1.33352e-5 1.41254e-5 1.49624e-5 1.58489e-5 1.67880e-5 &
1.77828e-5 1.88365e-5 1.99526e-5 2.11349e-5 2.23872e-5 &
2.37137e-5 2.51189e-5 2.66073e-5 2.81838e-5 2.98538e-5 &
3.16228e-5 3.34965e-5 3.54813e-5 3.75837e-5 3.98107e-5 &
4.21697e-5 4.46684e-5 4.73151e-5 5.01187e-5 5.30884e-5 &
5.62341e-5 5.95662e-5 6.30957e-5 6.68344e-5 7.07946e-5 &
7.49894e-5 7.94328e-5 8.41395e-5 8.91251e-5 9.44061e-5 &
1.00000e-4 1.05925e-4 1.12202e-4 1.18850e-4 1.25893e-4 &
1.33352e-4 1.41254e-4 1.49624e-4 1.58489e-4 1.67880e-4 &
1.77828e-4 1.88365e-4 1.99526e-4 2.11349e-4 2.23872e-4 &
2.37137e-4 2.51189e-4 2.66073e-4 2.81838e-4 2.98538e-4 &
3.16228e-4 3.34965e-4 3.54813e-4 3.75837e-4 3.98107e-4 &
4.21697e-4 4.46684e-4 4.73151e-4 5.01187e-4 5.30884e-4 &
5.62341e-4 5.95662e-4 6.30957e-4 6.68344e-4 7.07946e-4 &
7.49894e-4 7.94328e-4 8.41395e-4 8.91251e-4 9.44061e-4 &
1.00000e-3 1.05925e-3 1.12202e-3 1.18850e-3 1.25893e-3 &
1.33352e-3 1.41254e-3 1.49624e-3 1.58489e-3 1.67880e-3 &
1.77828e-3 1.88365e-3 1.99526e-3 2.11349e-3 2.23872e-3 &
2.37137e-3 2.51189e-3 2.66073e-3 2.81838e-3 2.98538e-3 &
3.16228e-3 3.34965e-3 3.54813e-3 3.75837e-3 3.98107e-3 &
4.21697e-3 4.46684e-3 4.73151e-3 5.01187e-3 5.30884e-3 &
5.62341e-3 5.95662e-3 6.30957e-3 6.68344e-3 7.07946e-3 &
7.49894e-3 7.94328e-3 8.41395e-3 8.91251e-3 9.44061e-3 &
1.00000e-2 1.05925e-2 1.12202e-2 1.18850e-2 1.25893e-2 &
1.33352e-2 1.41254e-2 1.49624e-2 1.58489e-2 1.67880e-2 &
1.77828e-2 1.88365e-2 1.99526e-2 2.11349e-2 2.23872e-2 &
2.37137e-2 2.51189e-2 2.66073e-2 2.81838e-2 2.98538e-2 &
3.16228e-2 3.34965e-2 3.54813e-2 3.75837e-2 3.98107e-2 &
4.21697e-2 4.46684e-2 4.73151e-2 5.01187e-2 5.30884e-2 &
5.62341e-2 5.95662e-2 6.30957e-2 6.68344e-2 7.07946e-2 &
7.49894e-2 7.94328e-2 8.41395e-2 8.91251e-2 9.44061e-2 &
1.00000e-1 1.05925e-1 1.12202e-1 1.18850e-1 1.25893e-1 &
1.33352e-1 1.41254e-1 1.49624e-1 1.58489e-1 1.67880e-1 &
1.77828e-1 1.88365e-1 1.99526e-1 2.11349e-1 2.23872e-1 &
2.37137e-1 2.51189e-1 2.66073e-1 2.81838e-1 2.98538e-1 &
3.16228e-1 3.34965e-1 3.54813e-1 3.75837e-1 3.98107e-1 &
4.21697e-1 4.46684e-1 4.73151e-1 5.01187e-1 5.30884e-1 &
5.62341e-1 5.95662e-1 6.30957e-1 6.68344e-1 7.07946e-1 &
```

```
    7.49894e-1 7.94328e-1 8.41395e-1 8.91251e-1 9.44061e-1 &
    1.00000e+0 1.05925e+0 1.12202e+0 1.18850e+0 1.25893e+0 &
    1.33352e+0 1.41254e+0 1.49624e+0 1.58489e+0 1.67880e+0 &
    1.77828e+0 1.88365e+0 1.99526e+0 2.11349e+0 2.23872e+0 &
    2.37137e+0 2.51189e+0 2.66073e+0 2.81838e+0 2.98538e+0 &
    3.16228e+0 3.34965e+0 3.54813e+0 3.75837e+0 3.98107e+0 &
    4.21697e+0 4.46684e+0 4.73151e+0 5.01187e+0 5.30884e+0 &
    5.62341e+0 5.95662e+0 6.30957e+0 6.68344e+0 7.07946e+0 &
    7.49894e+0 7.94328e+0 8.41395e+0 8.91251e+0 9.44061e+0 &
    1.00000e+1 1.05925e+1 1.12202e+1 1.18850e+1 1.25893e+1 &
    1.33352e+1 1.41254e+1 1.49624e+1 1.58489e+1 1.67880e+1 &
    1.77828e+1 1.88365e+1 1.99526e+1 2.11349e+1 2.23872e+1 &
    2.37137e+1 2.51189e+1 2.66073e+1 2.81838e+1 2.98538e+1 &
    3.16228e+1 3.34965e+1 3.54813e+1 3.75837e+1 3.98107e+1 &
    4.21697e+1 4.46684e+1 4.73151e+1 5.01187e+1 5.30884e+1 &
    5.62341e+1 5.95662e+1 6.30957e+1 6.68344e+1 7.07946e+1 &
    7.49894e+1 7.94328e+1 8.41395e+1 8.91251e+1 9.44061e+1 &
    1.00000e+2 &
    eints=1 1 &
    1 1 1 1 1 1 1 1 1 1 1 1 1 1 1 1 1 1 1 1 &
    1 1 1 1 1 1 1 1 1 1 1 1 1 1 1 1 1 1 1 1 &
    1 1 1 1 1 1 1 1 1 1 1 1 1 1 1 1 1 1 1 1 &
    1 1 1 1 1 1 1 1 1 1 1 1 1 1 1 1 1 1 1 1 &
    1 1 1 1 1 1 1 1 1 1 1 1 1 1 1 1 1 1 1 1 &
    1 1 1 1 1 1 1 1 1 1 1 1 1 1 1 1 1 1 1 1 &
    1 1 1 1 1 1 1 1 1 1 1 1 1 1 1 1 1 1 1 1 &
    1 1 1 1 1 1 1 1 1 1 1 1 1 1 1 1 1 1 1 1 &
    1 1 1 1 1 1 1 1 1 1 1 1 1 1 1 1 1 1 1 1 &
    1 1 1 1 1 1 1 1 1 1 1 1 1 1 1 1 1 1 1 1 &
    1 1 1 1 1 1 1 1 1 1 1 1 1 1 1 1 1 1 1 1 &
    1 1 1 1 1 1 1 1 1 1 1 1 1 1 1 1 1 1 1 1 &
    1 1 1 1 1 1 1 1 1 1 1 1 1 1 1 1 1 1 1 1 &
    1 1 1 1 1 1 1 1 1 1 1 1 1 1 1 1 1 1 1 1 &
    1 1 1 1 1 1 1 1 1 1 1 1 1 1 1 1 1 1 1 1 &
    1 1 1 1 1 1 1 1 1 1 1 1 1 1 1 1 1 1 1 1 &
    1 1 1 1 1 1 1 1 1 1 1 1 1 1 1 1 1 1 1 1 &
    1 1 1 1 1 1 1 1 1 1 1 1 1 1 1 1 1 1 1 1 &
    1 1 1 1 1 1 1 1 1 1 1 1 1 1 1 1 1 1 1 1 &
    1 1 1 1 1 1 1 1 1 1 1 1 1 1 1 1 1 1 1 1 &
    1 1 1 1 1 1 1 1 1 1 1 1 1 1 1 1 1 1 1 1 &
    1 1 1 1 1 1 1 1 1 1 1 1 1 1 1 1 1 1 1 1
fm4 4.622e+19      $ Source (n/sec) @cycle-3, timestep-0 (BOC3)
c
fc14   Sr90 reaction rates
fmesh14:n geom=cyl origin=0 0 -174 axs=0 0 1 vec=1 0 0 &
          imesh=20.7846 301.3768 iints=1 9 jmesh=1044 jints=18 &
          kmesh=1 kints=1
fm14 -1 40 -2
c
fc24   Zr93 reaction rates
fmesh24:n geom=cyl origin=0 0 -174 axs=0 0 1 vec=1 0 0 &
          imesh=20.7846 301.3768 iints=1 9 jmesh=1044 jints=18 &
          kmesh=1 kints=1
fm24 -1 41 -2
c
fc34   Tc99 reaction rates
fmesh34:n geom=cyl origin=0 0 -174 axs=0 0 1 vec=1 0 0 &
```

```
          imesh=20.7846 301.3768 iints=1 9 jmesh=1044 jints=18 &
          kmesh=1 kints=1
fm34 -1 42 -2
c
fc44   I129 reaction rates
fmesh44:n geom=cyl origin=0 0 -174 axs=0 0 1 vec=1 0 0 &
          imesh=20.7846 301.3768 iints=1 9 jmesh=1044 jints=18 &
          kmesh=1 kints=1
fm44 -1 43 -2
c
fc54   Cs135 reaction rates
fmesh54:n geom=cyl origin=0 0 -174 axs=0 0 1 vec=1 0 0 &
          imesh=20.7846 301.3768 iints=1 9 jmesh=1044 jints=18 &
          kmesh=1 kints=1
fm54 -1 44 -2
c
fc64   Cs137 reaction rates
fmesh64:n geom=cyl origin=0 0 -174 axs=0 0 1 vec=1 0 0 &
          imesh=20.7846 301.3768 iints=1 9 jmesh=1044 jints=18 &
          kmesh=1 kints=1
fm64 -1 45 -2
c
prdmp j 25
```

C-2: SAMPLE MCNPX INPUT DECK

```
VHTR Prismatic Power Core
c based on Japan's HTTR fuel and block design
c  -- Cell cards --
c  TRISO particle
c    Zone 1
1    11 6.982E-02  -10     u=10 imp:n=1 VOL=1.13097e-04 $ Fuel kernel
(15% u235 enrichment)
2    2  -1.14       10 -11 u=10 imp:n=1  $ Porous buffer
3    2  -1.89       11 -12 u=10 imp:n=1  $ IPyC
4    3  -3.2        12 -13 u=10 imp:n=1  $ SiC containment
5    2  -1.87       13 -14 u=10 imp:n=1  $ OPyC
6    6  -1.69       14     u=10 imp:n=1  $ Graphite matrix
c
c    Zone 2
7    21 6.983E-02  -10     u=11 imp:n=1 VOL=1.13097e-04 $ Fuel kernel
(15% enrichment)
8    2  -1.14       10 -11 u=11 imp:n=1  $ Porous buffer
9    2  -1.89       11 -12 u=11 imp:n=1  $ IPyC
10   3  -3.2        12 -13 u=11 imp:n=1  $ SiC containment
11   2  -1.87       13 -14 u=11 imp:n=1  $ OPyC
12   6  -1.69       14     u=11 imp:n=1  $ Graphite matrix
c
c    Zone 3
13   31 -10.41     -10     u=12 imp:n=1 VOL=1.13097e-04 $ Fuel kernel
(15% enrichment)
14   2  -1.14       10 -11 u=12 imp:n=1  $ Porous buffer
15   2  -1.89       11 -12 u=12 imp:n=1  $ IPyC
16   3  -3.2        12 -13 u=12 imp:n=1  $ SiC containment
17   2  -1.87       13 -14 u=12 imp:n=1  $ OPyC
18   6  -1.69       14     u=12 imp:n=1  $ Graphite matrix
c
19   0             -21 22 -23 24 -25 26 lat=1 u=15 fill=10 imp:n=1  $
Unit of compact lattice
20   0             -21 22 -23 24 -25 26 lat=1 u=16 fill=11 imp:n=1  $
Unit of compact lattice
21   0             -21 22 -23 24 -25 26 lat=1 u=17 fill=12 imp:n=1  $
Unit of compact lattice
c  Fuel compact
c    Zone 1
22   4  -0.001708   36 -37 -30      u=20         imp:n=1  $ Helium in
inner annulus
23   0              36 -37  30 -31  u=20 fill=15 imp:n=1  $ Fuel
compact annulus
24   8  -1.77       35 -38  31 -32  u=20         imp:n=1  $ Graphite
sleeve
25   4  -0.001708   35 -38  32 -33  u=20         imp:n=1  $ Coolant
channel
26   4  -0.001708  -35 -33          u=20         imp:n=1  $ Helium
below fuel rod
27   4  -0.001708   38 -33          u=20         imp:n=1  $ Helium
above fuel rod
28   8  -1.77       35 -36 -31      u=20         imp:n=1  $ Graphite
sleeve bottom-cap
```

```
29   8  -1.77       37 -38 -31      u=20         imp:n=1  $ Graphite
sleeve top-cap
30   7  -1.77       33              u=20         imp:n=1  $ Surrounding
Graphite
c
c    Zone 2
31   4  -0.001708   36 -37 -30      u=21         imp:n=1  $ Helium in
inner annulus
32   0              36 -37  30 -31  u=21 fill=16 imp:n=1  $ Fuel region
of rod
33   8  -1.77       35 -38  31 -32  u=21         imp:n=1  $ Graphite
sleeve
34   4  -0.001708   35 -38  32 -33  u=21         imp:n=1  $ Helium
coolant channel
35   4  -0.001708  -35 -33          u=21         imp:n=1  $ Helium
below fuel rod
36   4  -0.001708   38 -33          u=21         imp:n=1  $ Helium
above fuel rod
37   8  -1.77       35 -36 -31      u=21         imp:n=1  $ Graphite
sleeve bottom-cap
38   8  -1.77       37 -38 -31      u=21         imp:n=1  $ Graphite
sleeve top-cap
39   7  -1.77       33              u=21         imp:n=1  $ Surrounding
Graphite
c
c    Zone 3
40   4  -0.001708   36 -37 -30      u=22         imp:n=1  $ Helium in
inner annulus
41   0              36 -37  30 -31  u=22 fill=17 imp:n=1  $ Fuel region
of rod
42   8  -1.77       35 -38  31 -32  u=22         imp:n=1  $ Graphite
sleeve
43   4  -0.001708   35 -38  32 -33  u=22         imp:n=1  $ Helium
coolant channel
44   4  -0.001708  -35 -33          u=22         imp:n=1  $ Helium
below fuel rod
45   4  -0.001708   38 -33          u=22         imp:n=1  $ Helium
above fuel rod
46   8  -1.77       35 -36 -31      u=22         imp:n=1  $ Graphite
sleeve bottom-cap
47   8  -1.77       37 -38 -31      u=22         imp:n=1  $ Graphite
sleeve top-cap
48   7  -1.77       33              u=22         imp:n=1  $ Surrounding
Graphite
c
c  Burnable poison rod
c    Zone 1
49   15  9.147E-02  41 -42 -40      u=23 imp:n=1 VOL=35.3429 $ Lower
portion of BP rod
50   2  -1.77       42 -43 -40      u=23         imp:n=1  $ Middle
(graphite) portion of BP rod
51   15  9.147E-02  43 -44 -40      u=23 imp:n=1 VOL=35.3429 $ Upper
portion of BP rod
52   7  -1.77       40              u=23         imp:n=1  $ Surrounding
Graphite
53   7  -1.77       44 -40          u=23         imp:n=1  $ Graphite
above BP rod
```

```
54   7  -1.77      -41 -40          u=23         imp:n=1  $ Graphite
below BP rod
c
c    Zone 2
55   25  9.147E-02  41 -42 -40      u=24 imp:n=1 VOL=35.3429 $ Lower
portion of BP rod
56   2  -1.77       42 -43 -40      u=24         imp:n=1  $ Middle
(graphite) portion of BP rod
57   25  9.147E-02   43 -44 -40      u=24 imp:n=1 VOL=35.3429 $ Upper
portion of BP rod
58   7  -1.77       40              u=24         imp:n=1  $ Surrounding
Graphite
59   7  -1.77       44 -40          u=24         imp:n=1  $ Graphite
above BP rod
60   7  -1.77      -41 -40          u=24         imp:n=1  $ Graphite
below BP rod
c
c    Zone 3
61   35 -1.82       41 -42 -40      u=25 imp:n=1 VOL=35.3429 $ Lower
portion of BP rod
62   2  -1.77       42 -43 -40      u=25         imp:n=1  $ Middle
(graphite) portion of BP rod
63   35 -1.82       43 -44 -40      u=25 imp:n=1 VOL=35.3429 $ Upper
portion of BP rod
64   7  -1.77       40              u=25         imp:n=1  $ Surrounding
Graphite
65   7  -1.77       44 -40          u=25         imp:n=1  $ Graphite
above BP rod
66   7  -1.77      -41 -40          u=25         imp:n=1  $ Graphite
below BP rod
c
c  Empty BP location
67   4  -0.001708   41 -44 -40      u=27         imp:n=1
68   7  -1.77      #67              u=27         imp:n=1
c
c  Block handling hole
69   4  -0.001708   53 -54 -50      u=28         imp:n=1  $ Lower block
handling hole
70   4  -0.001708   54 -55 -51      u=28         imp:n=1  $ Middle
block handling hole
71   4  -0.001708   55 -52          u=28         imp:n=1  $ Upper block
handling hole
72   7  -1.77      #71 #70 #69      u=28         imp:n=1  $ Surrounding
graphite
c  Graphite part of fuel block
73   7  -1.77      -34              u=29         imp:n=1
c
c  Fuel block
c    Zone 1
74   0  -60 lat=2 imp:n=1 u=30 fill=-4:4 -4:4 0:0   $ Pitch = 5.15 cm
      29 29 29 29 29 29 29 29 29  $ROW 1
       29 29 29 29 27 20 20 20 29  $ROW 2
        29 29 29 20 20 20 20 20 29  $ROW 3
         29 29 20 20 20 20 20 20 29  $ROW 4
          29 20 20 20 28 20 20 23 29  $ROW 5
           29 20 20 20 20 20 20 29 29  $ROW 6
            29 20 20 20 20 20 29 29 29  $ROW 7
```

```
             29 23 20 20 20 29 29 29 29  $ROW 8
              29 29 29 29 29 29 29 29 29  $ROW 9
75   0  -61  fill=30 u=31 imp:n=1
76   0  #75          u=31 imp:n=0
c
c    Zone 2
77   0  -60 lat=2 imp:n=1 u=35 fill=-4:4 -4:4 0:0   $ Pitch = 5.15 cm
      29 29 29 29 29 29 29 29 29  $ROW 1
       29 29 29 29 27 21 21 21 29  $ROW 2
        29 29 29 21 21 21 21 21 29  $ROW 3
         29 29 21 21 21 21 21 21 29  $ROW 4
          29 21 21 21 28 21 21 24 29  $ROW 5
           29 21 21 21 21 21 21 29 29  $ROW 6
            29 21 21 21 21 21 29 29 29  $ROW 7
             29 24 21 21 21 29 29 29 29  $ROW 8
              29 29 29 29 29 29 29 29 29  $ROW 9
78   0  -61  fill=35 u=32 imp:n=1
79   0  #78          u=32 imp:n=0
c
c    Zone 3
80   0  -60 lat=2 imp:n=1 u=36 fill=-4:4 -4:4 0:0   $ Pitch = 5.15 cm
      29 29 29 29 29 29 29 29 29  $ROW 1
       29 29 29 29 27 22 22 22 29  $ROW 2
        29 29 29 22 22 22 22 22 29  $ROW 3
         29 29 22 22 22 22 22 22 29  $ROW 4
          29 22 22 22 28 22 22 25 29  $ROW 5
           29 22 22 22 22 22 22 29 29  $ROW 6
            29 22 22 22 22 22 29 29 29  $ROW 7
             29 25 22 22 22 29 29 29 29  $ROW 8
              29 29 29 29 29 29 29 29 29  $ROW 9
81   0  -61  fill=36 u=33 imp:n=1
82   0  #81          u=33 imp:n=0
c
c  Control rod block
83   4  -0.001708   53 -54 -50             u=38 imp:n=1  $ Lower block
handling hole
84   4  -0.001708   54 -55 -51             u=38 imp:n=1  $ Middle
block handling hole
85   4  -0.001708   55 -52                 u=38 imp:n=1  $ Upper block
handling hole
86   4  -0.001708  -70                     u=38 imp:n=1  $ Control rod
channel
87   4  -0.001708  -71                     u=38 imp:n=1  $ Control rod
channel
88   4  -0.001708  -72                     u=38 imp:n=1  $ Control rod
channel
89   7  -1.77      -61 70 71 72 #83 #84 #85 u=38 imp:n=1  $ Graphite
Control rod block
90   0              61  u=38    imp:n=0
c
c  Graphite Reflector block
91   4  -0.001708   53 -54 -50      u=39 imp:n=1  $ Lower block
handling hole
92   4  -0.001708   54 -55 -51      u=39 imp:n=1  $ Middle block
handling hole
93   4  -0.001708   55 -52          u=39 imp:n=1  $ Upper block
handling hole
```

```
94   7  -1.77      -61 #91 #92 #93  u=39 imp:n=1  $ Prismatic block
95   0              61              u=39 imp:n=0
c
c  Columns
96   0   80 -81 lat=1 imp:n=1 u=1 fill=31  $ Fuel block column - Zone 1
97   0   80 -81 lat=1 imp:n=1 u=2 fill=32  $ Fuel block column - Zone 2
98   0   80 -81 lat=1 imp:n=1 u=3 fill=33  $ Fuel block column - Zone 3
99   0   80 -81 lat=1 imp:n=1 u=8 fill=38  $ Control block column
100  0   80 -81 lat=1 imp:n=1 u=9 fill=39  $ Graphite block column
c
c  Core
101  0  -61 lat=2  imp:n=1 u=100  fill=-10:10 -10:10 0:0
      9 9 9 9 9 9 9 9 9 9 9 9 9 9 9 9 9 9 9 9 9 9 9  $ROW 1
       9 9 9 9 9 9 9 9 9 9 9 9 9 9 9 9 9 9 9 9 9 9 9  $ROW 2
        9 9 9 9 9 9 9 9 9 9 9 9 9 9 9 9 9 9 9 9 9 9 9  $ROW 3
         9 9 9 9 9 9 9 9 9 9 9 8 3 8 1 8 2 9 9 9 9 9  $ROW 4
          9 9 9 9 9 9 9 9 9 9 8 1 2 1 2 3 1 8 3 9 9 9 9  $ROW 5
           9 9 9 9 9 9 9 9 9 2 3 8 3 8 1 8 2 1 8 9 9 9 9  $ROW 6
            9 9 9 9 9 9 9 9 8 1 2 9 9 9 9 9 8 2 1 9 9 9 9  $ROW 7
             9 9 9 9 9 9 9 1 3 8 9 9 9 9 9 9 3 3 8 9 9 9 9  $ROW 8
              9 9 9 9 9 9 8 2 1 9 9 9 9 9 9 9 8 2 2 9 9 9 9  $ROW 9
               9 9 9 9 9 3 1 8 9 9 9 9 9 9 9 9 1 3 8 9 9 9 9  $ROW 10
                9 9 9 9 9 8 3 9 9 9 9 9 9 9 9 9 8 1 9 9 9 9 9  $ROW 11
                 9 9 9 9 2 1 8 9 9 9 9 9 9 9 9 2 2 8 9 9 9 9 9  $ROW 12
                  9 9 9 9 8 3 2 9 9 9 9 9 9 9 9 8 1 3 9 9 9 9 9 9  $ROW 13
                   9 9 9 9 1 2 8 9 9 9 9 9 9 9 3 3 8 9 9 9 9 9 9 9  $ROW 14
                    9 9 9 9 8 3 1 9 9 9 9 9 9 8 2 1 9 9 9 9 9 9 9 9  $ROW 15
                     9 9 9 9 3 2 8 3 8 2 8 1 3 8 9 9 9 9 9 9 9 9 9 9  $ROW 16
                      9 9 9 9 8 1 3 1 2 3 2 8 2 9 9 9 9 9 9 9 9 9 9 9  $ROW
17
                       9 9 9 9 9 8 2 8 1 8 3 9 9 9 9 9 9 9 9 9 9 9 9 9  $ROW
18
                        9 9 9 9 9 9 9 9 9 9 9 9 9 9 9 9 9 9 9 9 9 9 9 9 9  $ROW
19
                          9 9 9 9 9 9 9 9 9 9 9 9 9 9 9 9 9 9 9 9 9 9 9 9 9
$ROW 20
                           9 9 9 9 9 9 9 9 9 9 9 9 9 9 9 9 9 9 9 9 9 9 9 9 9
$ROW 21
102  0          -91  80 -93 fill=100 imp:n=1  $ Core
103  7  -1.77    91 -92 -93          imp:n=1  $ Upper reflector
104  7  -1.77   -80  90 -93          imp:n=1  $ Lower reflector
105  9  -1.732   90 -92  93 -94      imp:n=1  $ Outer reflector
106  0          #102 #103 #104 #105  imp:n=0

c  -- Surface Cards --
c    TRISO Particle surfaces
10   so 0.03     $ U kernel, diameter = 0.03cm
11   so 0.0359   $ Carbon buffer, thickness = 0.0059cm
12   so 0.039    $ IPyC, thickness = 0.0031cm
13   so 0.0419   $ SiC, thickness = 0.0029cm
14   so 0.0465   $ OPyC, thickness = 0.0046cm
c    TRISO lattice boundary, VF=0.3, side length=R[(4pi/3VF)^(1/3)]
21   pz  0.055986
22   pz -0.055986
23   px  0.055986
24   px -0.055986
25   py  0.055986
```

```
26   py -0.055986
c  Fuel compact surfaces
30   cz  0.5   $ Inner compact radius
31   cz  1.3   $ Outer compact radius
32   cz  1.7   $ Graphite sleeve, thickness = 0.4cm
33   cz  2.05  $ Helium coolant channel O/Dia.
34   cz  8.5   $ Graphite for remaining area
35   pz  0.15  $ Bottom plane - sleeve
36   pz  1.7   $ Bottom plane - compact
37   pz  56.3  $ Top plane - compact
38   pz  57.85 $ Top plane - sleeve
c  Burnable poison (BP) surfaces
40   cz  0.75  $ BP rod
41   pz  4.2   $ Bottom - lower part of BP rod
42   pz  24.2  $ Top - lower part of BP rod
43   pz  34.2  $ Bottom - upper part of BP rod
44   pz  54.2  $ Top - upper part of BP rod
c    Block handling hole surfaces
50   cz  2.25  $ Lower cylindrical section of handling hole
51   cz  1.5   $ Middle cylindrical section of handling hole
52   cz  2     $ Upper cylindrical section of handling hole
53   pz  33    $ Lower plane
54   pz  43    $ Middle plane
55   pz  49    $ Upper plane
c    Fuel element hexagonal surface
60   rhp 0 0 0  0 0 754  2.575 0 0   $ Pitch = 5.15 cm
c    Fuel/Reflector/Control block hexagonal surface
61   rhp 0 0 0  0 0 754  0 18 0      $ Pitch = 36 cm
c  Control rod channels
70   c/z -5.4   9.353 6.15
71   c/z -5.4  -9.353 6.15
72   c/z  10.8  0     6.15
c  Fuel/Control/Reflector block planes
80   pz   0     $ Bottom of active core
81   pz   58    $ Top of fuel/control block
c  Core and reflector
90   pz  -174   $ Lower plane of lower reflector
91   pz   754   $ Top plane of active core
92   pz   870   $ Top plane of upper reflector
93   cz   310   $ core
94   cz   340   $ outer reflector

c  Data cards
c  Criticality control cards
 kcode 2500 1.0 50 250
c USE SOURCE DISTRIBUTION IN FILE VHTR_3ZN_SRC
c sdef pos=0 0 0 rad=d1 axs=0 0 1 ext=d2
c si1 144 252
c si2 0  754
c
 BURN TIME = 100 2r 105 5
     MAT = 11 21 31 15 25 35
     POWER = 600
     PFRAC = 1 4r
     OMIT = 11 52 6014  8016  7016  8018  9018  44105 90234 91232
                  31070 32071 32075 34075 34081 35080 36079 36081
                  38085 41099 44097 45104 45106 45107 45108 45109
```

```
                45110 45111 46103 46111 48107 48109 49114 49116
                49117 49118 49119 49120 49121 50113 52121 53128
                54125 54127 56131 56133 58139 60149 61146 62145
                62146 66157 66159 68165
           21 52 6014  8016  7016  8018  9018  44105 90234 91232
                31070 32071 32075 34075 34081 35080 36079 36081
                38085 41099 44097 45104 45106 45107 45108 45109
                45110 45111 46103 46111 48107 48109 49114 49116
                49117 49118 49119 49120 49121 50113 52121 53128
                54125 54127 56131 56133 58139 60149 61146 62145
                62146 66157 66159 68165
           31 52 6014  8016  7016  8018  9018  44105 90234 91232
                31070 32071 32075 34075 34081 35080 36079 36081
                38085 41099 44097 45104 45106 45107 45108 45109
                45110 45111 46103 46111 48107 48109 49114 49116
                49117 49118 49119 49120 49121 50113 52121 53128
                54125 54127 56131 56133 58139 60149 61146 62145
                62146 66157 66159 68165
           15 5 8016 6014 7016 8018 9018
           25 5 8016 6014 7016 8018 9018
           35 5 8016 6014 7016 8018 9018
     AFMIN = 1.0E-10 5r
     BOPT = 1.0 14 1
     MATVOL = 1.824963e5 2r 4.043233e4 2r
c
c  Material cards
m2   6000   1               $ Carbon coatings
mt2  grph.06t
m3   14028 -0.64561         $ SiC coating
     14029 -0.03278
     14030 -0.02161
     6000  -0.3
mt3  grph.06t
m4   2003  -0.00000137      $ Helium coolant, density = 0.001708 g/cm3
(300K)
     2004  -0.99999863
m6   6000  -0.9999992       $ Graphite matrix (compact)
     5010  -0.0000001631    $ B10 impurities
     5011  -0.0000006569    $ B11 impurities
mt6  grph.06t
m7   6000  -0.9999996       $ Graphite prismatic block
     5010  -0.0000000796    $ B10 impurities
     5011  -0.0000003204    $ B11 impurities
mt7  grph.06t
m8   6000  -0.99999963      $ Graphite sleeve (rod)
     5010  -0.0000000736    $ B10 impurities
     5011  -0.0000002964    $ B11 impurities
mt8  grph.06t
m9   6000  -0.999998        $ Graphite outer cylinder
     5010  -0.000000398     $ B10 impurities
     5011  -0.000001602     $ B11 impurities
mt9  grph.06t
m11  92235 -0.13222  $  Zone 1: UO2, density = 10.41 g/cm3
     92238 -0.74925  $          enrichment = 15%
     8016  -0.11853
     93237 -1e-36    $          Start of TRU
     94238 -1e-36
```

```
94239 -1e-36
94240 -1e-36
94241 -1e-36
95241 -1e-36
95242 -1e-36
95243 -1e-36
96242 -1e-36
96243 -1e-36
96244 -1e-36
96245 -1e-36
33074 -1e-36    $          Start of (tier 2) fission products
33075 -1e-36
35079 -1e-36
35081 -1e-36
36078 -1e-36
36080 -1e-36
36082 -1e-36
36083 -1e-36
36084 -1e-36
36086 -1e-36
37085 -1e-36
37087 -1e-36
39089 -1e-36
40090 -1e-36
40091 -1e-36
40092 -1e-36
40093 -1e-36
40094 -1e-36
40096 -1e-36
41093 -1e-36
42095 -1e-36
43099 -1e-36
44101 -1e-36
44103 -1e-36
44105 -1e-36
46102 -1e-36
46104 -1e-36
46105 -1e-36
46106 -1e-36
46108 -1e-36
46110 -1e-36
47107 -1e-36
47109 -1e-36
48106 -1e-36
48108 -1e-36
48110 -1e-36
48111 -1e-36
48112 -1e-36
48113 -1e-36
50120 -1e-36
53127 -1e-36
53129 -1e-36
54124 -1e-36
54126 -1e-36
54128 -1e-36
54129 -1e-36
54130 -1e-36
```

```
      54131 -1e-36
      54132 -1e-36
      54134 -1e-36
      54135 -1e-36
      54136 -1e-36
      55133 -1e-36
      55134 -1e-36
      55135 -1e-36
      55136 -1e-36
      55137 -1e-36
      56138 -1e-36
      59141 -1e-36
      60143 -1e-36
      60145 -1e-36
      60147 -1e-36
      60148 -1e-36
      60150 -1e-36
      61147 -1e-36
      61149 -1e-36
      62147 -1e-36
      62149 -1e-36
      62150 -1e-36
      62151 -1e-36
      62152 -1e-36
      63151 -1e-36
      63152 -1e-36
      63153 -1e-36
      63154 -1e-36
      63155 -1e-36
      64152 -1e-36
      64154 -1e-36
      64155 -1e-36
      64156 -1e-36
      64157 -1e-36
      64158 -1e-36
      64160 -1e-36
      67165 -1e-36
m15   6000  -0.978556        $ Burnable poison rod B4C
      5010  -0.004267
      5011  -0.017177
mt15 grph.06t
m21   92235  1.765E-03       $ Fuel - 1cyc depl
      92238  1.941E-02
      8016   4.645E-02
      93237  8.408E-06
      94238  1.473E-06
      94239  7.278E-05
      94240  4.302E-05
      94241  2.119E-05
      95241  1.859E-07
      95242  1.461E-09
      95243  3.640E-07
      96242  9.141E-08
      96243  6.932E-10
      96244  4.471E-08
      96245  7.751E-10
      33074  1.000E-36
```

33075	1.667E-08
35079	1.000E-36
35081	3.063E-06
36078	1.000E-36
36080	1.000E-36
36082	5.175E-08
36083	7.200E-06
36084	1.579E-05
36086	3.132E-05
37085	1.404E-05
37087	3.876E-05
39089	5.609E-05
40090	9.886E-07
40091	6.616E-05
40092	9.014E-05
40093	9.527E-05
40094	1.004E-04
40096	9.669E-05
41093	1.000E-36
42095	5.821E-05
43099	8.940E-05
44101	7.984E-05
44103	9.517E-06
44105	2.313E-08
46102	1.000E-36
46104	6.480E-06
46105	1.656E-05
46106	5.646E-06
46108	3.050E-06
46110	1.071E-06
47107	1.000E-36
47109	1.775E-06
48106	1.000E-36
48108	1.000E-36
48110	2.158E-07
48111	5.227E-07
48112	3.250E-07
48113	5.240E-09
50120	2.017E-07
53127	2.630E-06
53129	9.348E-06
54124	1.000E-36
54126	1.000E-36
54128	5.378E-08
54129	1.781E-10
54130	2.996E-07
54131	3.941E-05
54132	7.581E-05
54134	1.262E-04
54135	2.996E-08
54136	1.835E-04
55133	9.728E-05
55134	5.081E-06
55135	2.341E-05
55136	5.579E-08
55137	9.754E-05
56138	1.069E-04

```
      59141  7.678E-05
      60143  7.051E-05
      60145  5.714E-05
      60147  1.703E-06
      60148  2.701E-05
      60150  1.053E-05
      61147  2.016E-05
      61149  2.486E-07
      62147  2.591E-06
      62149  2.575E-07
      62150  1.872E-05
      62151  1.457E-06
      62152  8.189E-06
      63151  4.949E-10
      63152  1.044E-09
      63153  4.737E-06
      63154  5.369E-07
      63155  1.305E-07
      64152  1.008E-09
      64154  1.359E-08
      64155  6.925E-10
      64156  1.430E-06
      64157  5.069E-09
      64158  4.112E-07
      64160  1.804E-08
      67165  6.066E-10
m25   3007   2.331E-04       $ Burnable poison rod B4C - 1cyc depl
      4009   4.182E-11
      5010   2.165E-08
      5011   1.943E-03
      6000   8.929E-02
      6012   1.372E-08
mt25 grph.06t
m31   92235  3.211E-04       $ Fuel - 2cyc depl
      92238  1.883E-02
      8016   4.645E-02
      93237  1.374E-05
      94238  1.269E-05
      94239  4.845E-05
      94240  5.652E-05
      94241  2.780E-05
      95241  3.770E-07
      95242  2.915E-09
      95243  4.352E-06
      96242  7.215E-07
      96243  1.648E-08
      96244  2.831E-06
      96245  9.491E-08
      33074  1.000E-36
      33075  3.242E-08
      35079  3.062E-11
      35081  5.817E-06
      36078  1.000E-36
      36080  2.088E-11
      36082  2.776E-07
      36083  9.612E-06
      36084  3.481E-05
```

36086	5.946E-05
37085	2.720E-05
37087	7.396E-05
39089	1.221E-04
40090	4.837E-06
40091	1.484E-04
40092	1.741E-04
40093	1.827E-04
40094	1.999E-04
40096	1.908E-04
41093	1.000E-36
42095	1.478E-04
43099	1.653E-04
44101	1.596E-04
44103	4.547E-06
44105	1.500E-08
46102	1.000E-36
46104	3.451E-05
46105	4.608E-05
46106	2.452E-05
46108	1.351E-05
46110	4.790E-06
47107	1.000E-36
47109	6.770E-06
48106	1.000E-36
48108	1.000E-36
48110	3.481E-06
48111	2.217E-06
48112	1.194E-06
48113	3.003E-09
50120	3.784E-07
53127	6.105E-06
53129	1.961E-05
54124	1.000E-36
54126	1.000E-36
54128	3.964E-07
54129	4.884E-09
54130	2.503E-06
54131	6.014E-05
54132	1.844E-04
54134	2.585E-04
54135	8.645E-09
54136	3.744E-04
55133	1.763E-04
55134	2.283E-05
55135	5.794E-05
55136	1.104E-07
55137	1.945E-04
56138	2.175E-04
59141	1.624E-04
60143	8.397E-05
60145	1.006E-04
60147	6.153E-07
60148	5.502E-05
60150	2.245E-05
61147	1.482E-05
61149	1.226E-07

```
      62147  1.021E-05
      62149  9.486E-08
      62150  3.658E-05
      62151  1.115E-06
      62152  1.425E-05
      63151  3.053E-10
      63152  5.761E-10
      63153  1.369E-05
      63154  1.679E-06
      63155  3.779E-07
      64152  1.417E-09
      64154  1.883E-07
      64155  2.178E-09
      64156  1.332E-05
      64157  8.416E-09
      64158  2.158E-06
      64160  7.673E-08
      67165  3.376E-09
m35   1003   1.220E-09       $ Burnable poison rod B4C - 2cyc depl
      2004   1.857E-08
      3007   2.332E-04
      4009   5.366E-11
      5011   1.943E-03
      6000   8.929E-02
      6012   1.733E-08
mt35 grph.06t
c
c  Tallies
c
c  Total flux in the Triso kernels
f4:n 1 7 13 23 32 41 75 78 81 102
sd4 194269 2r 2.3313E6 2r 1.862E7 2r 2.276E8
c e4  1.05000e-10 &
c    1.00000e-9 1.05925e-9 1.12202e-9 1.18850e-9 1.25893e-9 &
c    1.33352e-9 1.41254e-9 1.49624e-9 1.58489e-9 1.67880e-9 &
c    1.77828e-9 1.88365e-9 1.99526e-9 2.11349e-9 2.23872e-9 &
c    2.37137e-9 2.51189e-9 2.66073e-9 2.81838e-9 2.98538e-9 &
c    3.16228e-9 3.34965e-9 3.54813e-9 3.75837e-9 3.98107e-9 &
c    4.21697e-9 4.46684e-9 4.73151e-9 5.01187e-9 5.30884e-9 &
c    5.62341e-9 5.95662e-9 6.30957e-9 6.68344e-9 7.07946e-9 &
c    7.49894e-9 7.94328e-9 8.41395e-9 8.91251e-9 9.44061e-9 &
c    1.00000e-8 1.05925e-8 1.12202e-8 1.18850e-8 1.25893e-8 &
c    1.33352e-8 1.41254e-8 1.49624e-8 1.58489e-8 1.67880e-8 &
c    1.77828e-8 1.88365e-8 1.99526e-8 2.11349e-8 2.23872e-8 &
c    2.37137e-8 2.51189e-8 2.66073e-8 2.81838e-8 2.98538e-8 &
c    3.16228e-8 3.34965e-8 3.54813e-8 3.75837e-8 3.98107e-8 &
c    4.21697e-8 4.46684e-8 4.73151e-8 5.01187e-8 5.30884e-8 &
c    5.62341e-8 5.95662e-8 6.30957e-8 6.68344e-8 7.07946e-8 &
c    7.49894e-8 7.94328e-8 8.41395e-8 8.91251e-8 9.44061e-8 &
c    1.00000e-7 1.05925e-7 1.12202e-7 1.18850e-7 1.25893e-7 &
c    1.33352e-7 1.41254e-7 1.49624e-7 1.58489e-7 1.67880e-7 &
c    1.77828e-7 1.88365e-7 1.99526e-7 2.11349e-7 2.23872e-7 &
c    2.37137e-7 2.51189e-7 2.66073e-7 2.81838e-7 2.98538e-7 &
c    3.16228e-7 3.34965e-7 3.54813e-7 3.75837e-7 3.98107e-7 &
c    4.21697e-7 4.46684e-7 4.73151e-7 5.01187e-7 5.30884e-7 &
c    5.62341e-7 5.95662e-7 6.30957e-7 6.68344e-7 7.07946e-7 &
c    7.49894e-7 7.94328e-7 8.41395e-7 8.91251e-7 9.44061e-7 &
```

```
c    1.00000e-6 1.05925e-6 1.12202e-6 1.18850e-6 1.25893e-6 &
c    1.33352e-6 1.41254e-6 1.49624e-6 1.58489e-6 1.67880e-6 &
c    1.77828e-6 1.88365e-6 1.99526e-6 2.11349e-6 2.23872e-6 &
c    2.37137e-6 2.51189e-6 2.66073e-6 2.81838e-6 2.98538e-6 &
c    3.16228e-6 3.34965e-6 3.54813e-6 3.75837e-6 3.98107e-6 &
c    4.21697e-6 4.46684e-6 4.73151e-6 5.01187e-6 5.30884e-6 &
c    5.62341e-6 5.95662e-6 6.30957e-6 6.68344e-6 7.07946e-6 &
c    7.49894e-6 7.94328e-6 8.41395e-6 8.91251e-6 9.44061e-6 &
c    1.00000e-5 1.05925e-5 1.12202e-5 1.18850e-5 1.25893e-5 &
c    1.33352e-5 1.41254e-5 1.49624e-5 1.58489e-5 1.67880e-5 &
c    1.77828e-5 1.88365e-5 1.99526e-5 2.11349e-5 2.23872e-5 &
c    2.37137e-5 2.51189e-5 2.66073e-5 2.81838e-5 2.98538e-5 &
c    3.16228e-5 3.34965e-5 3.54813e-5 3.75837e-5 3.98107e-5 &
c    4.21697e-5 4.46684e-5 4.73151e-5 5.01187e-5 5.30884e-5 &
c    5.62341e-5 5.95662e-5 6.30957e-5 6.68344e-5 7.07946e-5 &
c    7.49894e-5 7.94328e-5 8.41395e-5 8.91251e-5 9.44061e-5 &
c    1.00000e-4 1.05925e-4 1.12202e-4 1.18850e-4 1.25893e-4 &
c    1.33352e-4 1.41254e-4 1.49624e-4 1.58489e-4 1.67880e-4 &
c    1.77828e-4 1.88365e-4 1.99526e-4 2.11349e-4 2.23872e-4 &
c    2.37137e-4 2.51189e-4 2.66073e-4 2.81838e-4 2.98538e-4 &
c    3.16228e-4 3.34965e-4 3.54813e-4 3.75837e-4 3.98107e-4 &
c    4.21697e-4 4.46684e-4 4.73151e-4 5.01187e-4 5.30884e-4 &
c    5.62341e-4 5.95662e-4 6.30957e-4 6.68344e-4 7.07946e-4 &
c    7.49894e-4 7.94328e-4 8.41395e-4 8.91251e-4 9.44061e-4 &
c    1.00000e-3 1.05925e-3 1.12202e-3 1.18850e-3 1.25893e-3 &
c    1.33352e-3 1.41254e-3 1.49624e-3 1.58489e-3 1.67880e-3 &
c    1.77828e-3 1.88365e-3 1.99526e-3 2.11349e-3 2.23872e-3 &
c    2.37137e-3 2.51189e-3 2.66073e-3 2.81838e-3 2.98538e-3 &
c    3.16228e-3 3.34965e-3 3.54813e-3 3.75837e-3 3.98107e-3 &
c    4.21697e-3 4.46684e-3 4.73151e-3 5.01187e-3 5.30884e-3 &
c    5.62341e-3 5.95662e-3 6.30957e-3 6.68344e-3 7.07946e-3 &
c    7.49894e-3 7.94328e-3 8.41395e-3 8.91251e-3 9.44061e-3 &
c    1.00000e-2 1.05925e-2 1.12202e-2 1.18850e-2 1.25893e-2 &
c    1.33352e-2 1.41254e-2 1.49624e-2 1.58489e-2 1.67880e-2 &
c    1.77828e-2 1.88365e-2 1.99526e-2 2.11349e-2 2.23872e-2 &
c    2.37137e-2 2.51189e-2 2.66073e-2 2.81838e-2 2.98538e-2 &
c    3.16228e-2 3.34965e-2 3.54813e-2 3.75837e-2 3.98107e-2 &
c    4.21697e-2 4.46684e-2 4.73151e-2 5.01187e-2 5.30884e-2 &
c    5.62341e-2 5.95662e-2 6.30957e-2 6.68344e-2 7.07946e-2 &
c    7.49894e-2 7.94328e-2 8.41395e-2 8.91251e-2 9.44061e-2 &
c    1.00000e-1 1.05925e-1 1.12202e-1 1.18850e-1 1.25893e-1 &
c    1.33352e-1 1.41254e-1 1.49624e-1 1.58489e-1 1.67880e-1 &
c    1.77828e-1 1.88365e-1 1.99526e-1 2.11349e-1 2.23872e-1 &
c    2.37137e-1 2.51189e-1 2.66073e-1 2.81838e-1 2.98538e-1 &
c    3.16228e-1 3.34965e-1 3.54813e-1 3.75837e-1 3.98107e-1 &
c    4.21697e-1 4.46684e-1 4.73151e-1 5.01187e-1 5.30884e-1 &
c    5.62341e-1 5.95662e-1 6.30957e-1 6.68344e-1 7.07946e-1 &
c    7.49894e-1 7.94328e-1 8.41395e-1 8.91251e-1 9.44061e-1 &
c    1.00000e+0 1.05925e+0 1.12202e+0 1.18850e+0 1.25893e+0 &
c    1.33352e+0 1.41254e+0 1.49624e+0 1.58489e+0 1.67880e+0 &
c    1.77828e+0 1.88365e+0 1.99526e+0 2.11349e+0 2.23872e+0 &
c    2.37137e+0 2.51189e+0 2.66073e+0 2.81838e+0 2.98538e+0 &
c    3.16228e+0 3.34965e+0 3.54813e+0 3.75837e+0 3.98107e+0 &
c    4.21697e+0 4.46684e+0 4.73151e+0 5.01187e+0 5.30884e+0 &
c    5.62341e+0 5.95662e+0 6.30957e+0 6.68344e+0 7.07946e+0 &
c    7.49894e+0 7.94328e+0 8.41395e+0 8.91251e+0 9.44061e+0 &
c    1.00000e+1 1.05925e+1 1.12202e+1 1.18850e+1 1.25893e+1 &
```

```
c    1.33352e+1 1.41254e+1 1.49624e+1 1.58489e+1 1.67880e+1 &
c    1.77828e+1 1.88365e+1 1.99526e+1 2.11349e+1 2.23872e+1 &
c    2.37137e+1 2.51189e+1 2.66073e+1 2.81838e+1 2.98538e+1 &
c    3.16228e+1 3.34965e+1 3.54813e+1 3.75837e+1 3.98107e+1 &
c    4.21697e+1 4.46684e+1 4.73151e+1 5.01187e+1 5.30884e+1 &
c    5.62341e+1 5.95662e+1 6.30957e+1 6.68344e+1 7.07946e+1 &
c    7.49894e+1 7.94328e+1 8.41395e+1 8.91251e+1 9.44061e+1 &
c    1.00000e+2
prdmp j 250
```

C-3: SAMPLE ORIGEN-S INPUT FILE

```
=origens
'-------------------------------------------------------------------------
---
'    This input file irradiates Zr93 (with other Zr isotopes from U235
' fission yield. The neutronic parameters are from MCNP model of VHTR.
' Result requested is the status of the FP up to 30yrs from initial
' loading into VHTR core.
'-------------------------------------------------------------------------
---
'    The 0$$ is the logical unit assignment card. The 8th entry (a8) =
26
' implies binary library on 3rd entry of 81$$ card. a11 = 71 implies
the
' unit number of the file where concentrations and binary photon
library
' are stored. Note that unit 71 is origen's binary density file.
'-------------------------------------------------------------------------
---
0$$ a8 26 a11 71 e
'-------------------------------------------------------------------------
---
'    THE LINE AFTER "1t" IS THE TITLE CARD. IT MUST ALWAYS BE PRESENT!
'-------------------------------------------------------------------------
---
1t
-- Post Irradiation Decay of Fission Product --
'-------------------------------------------------------------------------
---
'    The 3$$ is the library integer constants card. The 1st 3 entries
are
' default values. 4th entry = -82 implies neutron energy group
structure
' read from logical unit 81 of SCALE library (this is a 27 grp
structure).
' a16 = 2 implies the unit of input concentrations is in grams. a33 =
18
' implies an 18 group gamma energy structure, specified on 83** card.
'-------------------------------------------------------------------------
---
3$$ 28 0 0 0 a16 2 a33 18 e
'-------------------------------------------------------------------------
---
'    The 4** is the library constants for NTYPE=0.
' 1st entry is the ratio of thermal neutron xsection to 2200m/s neutron
xs.
'    THERM = sqrt((pi/4)*(T_0/T)); where T_0=293.16K, T=moderator temp.
' 2nd entry is RES, which is ratio of resonance flux to thermal flux:
'    RES = integral phi(E) over E=(0.625eV,1Mev] divided by phi_therm;
'              phi_therm = integral phi(E) over E=[0eV,0.625eV].
' 3rd entry is FAST, which is the ratio of fast flux to thermal flux
'    FAST = integral phi(E) over E=(1MeV,E_max] divided by phi_therm.
' 4th entry is a truncation error limit below which the values computed
'    by the code will be considered to be zero.
```

```
'-------------------------------------------------------------------
---
4** 0.41395 1.54552 0.19718 1e-25
2t
'-------------------------------------------------------------------
---
'    The 35$$ explains the gamma energy group structure. Entry "0"
implies
' group structure is available in library or provided in 83** card.
35$$ 0 4t
'-------------------------------------------------------------------
---
'    The 54$$ is a special calculation card. a11 = 2 implies
application
' of problem-dependent compositions for the (alpha,n) calculation.
'    The 56$$ is subcase control constants card. 1st entry = 0 implies
a
' decay calculation (note: 1st entry is number of irradiation
intervals).
' 2nd entry = 6 implies number of time intervals in this case.
' 2nd entry = 0/1 implies irradiation case input in
POWER(58*)/FLUX(59*)
' a13 = 3 implies number of nuclides in input cards 73$$, 74** $ 75$$.
' 14th entry = 1/2/3/4/5 implies unit of time is
"seconds/minutes/hours/
' days/years".
' 15th entry = 3 implies input cards should be read for both problem
' title and basis, from the 2 lines after the "5t" block termination
flag.
' a17 =  2 implies output tables to be suppressed are indicated on 65$$
' (decay print) and 66$$ (irradiation print) cards. 18th entry= 0
implies
' suppression of element output tables during irradiation, which is not
' necessary for a decay-only problem.
'    The 60** is the interval times in the unit specified on a14 of
56$$.
'    The 61** is print cut-offs for decay tables requested in 65$$
cards.
' There are 7 cut-off entries in the following other: gram-atoms,
grams,
' curies, watts decay heat, watts gamma heat, m^3 of rcg-
air(inhalation),
' & m^3 of rcg-water(ingestion) [rcg = radioactivity concentration
guides]
'-------------------------------------------------------------------
---
54$$ a11 2 e  56$$ 12 12 1 a13 7 4 3 a17 2 0 e  5t
 Zr93 irradiation in VHTR system
 kg of Zirconium
59**  3.26E+14 3.49E+14 3.53E+14 3.74E+14
      3.26E+14 3.49E+14 3.53E+14 3.74E+14
      3.26E+14 3.49E+14 3.53E+14 3.74E+14
60**  100 200 300 405 505 605 705 810 910 1010 1110 1215
61** 5r1-6 1+6 1+4
'-------------------------------------------------------------------
---
'    The 65$$ is the decay period print control card with a total of 63
```

```
' entries. Each entry number in the table below corresponds to the
control
' of the row and column it represents. e.g. entry 5 is print control
for
' light element concentrations in grams printed by elements, entry 31
is
' the control for actinide decay heat in watts printed by nuclides, and
' entry 57 is the control for printing total fission product gamma
heat.
' All 63 entries are default to "0" (i.e. turned-off). To turn any
entry
' on, set the value to "1".
'  ____________________________________________________________________
''|Output Print Unit| Light Elements |    Actinide    |Fission Products|
''|                 | Nuc.  El.  Sum | Nuc.  El.  Sum | Nuc.  El.  Sum |
''|_________________|________________|________________|________________|
''|atom-grams       |  1     2    3  |  22   23   24  | 43    44   45  |
''|grams            |  4     5    6  |  25   26   27  | 46    47   48  |
''|curies           |  7     8    9  |  28   29   30  | 49    50   51  |
''|decay heat(Watts)| 10    11   12  |  31   32   33  | 52    53   54  |
''|gamma heat(Watts)| 13    14   15  |  34   35   36  | 55    56   57  |
''|inhalation hazard| 16    17   18  |  37   38   39  | 58    59   60  |
''|ingestion hazard | 19    20   21  |  40   41   42  | 61    62   63  |
''|_________________|________________|________________|________________|
'-----------------------------------------------------------------------
---
'65$$ f1 e
65$$ a46 1 a49 1 a52 1 a55 1 e
'-----------------------------------------------------------------------
---
'    The 81$$ is the gamma source term and library update card. 1st
entry
' = 2 implies master photon library is requested. 2nd entry is no
longer
' required. 3rd entry = 26 is the master photon library unit number.
4th
' entry = 1 implies photon library is in binary format.
'    The 82$$ is the gamma source print flag. entry = f2 implies fill
all
' entries with value 2 for all decay time intervals (10 in this case).
' The value "2"  implies printing of total gamma source per second.
'    The 83** card is the user-specified gamma energy group boundaries.
'-----------------------------------------------------------------------
---
81$$ 2 0 26 1 e  82$$ f2
' 83** 1.5+7  1.3+7  1.1+7  9.0+6  7.5+6  6.8+6  6.3+6  5.8+6  5.3+6
'      5.0+6  4.8+6  4.3+6  3.8+6  3.3+6  2.8+6  2.6+6  2.2+6  1.8+6
'      1.4+6  1.0+6  8.0+5  7.0+5  6.5+5  6.0+5  5.5+5  5.0+5  4.5+5
'      4.0+5  3.5+5  3.0+5  2.5+5  2.0+5  1.5+5  1.0+5  7.0+4  5.0+4
'      3.0+4  1.0+4  0.0+0  e
' 84** 2.0+7  1.4+7  1.0+7  7.0+6  5.0+6  2.5+6  1.0+6  5.0+5  1.0+5
'      1.0+4  1.0+3  1.0+2  1.0+1  1.0+0  1.0-1  2.5-2  0.0+0  e
'-----------------------------------------------------------------------
---
'    The 73$$ is the input nuclide ID.
'    The 74** is the concentrations of each nuclide in 73$$ in the unit
' specified on a16 of 3$$.
```

```
'    The 75$$ card indicates the type of library required with 73$$:
' 1 => light elements lib; 2 => actinides lib; 3 => fission products
lib;
' 4 => element from light elements lib.
'    Entries in 73$$, 74** & 75$$ retain the same order. The order of
the
' (3) nuclides is given below:
'Nuclides Zr90   Zr91   Zr92   Zr93   Zr94   Zr95   Zr96
'-------------------------------------------------------------------
---
73$$      400900 400910 400920 400930 400940 400950 400960
'...................................................................
.
74**      133.56 134.62 139.09 146.59 149.50 150.21 146.43
'...................................................................
.
75$$      7r3
'-------------------------------------------------------------------
---
6t
'-------------------------------------------------------------------
---
'    The following (2) 56$$ cards are described here.
' Top 56$$: 1st entry = 0 implies decay. 2nd entry = -10 & a10 = 0
implies
'           results in g-atoms for steps 0 through 10 are written on
file
'           unit #71 (origen density file). a6 = 1 implies a
continuation
'           problem with old concentrations and same libraries, next
sub-
'           case begin with data block 5 (this is the default).
' Bottom 56$$: Entry = f0 implies all entries filled with "0". This is
the
'           termination of the origen calculation.
'-------------------------------------------------------------------
---
56$$ 0 -12 a6 1 a10 0 e t
56$$ f0 t
end
'-------------------------------------------------------------------
---
'    There are 6 opus requests below this block.
' 1st opus: prints the mass per kg (grams) for selected nuclides at
'           times specified throughout irradiation period.
' 2nd opus: prints the radioactivity per kg (Ci) for selected nuclides
at
'           times specified throughout irradiation period.
' 3rd opus: prints the decay heat per kg (watts) for selected nuclides
at
'           times specified throughout irradiation period.
' 4th opus: prints the gamma heat per kg (watts) for selected nuclides
at
'           times specified throughout irradiation period.
'-------------------------------------------------------------------
---
=opus
```

```
typarams=nuclides   units=grams   libtype=all
symnuc=zr-90 zr-91 zr-92 zr-93 zr-94 zr-95 zr-96
  zr-97 zr-98 zr-99 nb-93 nb-94 nb-95 nb-96 nb-97
  nb-98 nb-99 nb-100 mo-94 mo-95 mo-96 mo-97 mo-98
  mo-99 mo-100 mo-101 mo-102 tc-99 tc-100 tc-101 tc-102
  tc-103 ru-100 ru-101 ru-102 ru-103 ru-104 rh-103
 end   sort=no   time=days
nposition=1 2 3 4 5 6 7 8 9 10 11 12 13 end
end
=opus
typarams=nuclides   units=curies   libtype=all
symnuc=zr-90 zr-91 zr-92 zr-93 zr-94 zr-95 zr-96
  zr-97 zr-98 zr-99 nb-93 nb-94 nb-95 nb-96 nb-97
  nb-98 nb-99 nb-100 mo-94 mo-95 mo-96 mo-97 mo-98
  mo-99 mo-100 mo-101 mo-102 tc-99 tc-100 tc-101 tc-102
  tc-103 ru-100 ru-101 ru-102 ru-103 ru-104 rh-103
 end   sort=no   time=days
nposition=1 2 3 4 5 6 7 8 9 10 11 12 13 end
end
=opus
typarams=nuclides   units=watts   libtype=all
symnuc=zr-90 zr-91 zr-92 zr-93 zr-94 zr-95 zr-96
  zr-97 zr-98 zr-99 nb-93 nb-94 nb-95 nb-96 nb-97
  nb-98 nb-99 nb-100 mo-94 mo-95 mo-96 mo-97 mo-98
  mo-99 mo-100 mo-101 mo-102 tc-99 tc-100 tc-101 tc-102
  tc-103 ru-100 ru-101 ru-102 ru-103 ru-104 rh-103
 end   sort=no   time=years
nposition=1 2 3 4 5 6 7 8 9 10 11 12 13 end
end
=opus
typarams=nuclides   units=gamwatts   libtype=all
symnuc=zr-90 zr-91 zr-92 zr-93 zr-94 zr-95 zr-96
  zr-97 zr-98 zr-99 nb-93 nb-94 nb-95 nb-96 nb-97
  nb-98 nb-99 nb-100 mo-94 mo-95 mo-96 mo-97 mo-98
  mo-99 mo-100 mo-101 mo-102 tc-99 tc-100 tc-101 tc-102
  tc-103 ru-100 ru-101 ru-102 ru-103 ru-104 rh-103
 end   sort=no   time=years
nposition=1 2 3 4 5 6 7 8 9 10 11 12 13 end
end
```

VITA

Name:	Ayodeji Babatunde Alajo
Address:	Nuclear Engineering Department, 129 Zachary Engineering Building, 3133 TAMU, College Station TX 77843
Email Address:	dejialajo@yahoo.com, dejialajo@tamu.edu
Education:	Ph.D., Nuclear Engineering, Texas A&M University, 2010 M.S., Nuclear Engineering, Texas A&M University, 2007 B.Sc., Mechanical Engineering, University of Ibadan, Nigeria, 2001